



Master Thesis

Detection and Visualization of Glacier Area Changes at the Lake Paiku Basin (Tibet, China) using Multi-Tem- poral Remote Sensing Imagery from 1974-2010

submitted by Maria Elena Vargas Amado

born on 05.03.1981 in Guadalajara, Jal, Mex.

submitted for the academic degree of
Master of Science (M.Sc.)

Date of Submission

[Date of Submission]

Supervisors:

Prof. Dr. Manfred F. Buchroithner
Technische Universität Dresden

Dipl. Ing. Nicolai Holzer
Technische Universität Dresden

Binding of the Original Sheet Containing the Task of the Thesis

Statement of Authorship

Herewith I declare that I am the sole author of the thesis named

„Detection and Visualization of Glacier Area Changes at the Lake Paiku Basin (Tibet, China) using Multi-Temporal Remote Sensing Imagery from 1974-2010“

which has been submitted to the study commission of geosciences today.

I have fully referenced the ideas and work of others, whether published or unpublished. Literal or analogous citations are clearly marked as such.

Dresden, [Date of Submission]

Signature

Abstract

The study area is located in the Tibetan Plateau and surrounding mountains, in an area known as the “Third Pole” due to its vast coverage of approximately 100,000km² glaciers. The area borders the Nepalese Bagmati region and the autonomous region of Tibet in China, otherwise known as Shigatse (Xizang). The response of glaciers to global warming in this extensive area is of both regional and worldwide significance. This project seeks to identify whether any changes in the glaciers’ surface area have occurred during the 1974 - 2010 study period.

To achieve this aim, a glacier inventory for the study area was created using multi-temporal analysis to identify the rate of change throughout the 36-year observation period. Remote sensed data from sensors such as Landsat TM/ETM+, HEXAGON, ALOS, ASTER DEM and SRTM was obtained and evaluated using image processing and GIS techniques. In order to distinguish the areas covered by glaciers, a ratio image was created using bands 4 and 5 from Landsat TM 2000. This was subsequently edited manually to allow for debris coverage. The resulting year 2000 glacier outlines were then duplicated and adjusted manually to fit the glacier outlines of 1974 and 2010, using HEXAGON and ALOS/Landsat ETM+ imagery respectively.

A total of 213 glaciers were delimited in the study area with an initial surface area of 817.76 ± 35.06 km² in 1974 and a surface area of 784.96 ± 17.42 km² in 2010. This equals a glacier shrinkage of 32.8 ± 34.64 km² in the region during the 36 year study period. The average annual loss was consistent throughout the years representing a continual loss of less than 1 km² per year. The multi-temporal analysis performed for the 1974-2010 period shows 66% of glaciers experienced retreat, 32% remained stable and only 2 percent of all glaciers advanced. The total count of retreat lengths during the 1974-2010 observation period was 56.248 ± 2.12 km based on distance measurements interpolated from the SRTM.

Kurzfassung

Gletscher gelten allgemein hin als Schlüsselindikatoren für Klimaänderungen und sind von größter Wichtigkeit für den Wasserhaushalt in den ariden Regionen Zentralasiens. Mit einer Gesamtgletscherausdehnung von circa 100.000 km² stellt das Tibetische Plateau die größte Agglomeration von Gletschern dar, weswegen diese Region auch als der „Dritte Pol“ bezeichnet wird. Die vorliegende Arbeit beschäftigt sich mit der Untersuchung von Gletscherflächenänderungen im Zeitraum 1974-2010 auf Basis optischer Fernerkundungsdaten für eine Region im Grenzgebiet zwischen der nepalesischen Provinz Bagmati und der Provinz Shigatse (Xizang) in der autonomen Region Tibet (China).

Auf Grundlage multi-temporalen optischer Satellitenbilddaten, beispielsweise Landsat TM/ETM+, HEXAGON, ALOS, und digitaler Geländemodelle (ASTER GDEM, SRTM) wurde ein Gletscherinventar für drei Zeitschnitte (1974, 2000, 2010) generiert und die jeweiligen Gletscherflächenänderungen über einen Gesamtzeitraum von 36 Jahren analysiert. Für das Jahr 2000, welches als Referenz für alle weiteren Zeitschnitte diente, wurde zur Unterscheidung glazialer und nichtglazialer Areale ein Ratio-Bild aus den Landsat TM Kanälen 4 und 5 berechnet. Im Anschluß erfolgte eine manuelle Korrektur hinsichtlich schuttbedeckter Gletscherbereiche, welche nicht durch das Ratio-Bild erfaßt wurden. Die 1974er und 2010er Gletscherumrisse wurden anschließend auf Grundlage der 2000er Umriss unter Zuhilfenahme von HEXAGON- bzw. ALOS/Landsat ETM+-Aufnahmen manuell kartiert.

In Summe umfaßt das erstellte Gletscherinventar 213 Einzelgletscher mit einer Gesamtfläche von $817,76 \pm 35,06$ km² zum Zeitpunkt 1974 bzw. $784,96 \pm 17,42$ km² zum Zeitpunkt 2010. Dies entspricht einem Gletscherflächenrückgang von $32,8 \pm 34,64$ km² innerhalb des 36 Jahre umfassenden Untersuchungszeitraums mit einer annähernd einheitlichen mittleren jährlichen Flächenabnahme von <1 km² pro Jahr. Insgesamt zeigt sich, dass 66% aller Gletscher eine Flächenabnahme, 2% eine Flächenzunahme und 32% stabile Bedingungen im Zeitraum 1974-2010 aufweisen. Die kumulierte Längenänderung im Untersuchungszeitraum, beruhend auf Distanzmessungen unter Einbeziehung des SRTM3 DGMs, beträgt $-56,248 \pm 2,12$ km.

Contents

Binding of the Original Sheet Containing the Task of the Thesis	I
Statement of Authorship	II
Abstract.....	III
Kurzfassung	IV
Contents	V
Figures	VII
Tables.....	IX
Table of Abbreviations	X
1 Introduction.....	1
1.1 Background.....	1
1.2 Research Outline.....	2
2 Study Region.....	3
2.1 General Description	3
2.2 Climate.....	4
3 Glaciers	9
3.1 An overview of the glaciers of the chosen area.	9
3.2 Glacier terminology	10
4 Data.....	13
4.1 HEXAGON KH-9 images	13
4.2 Landsat Images	15
4.2.1 Landsat 5 (TM)	16
4.2.2 Landsat 7 (ETM+).....	16
4.3 ALOS PRISM Images.....	18
4.4 SRTM.....	18
4.5 ASTER GDEM V2	19
4.6 WorldClim- Global Climate Data.	19
4.7 Global Land Ice Measurements from Space (GLIMS)	20
5 Methodology and Workflow.....	20
5.1 Creating A Glacier Inventory Based on Landsat 2000	21
5.1.1 Pre-processing (Semi-automatized Processing).....	22
5.1.2 Post-processing (Manual Editing).....	25

5.2	Adaptation of Glacier Outlines Based on Landsat and ALOS 2010.....	27
5.2.1	Landsat Image Selection	27
5.2.2	Manual Editing.....	29
5.3	Adaptation of Glacier Outlines Based on HEXAGON 1974.....	29
5.3.1	Image processing.....	29
5.3.2	Manual Edition.....	32
5.4	Lengths and Areas of Glaciers	33
5.4.1	Areas	34
5.4.2	Lengths.....	34
6	Uncertainty.....	38
6.1	Uncertainty Estimations for the Area.....	38
6.2	Uncertainty Estimations for the Lengths.....	39
7	Results.....	41
7.1	Area.....	41
7.2	Lengths.....	52
8	Discussion	57
9	Conclusions.....	60
10	Outlook	61
11	Appendix.....	63
	Acknowledgments.....	71
	References.....	72

Figures

Figure 1. Localization of the area of interest. (Personal compilation based on the raster layers: World Terrain Base, National Geographic World Map (Esri, 2014).	3
Figure 2. Average Monthly Mean Temperature for November (Personal compilation based on the raster layers: World Terrain Base, National Geographic World Map (Esri, 2014) and Global Climate data (Hijmans, Cameron and Parra, n.d.). The vector files were taken form DIVA-GIS (Hijmans, n.d.)).....	6
Figure 3. Average Monthly Mean Temperature for April (Personal compilation based on the raster layers: World Terrain Base, National Geographic World Map (Esri, 2014) and Global Climate data (Hijmans, Cameron and Parra, n.d.). The vector files were taken form DIVA-GIS (Hijmans, n.d.)).....	7
Figure 4. Average Monthly Mean Precipitation for November (Personal compilation based on the raster layers: World Terrain Base, National Geographic World Map (Esri, 2014) and Global Climate data (Hijmans, Cameron and Parra, n.d.). The vector files were taken form DIVA-GIS (Hijmans, n.d.)).....	8
Figure 5. Average Monthly Mean Precipitation for April (Personal compilation based on the raster layers: World Terrain Base, National Geographic World Map (Esri, 2014) and Global Climate data (Hijmans, Cameron and Parra, n.d.). The vector files were taken form DIVA-GIS (Hijmans, n.d.)).....	9
Figure 6. Components of the mass balance of a glacier. The arrows have arbitrary widths and do not indicate physical pathways of mass transfer (Cogley et al., 2011).	11
Figure 7. Landsat image 2000. In red the AOI.	21
Figure 8. The yellow line shows the edges of the vector layer coincided with the pixel size after the raster-vector transformation.....	24
Figure 9. The yellow line shows the original shape edge of the outlines after raster-vector transformation. The red line represents the edges result after smoothing the vector layer....	25
Figure 10. The red line represents the result of the vector layer after the semi-automatized process. The back line is the result of manual edition using the Landsat ETM+ 2000 as base image.....	26
Figure 11. Representation of ALOS image coverage over the AOI. The outlines are shown in red.	28
Figure 12. The black & white image corresponds to the chosen HEXAGON image to adapt outlines. In red, the AOI is shown.	30
Figure 13. Fig 10a shows the outlines from 2000 fitting perfectly in the ETM image not the same case in the HEXAGON images, where the yellow arrow shows the displacement.	31

Figure 14. Comparison between the HEXAGON input image (black and white) with different levels of geo-correction and Landsat ETM (color), used as the reference image. The Outlines are shown in orange. Images “c” and “d” display the matching after using AytoSync Tool..... 32

Figure 15. Flow chart of the model builder to get the flow lines..... 36

Figure 16. Group size proportion according to the total amount of glaciers (a) and the full surface (b). 44

Figure 17. Map showing the group size classification. (Personal compilation based on the raster layers: National Geographic World Map (Esri, 2014) and Shaded Relief from SRTM. The vector files were taken form DIVA-GIS (Hijmans, n.d.) and self-made outlines digitalization)..... 45

Figure 18. Changes per glacier occurred from 1974 to 2010 normalized by 1974’s surface. (Personal compilation based on the raster layers: National Geographic World Map (Esri, 2014) and Shaded Relief from SRTM. The vector files were taken form DIVA-GIS (Hijmans, n.d.) and self-made outlines digitalization)..... 46

Figure 19 Differences in area between 1974 and 2010. (Personal compilation based on the raster layers: National Geographic World Map (Esri, 2014) and Shaded Relief from SRTM. The vector files were taken form DIVA-GIS (Hijmans, n.d.) and self-made outlines digitalization)..... 47

Figure 20. Map showing glaciers sorted in descending order by area in 1974. (Personal compilation based on the raster layers: National Geographic World Map (Esri, 2014) and Shaded Relief from SRTM. The vector files were taken form DIVA-GIS (Hijmans, n.d.) and self-made outlines digitalization)..... 52

Figure 21. Charts that explain the changes of the glaciers in the AOI during different periods. 53

Figure 22. Length changes sorted by 3D Lengths during the period 1974-2010. . (Personal compilation based on the raster layers: National Geographic World Map (Esri, 2014) and Shaded Relief from SRTM. The vector files were taken form DIVA-GIS (Hijmans, n.d.) and self-made outlines digitalization)..... 55

Tables

Table 1. Mission Statistics of HEXAGON Program (Burnett, 2012).....	14
Table 2. Characteristics of search/surveillance system Cameras (Burnett, 2012)	15
Table 3 Band designations for Landsat 5 TM satellite (USGS, 2013).....	16
Table 4 Band designations for Landsat 7 ETM+ satellite (USGS, 2013).....	17
Table 5. Overall information of imagery used for the project.	29
Table 6 Details taken into account for the area accuracy (Bolch et al., 2010).....	38
Table 7. Uncertainty calculation for 2 dimensions lengths.....	40
Table 8. Uncertainty calculation for 3 dimensions lengths.....	40
Table 9. Totals in area in the AOI.....	41
Table 10. Absolute difference and averaged totals in area in the AOI	41
Table 11. Relative and averaged relative totals in area in the AOI.....	42
Table 12. Group Sizes of Glaciers	43
Table 13. Glacier changes sorted by the highest difference (descending order) in area during the period 1974-2010 (underlined field).	49
Table 14. Glaciers sorted in descending order by area in 1974 (underlined field).	51
Table 15. Percentage of dynamics of the glaciers over the AOI per period.	53
Table 16. Total length changes per period.....	54
Table 17. Lengths of the 11 more significant retreats.....	56
Table 18 Glaciers' mass and volume changes (Nikolakakou, 2014).....	58
Table 19. Area and differences in area for the Glaciers considered in Nikolakakou (2014)	59
Table 20 Length and length average for the Glaciers considered in Nikolakakou (2014).....	59
Table 21. Results per glacier.....	63

Equation

Equation 1. In this formula, “q” represents the result of the mathematical operation and “ δ ” is the uncertainty associated with that measurement (Appalachian State University, 2014). 39

Table of Abbreviations

2D	2-Dimensional
3D	Third Dimension
ALOS	Advanced Observing Satellite
AOI	Area Of Interest
APM	Automatic Point Measurement
ASTER	Advanced Spaceborne Thermal Emission and Reflection Radiometer
DEM	Digital Elevation Model
DLT	Direct Linear Transformation
EOM	Earth Observation Mission
ETM+	Enhanced Thematic Mapper Plus
GCPs	Ground Control Points
GDEM2	Global Digital Elevation Model Version 2
GIS	Geographic Information System
GLIMS	Global Land Ice Measurements from Space
JAXA	Japan Aerospace Exploration Agency
LPDAAC	Land Processes Distributed Active Archive Center
mw.e.a ⁻¹	Meter of Water Equivalent per Year
m a.s.l	meters above sea level
MEaSURES	Making Earth System Data Records for Use in Research Environments
METI	Ministry of Economy, Trade and Industry
NASA	National Aeronautics and Space Administration
NDVI	Normalized Difference Vegetation Index
NSIDC	National Snow and Ice Data Center
PAEK	Polynomial Approximation with Exponential Kernel
RGB	Red Green Blue
RMS	Root Mean Square
SAR	Synthetic Aperture Radar
SRTM	Shuttle Radar Topography Mission
TIN	Triangulated Irregular Network
TM	Landsat Thematic Mapper
TP	Tibetan Plateau
TPI	Tibetan Plateau Interior
USGS	United States Geological Survey
UTM	Universal Transverse Mercator
μm	Micrometer

1 Introduction

1.1 Background

Mountain glaciers represent just a small part of the cryosphere, yet they are no less important than the rest. These glaciers have proved to be an indicator of climate change because of their quick response to changes in the environment (Cubasch and Cess, 1990).

The area studied in this work is situated on the border between Tibet in China and Nepal, lying in the Himalayas Mountains. The Tibetan Plateau (TP) is part of the landscape.

The Tibetan Plateau and adjacent regions encompass nearly 46,300 glaciers spanning an area of 59,400 km². Just the Tibetan Plateau by itself holds 36,800 glaciers and a surface of 49,873 km². In the early 20th Century, glacier shrinking started in this area and since then, the glaciers have started to decrease rapidly due to the rising in air's temperature, result of the global warming (Yao et al., 2007).

Existing climate models predict the global warming trend because of the increasing levels of greenhouse gases in the atmosphere. This air temperature rise signifies consequences for the hydrological cycle, principally in regions where the most important water supply comes from melted snow or ice. A warmer world implies less snow falling in winter and therefore earlier spring melting of the winter snow (Barnett, Adam and Lettenmaier, 2005).

It is important to mention that more than one-sixth of the people in the Earth depends on glaciers for their water source. Climate change is jeopardizing the water reservoir linked to glaciers. With this panorama, life of thousands of people is being threatened by the fact that reach water human consumption will be very hard for them (Barnett, Adam and Lettenmaier, 2005).

The study area has become a research focus because of the large system of endorheic lakes that are part of the zone (Kropáček et al., 2013) and because of the huge amount of people, more than 1.4 billion, that depend on the water coming from the rivers:

Indus, Ganges, Brahmaputra, Yangtze, and Yellow. Those rivers are fed by the snow and ice from the glaciers. Climate change is jeopardizing the seasonal water availability (Immerzeel, van Beek and Bierkens, 2010).

It is also worth mentioning that drainage of glacial lakes represent one of the most significant threats to the Himalayas. Glacier outburst can result in discharges capable of destroying infrastructure and jeopardizing human lives (Richardson and Reynolds, 2000).

1.2 Research Outline

This thesis contains a total of nine chapters.

The first chapter or the introduction, starts explaining the situation of the zone to introduce to the reader to the glacier's conditions as well as to explain the reasons why these area became a focus attention to this study.

Chapter two includes a geographical and climatic impression of the area. A general panorama about precipitation, temperature of the area related to the location is given.

After given a general panorama of the Tibetan Plateau environment and how variables like weather and precipitation are behaving, in chapter three, we are going from generals to specifics with an overview of the glaciers of the chosen area. This Chapter is complemented with terminology that will be used through the development of this work.

Chapter four deals with the general explanation of the multi-temporal imagery used in this study and why the particular images were chosen.

The chapter five explains in detail the methodology used to get the outlines from the different years and also the results obtained afterwards. Chapter six explains the procedures flowed to calculate uncertainty for the results showed in chapter seven.

Chapter seven shows the results. A conclusion of the results is given in chapter eight, followed by the discussion in chapter nine. Finally the outlook in chapter 10 that shows suggestions to complement this job with further procedures and analyses taking more variables into consideration.

2 Study Region

2.1 General Description

The study area is situated between the south-west of the autonomous region in China known as Tibet or Shigatse (Xizang) and north-east of the region of Bagmati in Nepal, located in a succession of glaciers on the Himalayan mountains. The extreme coordinates, according to Google Earth, of this zone are: 85°13'1.82"E, 28°45'57.09"N and 85°56'6.76"E, 28° 4'41.19"N. (Fig. 1)

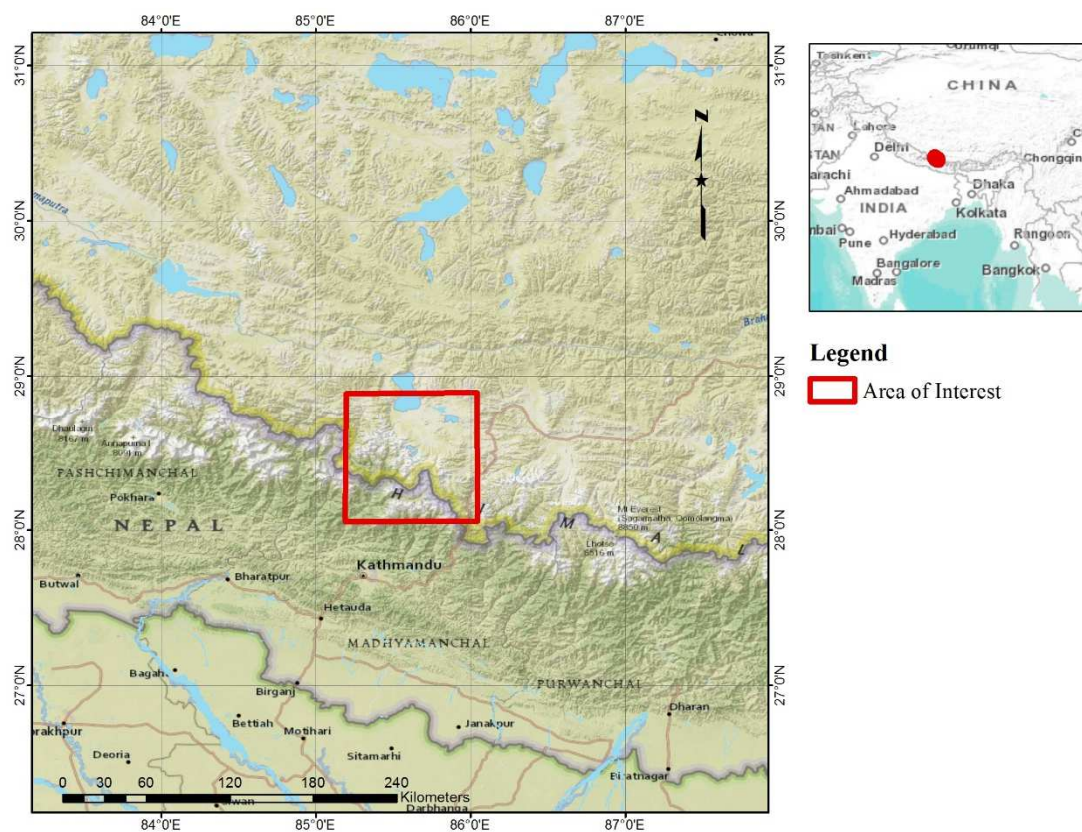


Figure 1. Localization of the area of interest. (Personal compilation based on the raster layers: World Terrain Base, National Geographic World Map (Esri, 2014).

Since the area of interest lies within the Himalayas, the landscape is characterized by the rugged terrain with mountain heights, taken from the SRTM, ranging from 624 to 7,975 meters above sea level. The fluctuation between the minimum and maximum altitude is more than 7,000 meters. This compares with information provided by the China Internet Information Center which states that the average elevation is 6000 meters (Center, n.d.).

More specifically the area is located in the Mont Qomolangma-Xixabangma, on the Himalayas. This zone has its boundaries on West in the basin of Gyirong-Woma, East in Paiku Lake basin, on the North, shares border with the basin of Penqu river and in the South with Gyirong Zangbo-Trisuli river, the Boqu - Bhote Kosi, Dudh Kosi (Zheng, 1988).

This study area is the result of the subduction between the Indian plate northward beneath the Eurasian Plate, (Ch'ang, Zheng, & Pan, 1977 in Zheng, 1988).

The differences in this area between the northern and southern slopes are clearly shown. In geomorphological terms, there is a huge distinction between the settings that harmonize in this landscape: from wide valleys and basins on the one hand to high mountains and deep valleys on the other hand (Zheng, 1988)

2.2 Climate

The strong insolar radiation is a characteristic of the Tibetan Plateau that produces winters with warm mornings but harsh temperatures at night. The extreme temperature oscillations occurring during the day are the result of low atmospheric pressure as well as relative low oxygen in the air (Center, n.d.).

The TP has considerable differences in altitude. The temperature variations are according to the region, for example, in the north and west regions, the mean temperature from October to April is 0° C, on the other hand, in Brahmaputra River basin, where the altitude is lower than 4,000 m, the cold season could last 2-3 months but during the summer, the average temperature is below 18° with a predominantly wet and cool weather. Changes in temperature according to altitude are not exclusive of this measure, also the precipitation presents differences. From the southeast to northwest precipitation gradually decreases. An annual precipitation of 1,000 mm or more is registered in the south of the Himalayas whereas in the rain shadow, located between the northern Himalayan footlands and the Brahmaputra River, the annual precipitation can reach less than 300 mm (Yu, 2010).

To complementing this section, a Climate Project in ArcGIS© was created using information from the “WorldClim- Global Climate Data” as input data. A brief explanation about the origin of this data is given in the section 4.6.

Even when some studies (Liu and Chen, 2000) and (Yao et al., 2012) have shown that the temperature in the TP have been increasing since the 1950s, the data used for the creation of the maps actually corresponds to that period 1950-2000, since the aim of this Climate Project created is *ex professo* to show a general view of the temperature and the precipitation of the study area.

The imagery used for the development of this thesis are from April and November. Therefore, the raster climate layers selected for the Climate Project correspond to these months.

Figure 2 shows the mean temperature for November. The study area presents temperatures that range from -24.7° to -3°C . It could be seen that in the whole area of Tibet, the temperatures correspond, by contrast however crossing the Himalayas, temperatures in Nepal, range from 6.5 to 26.1°C . The Himalayas act as a barrier stopping the escape of the cold winds.

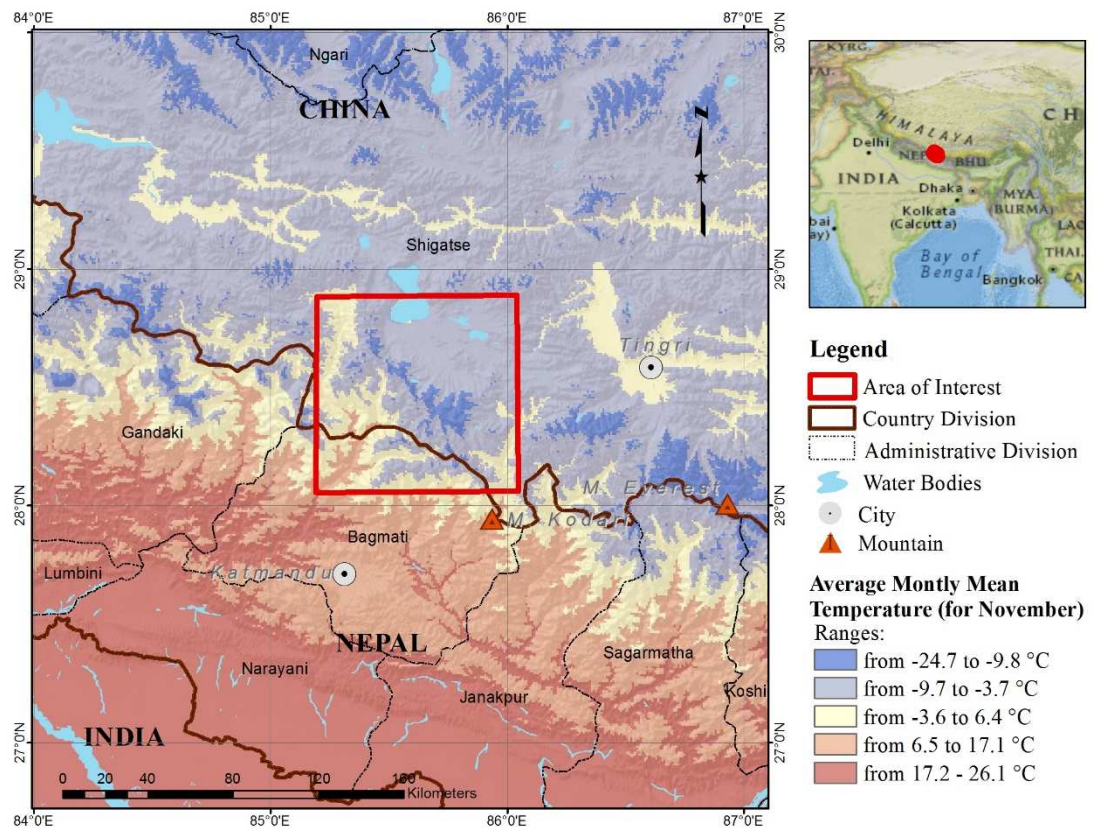


Figure 2. Average Monthly Mean Temperature for November (Personal compilation based on the raster layers: World Terrain Base, National Geographic World Map (Esri, 2014) and Global Climate data (Hijmans, Cameron and Parra, n.d.). The vector files were taken form DIVA-GIS (Hijmans, n.d.).

The temperature in April increases but not considerably. For the same area we can find temperatures from -21.9 to 3.7°C (see Fig.3). The Nepalese side can reach temperatures of 33.2°C , while the Tibet maintains low temperatures.

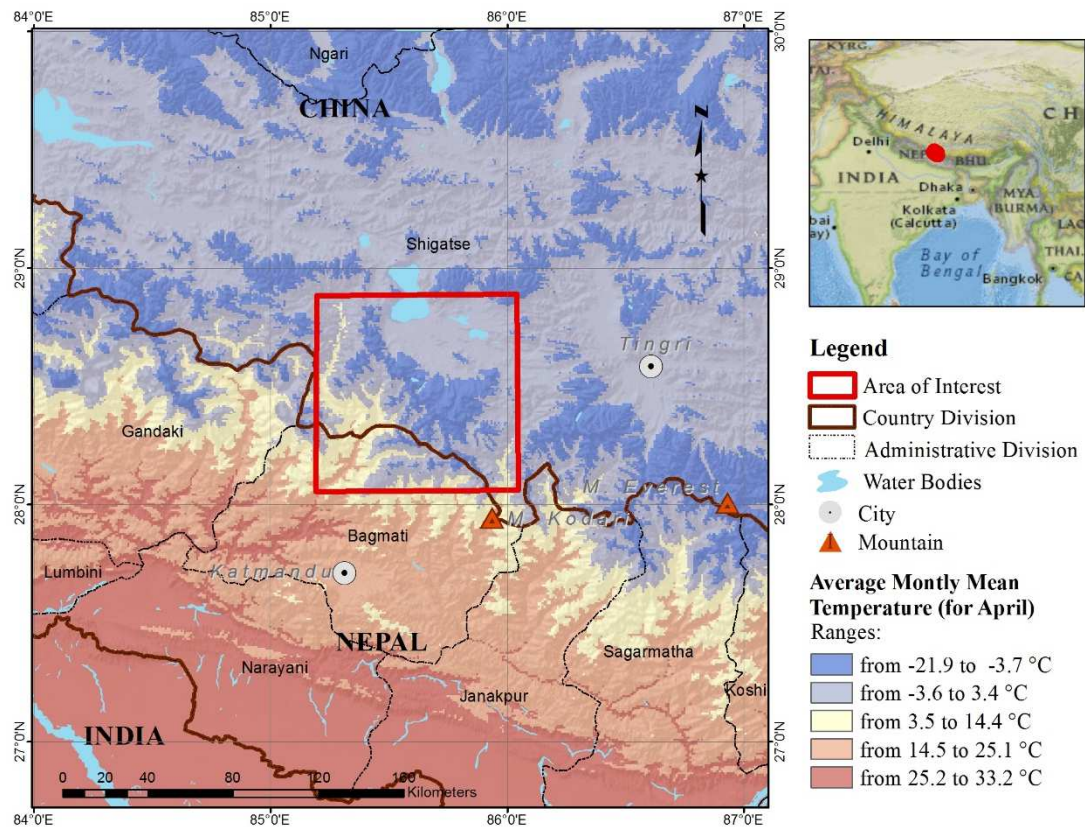


Figure 3. Average Monthly Mean Temperature for April (Personal compilation based on the raster layers: World Terrain Base, National Geographic World Map (Esri, 2014) and Global Climate data (Hijmans, Cameron and Parra, n.d.). The vector files were taken from DIVA-GIS (Hijmans, n.d.).

The precipitation in the area during November reaches amounts ranging from 1.1-3 mm (Fig. 4) meanwhile in April it reaches almost 13 mm (Fig. 5). The region in China

Shigatse or Tibet, holds a low amount of rain compared with the Nepalese region of Bagmati where quantities of 575 mm are reached during this month.

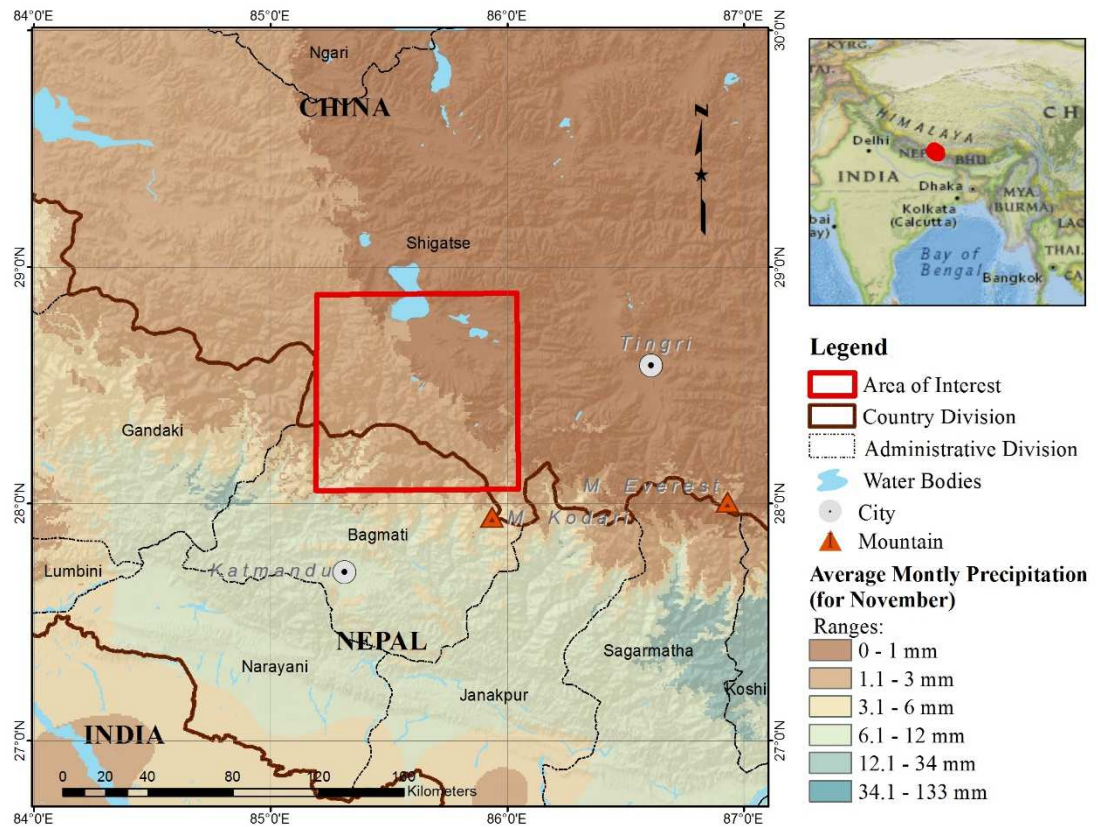


Figure 4. Average Monthly Mean Precipitation for November (Personal compilation based on the raster layers: World Terrain Base, National Geographic World Map (Esri, 2014) and Global Climate data (Hijmans, Cameron and Parra, n.d.). The vector files were taken from DIVA-GIS (Hijmans, n.d.).

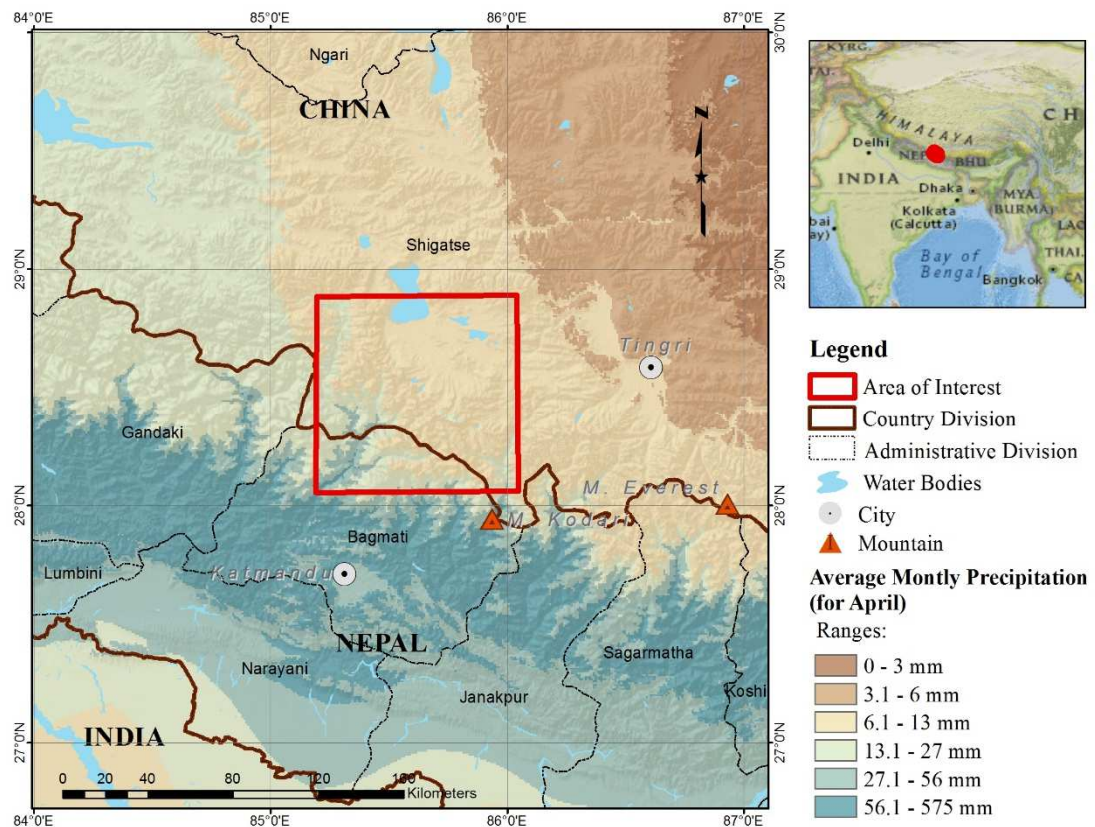


Figure 5. Average Monthly Mean Precipitation for April (Personal compilation based on the raster layers: World Terrain Base, National Geographic World Map (Esri, 2014) and Global Climate data (Hijmans, Cameron and Parra, n.d.). The vector files were taken from DIVA-GIS (Hijmans, n.d.).

3 Glaciers

3.1 An overview of the glaciers of the chosen area.

One of the largest ice masses on the planet is located in the Tibetan Plateau and surrounding mountains. Because of the huge amount of surface covered by glaciers in that region, the name “Third Pole” was given by the scientific community. The glacier coverage is about 100,000 km² and is prone to be affected by global warming changes (Yao et al., 2012).

The glacier progress in this region is impacted by the uplift of the Himalayan Mountains, particularly in Qinghai-Xizang. In the Quaternary period, this tectonic movement imprinted shapes to the terrain, determining the conditions for the development of glaciers and also influencing the zone with different kinds of climates, fluctuations and atmospheric movements from the Tibetan Plateau to its surroundings. During the

late Pleistocene, this uplift continued in the Qinghai-Xizang achieving up to 4,000 m a.s.l. and in the Himalayas up to 6,000 m a.s.l. This rise in the terrain not only brought a change in the precipitation's behavior but also a decrease of glaciers. This situation shows that the increasing elevation of the Himalayas is affecting the proliferation of the glaciers because mountains are acting as a barrier impeding the pass of the monsoon. Nowadays, most of the Indian monsoon precipitation occurs as rainfall over 1000 meters above the sea level nevertheless it changes to vapor form in heights about 6,000 m a.s.l. This movement in the Himalayas is also provoking the distance between first and second precipitation belts to increase and therefore the amount of rain in the second belt will be reduced (Zheng, 1988).

Elevation increase is not the only factor that contributes to glacier shrinkage, also global warming has been shown to have a huge influence on the glacier (Liu & Chen, 2000 and Yu, 2010). The increasing water level of the lakes in the zone confirms that the melted ice glacier is contributing to the water level rise. The intensification of the precipitation on the Tibetan Plateau Interior (TPI) product of the climate change can also be related with lake level rise (Lei et al., 2014). The topography and the climate are strongly related to accumulation and ablation and the interaction of these two process over the size and shape of the glaciers. How much a glacier decreases is not only dependent on the variation of temperature or climatic change but also topology will influence the reduction across the ice mass (Pellikka and Rees, 2009).

3.2 Glacier terminology

Glaciers are formed when in the course of one year, more snow was accumulated than melted or in other terms, when the accumulation exceeds ablation (Pellikka and Rees, 2009).

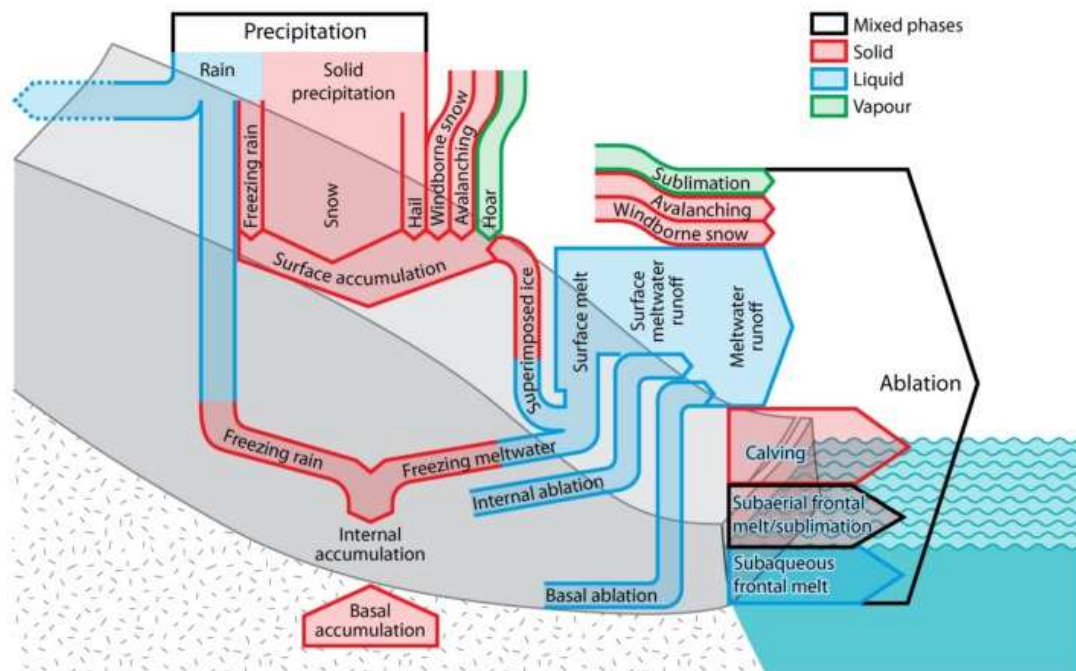


Figure 6. Components of the mass balance of a glacier. The arrows have arbitrary widths and do not indicate physical pathways of mass transfer (Cogley et al., 2011).

After the summer season, if there is enough snow left, this snow will consolidate as ice, it will grow and once the consistency of the ice gets dense enough because of its own weight, the resulting pressure may cause deformations on the glacier at depth (Pellikka and Rees, 2009). Because of this behavior and viscosity behavior, the glacier will start flowing down to lower heights following forces caused by acceleration due to gravity and the angle of slope (Nye, 1952). The figure 6 shows components and general behavior of the glacier.

Ablation this is the opposite of accumulation, the result of it will be reflected on the loss of ice from the glacier system. This decrease is caused by melting, sublimation, evaporation, ice loss by avalanches or calving (Pellikka and Rees, 2009), (Phillips, 2013).

Accumulation occurs when several process like snowfall, precipitation, avalanches, firnification or even snow in the wind, favor the addition of snow the glacier system (Pellikka and Rees, 2009), (Phillips, 2013).

Calving is when the terminus or the snout of the glacier is breaking off of ice into an ocean or lake (Pellikka and Rees, 2009), (Phillips, 2013).

Crevasse happens as a response of the stress caused by the movement of the glacier resulting in one or many cracks on the surface. It is important to mention that the orientation of the crack will be with respect of the glacier flow. (Phillips, 2013), (Cogley et al., 2011).

Cryosphere it is characterized by the existence of water in its solid form in a permanently way because of the lastingness of below zero temperatures. Typical landscape includes snow, floating ice, glaciers, ice caps, and permafrost (perennially frozen ground) (Cryosphere Glossary, 2014).

Debris-covered glacier is the trace of rocks, detritus or dust in different sizes that are deposited on the ablation zone (Cogley et al., 2011).

Equilibrium-line altitude (ELA) is the averaged altitude of the equilibrium line (Cogley et al., 2011). This is one of the most important factors to take into account because it separates the ablation from the accumulation zone (Braithwaite and Raper, 2009).

Firn is a step between snow and glacier ice. In no more than a year, the snow has been compressed in such a way that there is no more pores between the flakes or crystal that composes it (Phillips, 2013).

Flowline is the horizontal velocity vector that traces the glaciers from its highest to its lowest part (Cogley et al., 2011).

Glacier Flow is the movement of the glacier caused by the gravity's force in a descending direction (Phillips, 2013).

Iceberg is the result of a calving process as a block of ice floating in water (Phillips, 2013).

Ice-Dammed Lake happens when melted water cannot continue its course because it has being blocked by a valley or an ice dam (Phillips, 2013).

Moraine is a general term for unstratified and unsorted deposits of sediment that form through the direct action of, or contact with, glacier ice. Many different varieties are recognized on the basis of their position with respect to a glacier (Phillips, 2013).

4 Data

This work is the fruit of combining multiple data sources in order to fulfil the main objective of this thesis that is to find out how much the glaciers have shrunk during 36 years.

Multi-temporal data from sensors such as Landsat, HEXAGON and ALOS were used for remote sensing purposes. ASTER DEM and SRTM were used not only for imagery orthorectification but also for analysis including flow accumulation, used to determine the direction of the glacier flux. To complement the climate information, free downloadable data from the WorldClim web page was used.

More detailed information about the origin and how the data was used is provided in the next subsections.

4.1 HEXAGON KH-9 images

HEXAGON was the last of a three satellites constellation: “CORONA, GAMBIT and HEXAGON”, that were part of a surveillance program created by the United States during the Cold War (NGA, 2014), (Space, 2014). The obtained images were brought back to the earth as a photographic film by recovery vehicles (NGA, 2014).

The approval of HEXAGON took more than estimated because it cost more than twice what it was expected to be, as a result of the camera innovations that were added. Finally, it was in orbit on 15th June 1971 (Burnett, 2012).

The success of HEXAGON was reflected by the 12 successful missions where almost 30,000 terrain frames were taken (see Table 1) (Burnett, 2012).

Given the sensitive nature of the program, the images remained in the category of classified until 2002 when “The National Archives and Records Administration published the unrestricted availability to the 48,000 images taken from two significant satellite surveillance programs (KH-7 and KH-9)” (Archives, 2002) .

Table 1. Mission Statistics of HEXAGON Program (Burnett, 2012)

Mission	1205	1206	1207	1208	1209	1210	1211	1212	1213	1214	1215	1216	
Launch date	9-Mar-1973	13-Jul-1973	10-Nov-1973	10-Apr-1974	29-Oct-1974	8-Jun-1975	4-Dec-1975	8-July-1976	27-Jun-1977	16-Mar-1978	16-Mar-1979	18-Jun-1980	
Recovery date	20-Apr-1973	24-Aug-1973	7-Jan-1974	9-Jun-1974	27-Dec-1974	30-Jul-1975	2-Feb-1976	8-Sep-1976	17-Oct-1977	11-Jul-1978	12-Jul-1979	14-Oct-1980	
Days of operation	42	43	58	60	59	52	60	62	112	117	118	118	
Operational Summary													
Operates	141	153	148	200	167	198	202	279	252	386	488	529	
Terrain frames	2,026	2,118	2,145	2,120	2,077	2,090	2,066	2,090	2,109	3,144	3,947	3,840	
Terrain footage	3,245	3,393	3,442	3,402	3,333	3,354	3,316	3,354	3,385	5,046	6,335	6,163	
Terrain film type	3,400	----- ---	----- ---	----- ---	3,414	----- ---	----- ---	----- ---	----- ---	----- ---	1,414	SO-315	SO-315

Table one shows the statistics of the missions that were realized by the different launches during the project. The HEXAGON image used for this project is the “DZB1209-500101L007001” corresponding to the mission 1209 shown in bold font in table one. The acquisition date of the image corresponds to the 23th November 1974 with a format type black and white.

The satellite carried two panoramic cameras that were able to produce high quality stereoscopic images. The resolution that could be obtained at Nadir was 2.7 feet or higher. Table two shows characteristics about the cameras used for the program (Burnett, 2012).

Table 2. Characteristics of search/surveillance system Cameras (Burnett, 2012)

Optics	60-in. focal length, f/3 folded Wright (modified Schmidt) system (T 3.4 excluding filter factor)
Aperture diameter	20 in.
Field angle	$\pm 2.85^\circ$
Slit width range	0.91 in. (maximum); 0.08 in. (minimum)
Film	6.6-in.-wide (B&W) Type 1414 or SO-208 and others; currently SO-315. Also, 80-130 (infrared color) and SO-255 (natural color).
Resolution (2: 1 contrast)	Center of format ≥ 200 l/mm; Elsewhere in format ≥ 160 l/mm
Film. Load	Currently (1982) 155,000 ft. (per camera) mixed load of SO-315 and color. Total weight = 2,000 lb.
Film stack diameter Scan	68 in.
Scan modes	30° , 60° , 90° and 120°
Center of scan	0° , $\pm 15^\circ$, $\pm 30^\circ$, $\pm 45^\circ$
Maximum scan angle	$\pm 60^\circ$
Stereo convergence angle	20°
Frame format (120° scan)	6-in. By 125-in.
Film velocity	200 in./sec (maximum) at focal plane
Image motion compensation range	0.018 rad/sec to 0.054 rad/sec for V_x/H (orbital angular rate in-track) ± 0.0033 rad/sec for V_y/H (orbital angular rate cross-track)
Weight (less film)	5,375

4.2 Landsat Images

Landsat images are the result of the program managed through a series of Earth observation satellites with the same name. It was developed in the United States by the NASA and USGS and successfully operating since 1972 (USGS, 2013), (Lauer, Morain and Salomonson, 1997).

Thanks to this program, imagery has been obtained regularly and has helped for a better understanding of the earth in domains such as geology, agriculture and land surveying, providing the scientist with a clear panorama of how ecosystems and land process work (Lauer, Morain and Salomonson, 1997).

4.2.1 Landsat 5 (TM)

Landsat Thematic Mapper was launched on 1st March 1984 by NASA. This satellite was expected to have a 3-year life span but it exceeded that by orbiting for almost 29 years. In December 2012, it was turned off when one of the satellite's three gyroscopes stopped functioning (NASA, 2014)

Landsat TM images are composed of seven bands (see Table 3). Spatial resolution for the thermal infrared band is 120 meters, but is resampled to 30 meters. Each scene covers approximately 170 km (North-South) by 183 km (East-West) (USGS, 2013)

Table 3 Band designations for Landsat 5 TM satellite (USGS, 2013)

Mapper (TM)	Landsat 4-5	Wavelength (micrometers)	Resolution (meters)
	Band 1	0.45-0.52	30
	Band 2	0.52-0.60	30
	Band 3	0.63-0.69	30
	Band 4	0.76-0.90	30
	Band 5	1.55-1.75	30
	Band 6	10.40-12.50	120* (30)
	Band 7	2.08-2.35	30

4.2.2 Landsat 7 (ETM+)

The Earth observing instrument on Landsat 7, the Enhanced Thematic Mapper Plus (ETM+), was launched on 15th April 1999 as part of the Earth Observation Mission (EOM) with the purpose of monitoring land cover (Goward et al., 2001), since this is the most accurately calibrated earth-observing satellite compared with measurements made on ground (NASA, 2014). This satellite continues to orbit but in May 2003 a hardware component failed which resulting in gaps of data in the images but with each image still retaining 75% of its data (NASA, 2014).

The progress made to the calibration and radiometry of this satellite symbolized a huge improvement monitoring the planet and for the comprehension of the earth's processes. Not only has this information benefitted the scientific community, but it has

also been useful for education, commercial and research purposes. This is because the satellite is able to capture seasonal information given the temporal resolution of 16 days (Goward et al., 2001).

Landsat ETM+ images are constituted by eight spectral bands with 30 m spatial resolution from bands 1 to 7. The eighth band is panchromatic and has 15 m spatial resolution. Band 6 is acquired at 60 m spatial resolution but resampled to 30 in products after 25th February 2010. The swath width is 170 km North-South by 183 km East-West. (See table 4)

Table 4 Band designations for Landsat 7 ETM+ satellite (USGS, 2013).

Enhanced Thematic Mapper Plus (ETM+)	Landsat 7	Wavelength (micrometers)	Resolution (meters)
	Band 1	0.45-0.52	30
	Band 2	0.52-0.60	30
	Band 3	0.63-0.69	30
	Band 4	0.77-0.90	30
	Band 5	1.55-1.75	30
	Band 6	10.40-12.50	60 * (30)
	Band 7	2.09-2.35	30
	Band 8	.52-.90	15

Both of the Landsat images that were used for this study correspond to level 1T. This level of correction is provided directly by the USGS. “The Level 1T (L1T) data product provides systematic radiometric accuracy, geometric accuracy by incorporating ground control points, while also employing a digital elevation model (DEM) for topographic accuracy. Geodetic accuracy of the product depends on the accuracy of the ground control points and the resolution of the DEM used.” (U.S. Department of the Interior, 2013)

For the base outlines, Landsat image (ETM+) level 1T from 2000 image was used. This image was obtained freely from the United States Geological Survey (USGS) webpage¹.

4.3 ALOS PRISM Images

ALOS is a Japanese satellite designed for mapping and earth monitoring. This satellite has three sensors: PRISM that handles the panchromatic stereo pair for precision mapping, AVNIR-2 for land cover observation and the PALSAR or Phased Array “L” band SAR (Synthetic Aperture Radar). This satellite was launched on 24th January 2006 and since then it has been useful for monitoring natural disasters and human activities like agriculture. Communication with the satellite stopped on 22nd April 2011 due to power issues (JAXA, 2001)

4.4 SRTM

The version of SRTM used for this project was the Void-Filled NASA. This void-filled version of the Shuttle Radar Topography Mission digital elevation model, known as "SRTM Plus", was produced under the "Making Earth System Data Records for Use in Research Environments" (MEaSUREs) Program. To void fill or correct gaps in elevation that this data could have, the ASTER GDEM2 (Global Digital Elevation Model Version 2) was used in addition to the GMTED2010 elevation model (compiled by the USGS).

This information and also other products can be found free to download in NASA's Land Processes Distributed Active Archive Center (LPDAAC) webpage².

This product is available with a spatial resolution of approximately 90 m (3 arc- seconds). It is expected to release information at 1-arc-second (about 30-meter) pixel spacing to the rest of the regional SRTM data during 2014-2015. (Laboratory, 2014).

¹ <http://earthexplorer.usgs.gov/>

² https://lpdaac.usgs.gov/products/measures_products_table

4.5 ASTER GDEM V2

GDEM V2 is the product of an enhanced algorithm that provides better spatial resolution and increases the horizontal and vertical accuracy. This information was released on 17th October 2011 by Japan's Ministry of Economy, Trade and Industry (METI) in conjunction with the NASA (NASA, 2011).

Although this version is an improved version of the ASTER products, there are some issues that hamper using these data in some applications and the users are warned about this (NASA, 2011).

The information was freely downloaded in tiff format from the USGS web page³.

4.6 WorldClim- Global Climate Data.

This is climate data for ecological modelling and GIS, freely available online⁴. Among the available layers for free download are the mean, maximum air temperature and precipitation per month. This monthly information is the result of averaging data gathered from weather stations situated throughout the world. The spatial resolution of the layers is 30 arc seconds (ca.1 km) (Hijmans, Cameron and Parra, n.d.).

This information is the result of implementing the thin-plate smoothing spline algorithm over climatologic data available from different sources since 1950 to 2000. To quantify uncertainty, the following aspects were taken into account: the mapping weather station density, bias that might occur because of position of the weather station, the variation present on grid cells and through data partitioning and the cross validation. It was proved that these layers had better spatial resolution compared to previous climatological information because a higher amount of information was used and also because spatial patterns were taken into account for this project (Hijmans et al., 2005).

Since temperature and precipitation information were available per month and on a global scale, the chosen months to work with were November and April. The decision

³ <http://gdex.cr.usgs.gov/gdex/>

⁴ <http://www.worldclim.org/current>

was made based on the imagery available for this work: Landsat, ALOS and HEXAGON (see table 5). It was necessary to Clip⁵ the information to get layers adapted to the study area.

4.7 Global Land Ice Measurements from Space (GLIMS)

GLIMS started as a project allocated to monitor glaciers with satellite imagery (using ASTER). An international network of specialists was created to enrich the data and improve the results by having people with multiples backgrounds and knowledge. The results obtained by the joint group of experts included vector layers with the digitalization of the glaciers, snow lines, center flow lines, hypsometry, surface velocity fields and literature. The results are stored in the National Snow and Ice Data Center (NSIDC) (GLIMS, 2014).

5 Methodology and Workflow

This section endeavors to explain the adaptation of the multisource method for mapping supraglacial debris developed in 2004 (Paul, Huggel and Kääb, 2004), in order to determine the outlines of the glacier area of interest.

The aim of the following method was to optimize the time required to obtain the outlines from the Landsat image in a semi-automatic way. One of the important advantages of this process was to develop a way to consider the debris. This is based on the observation that debris accumulates in low slope angles. (Paul, Huggel and Kääb, 2004)

After image selection, the main steps of the mentioned method were to apply several image and geo-processing techniques to the images to gain new information and to choose a threshold that would reveal different results and allow comparisons made between them. In this method, a preliminary version of the outlines was achieved and subsequently modified manually.

⁵ Clip: “is a tool used to cut out a piece of one feature class using one or more of the features in another feature class as a cookie cutter” (ESRI, 2014).

5.1 Creating A Glacier Inventory Based on Landsat 2000

Selecting the best image for this task was quite challenging taking into account that images should be chosen in the summer season to avoid high concentrations of snow and also that the sequence of images should belong to the same months in order to compare them (Paul et al., 2009).

From the imagery available to accomplish this task (HEXAGON, Landsat ETM+, Landsat TM and ALOS), the 2000 Landsat ETM+ scene was selected as the starting point image to create the baselines because of 3 reasons: 1) the horizontal shift is nearly null (Bolch et al., 2010), 2) only one scene was needed to cover the whole area of interest (see fig. 7) and finally, the high standard of the terrain correction level that this image had originally, was used as the base to correct the rest.

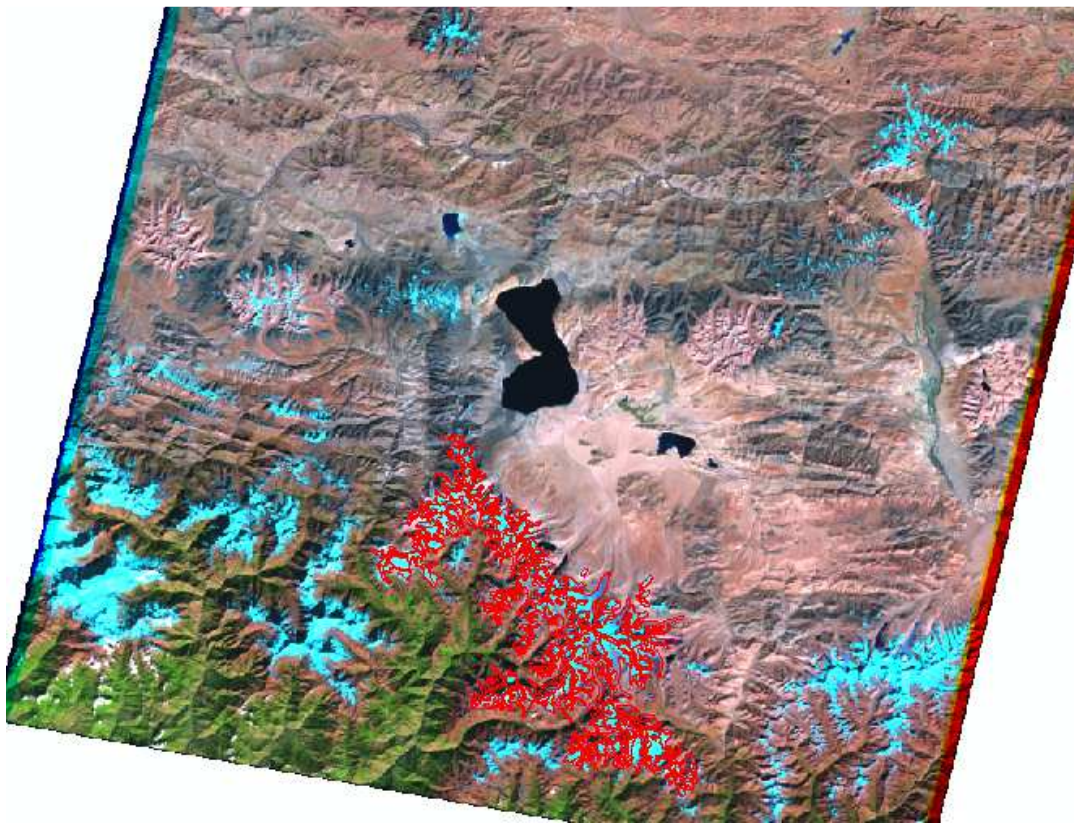


Figure 7. Landsat image 2000. In red the AOI.

5.1.1 Pre-processing (Semi-automatized Processing)

To automatically obtain the outlines, following the method developed by Paul, Huggel & Käab (2004), two models in ArcGIS© were created.

In the first model, four bands from Landsat ETM+ 3, 4, 5 and the panchromatic were taken and the SRTM was used in the development of the model. Bands 4 and 5 were used to get the ratio image that will be used to distinguish the glacier from no glacier in the image. The other viable combination to get a similar result could have been the ETM3/ETM5 ratio, but after trying both options, ETM4/ETM5 was chosen because it proved to give better results for this particular case. Snow and ice present a low reflectivity and thus the chosen bands allow their easy detection with this ratio (Paul et al., 2002)

Bands 3 and 4 were used to calculate the Normalized Difference Vegetation Index (NDVI) using this result to detect pixels that might be incorrectly classified from the previous ratio ETM4/ETM5. At the same time, an RGB layer was created using the bands 3, 4 and 5. It was needed to create a Pan Sharpening⁶ image and afterwards apply Principal Components Analysis⁷ to generate a single multiband raster which was then resampled again to have the corresponding pixel size with the rest of the layers. According to the followed method, a threshold of 126 was applied over this raster layer to detect glacier and no glacier and eventually debris from no debris. Several thresholds were tested and ultimately, 126 demonstrated the best results.

Queries developed on the SRTM were used to define where the debris tends to localize according to the slope. Debris are usually found on 0-24° slopes (Paul, Huggel and Käab, 2004), with other authors mentioning 0-10° (Pellikka and Rees, 2009) but since we are following the Paul, et al., (2004) method, their suggestions were followed. The other query applied over the SRTM had the purpose of isolating all the areas where

⁶ A Pan sharpening “produces a multiband raster layer with the resolution of the panchromatic raster where the two raster layers fully overlap” (ESRI, 2014).

⁷ Principal Components: “The value specified for the number of principal components determines the number of principal component bands in the output multiband raster. The number must not be larger than the total number of raster bands in the input” (ESRI, 2014).

the slope inclination exceeded 45° due to gravity force in a steep plane increasing the friction between the body (snow in this case) and the surface impeding the stability of it. The more mass that steep slope gets, the more unstable it becomes (de Blasio, 2011). Slopes with more than 45° are not able to sustain masses of ice and subsequently the snow ends up in gentler slopes where the accumulation process begins (Paul, Huggel and Kääh, 2004). The resulting layer was used to remove all these steep areas from the glacier outlines.

In this first model, a raster product of the ratio between the band 4 and 5 was also created to distinguish ice from no ice. When pixels values are equal or greater than 1.7, they were classified as ice. Different thresholds were also tested for each one of the raster products of different ratios. Nevertheless in the majority of cases, the one suggested in the method fitted perfectly well, except for the ETM4/ETM5 one. In this case, a lower threshold than that published in other papers: 2.0 in Paul, et al., (2004) and 2.4 in Pan et al., (2012) was chosen. The fact that a lower threshold was needed could have been result of the lesser snow coverage in this image. This model was built with the purpose of fulfilling all the methodology described by Paul et al., (2002).

Once the model was run, the resulting layers were checked one by one to verify the results. All the results were visually similar, therefore only one layer was chosen to work with. The ratio ETM4/ETM5 was transformed from raster into vector layer and the rest of the other results were used as a backup to double check debris and vegetation cover.

The second model is a simpler one. It uses the ETM4/ETM5 ratio raster layers and performs a transform into a vector layer. The median filter with a 3x3 pixel window is normally applied in this procedure in order to avoid misclassification (Paul, Huggel and Kääh, 2004), (Bolch et al., 2010), however this system was insufficient to clean up the strong segmentation resulting from the raster to polygon transformation, therefore the mapped areas with a size less than 11 pixels were merged into the larger area that contained them. One pixel surface in Landsat represents 900 m^2 in surface terrain, 11 pixels equals 9900 m^2 , almost one hectare. That was the minimum mapping unit by Bolch, et al., (2010) used to clean up the segmentation of the polygon layer.

After running the Eliminate⁸ geo-processing tool, a Dissolve⁹ tool was applied in order to simplify the layer from thousands of polygons to two groups: the ice (value 2) or no ice (value 1). When these two groups were created, the polygons were smoothed (Smooth Polygon¹⁰) to avoid the square edges product of the transformation from raster to polygon (see fig. 8). This was the layer used to manually modify and adapt it to the Landsat image.

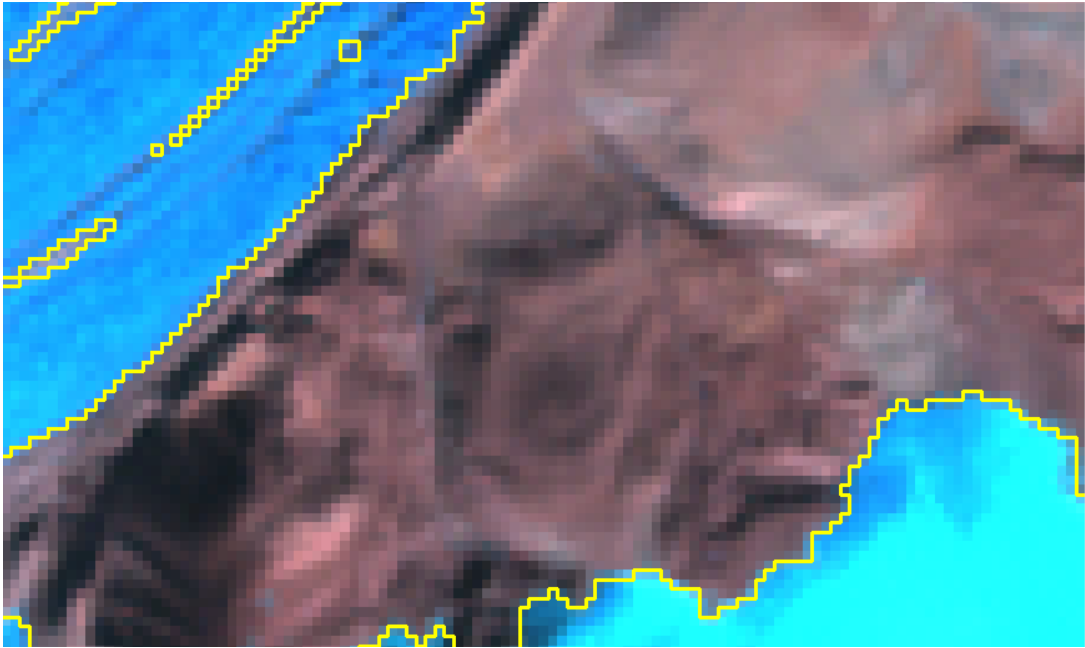


Figure 8. The yellow line shows the edges of the vector layer coincided with the pixel size after the raster-vector transformation

The semi algorithm used to smooth the polygon was the PAEK (Polynomial Approximation with Exponential Kernel) with a 500 m tolerance. Several options were tested as a tolerance, this one proved to be the most suitable for a good result to see different approaches (see fig 9). That was the last geoprocessing operation applied to the data in order to produce outlines semi-automatically.

⁸ “Eliminates polygons by merging them with neighboring polygons that have the largest area or the longest shared border” (ESRI, 2014).

⁹ Dissolve “reduces the number of features in the output when the original processing divided and processed the inputs using adaptive tiling” (ESRI, 2014).

¹⁰ “Smooth sharp angles in polygon outlines to improve aesthetic or cartographic quality” (ESRI, 2014).

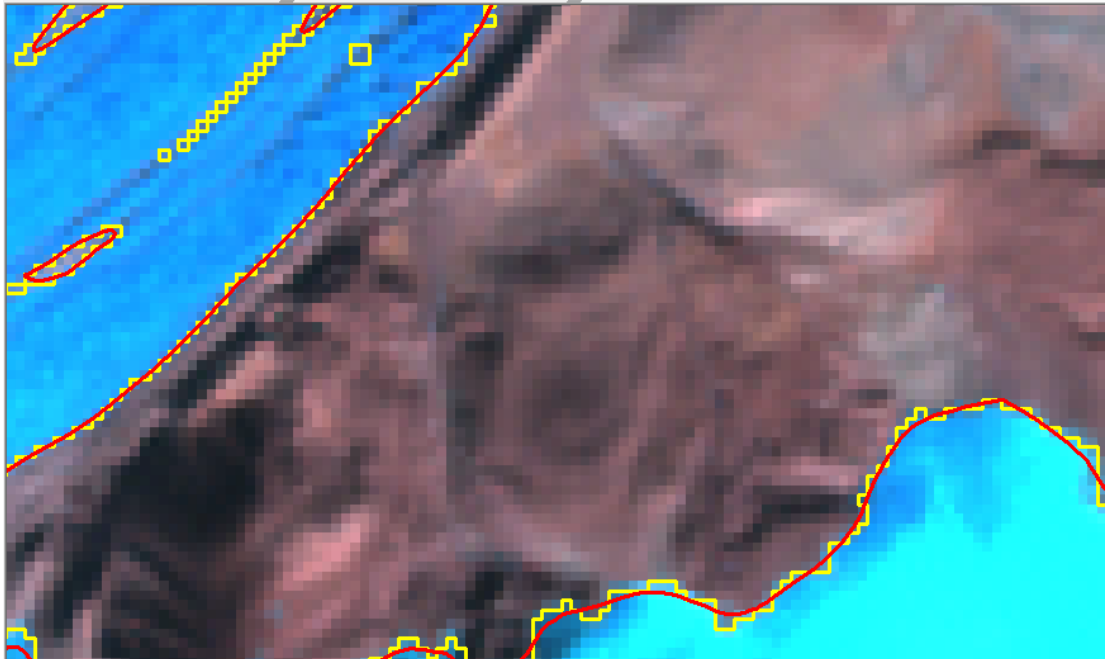


Figure 9. The yellow line shows the original shape edge of the outlines after raster-vector transformation. The red line represents the edges result after smoothing the vector layer.

5.1.2 Post-processing (Manual Editing)

Thus far, the semi-automatized method has differentiated ice from no ice in the image and excluded most of the debris coverage. Some of the products of the model were useful as a validation/cross reference, nevertheless, manual editing was necessary to adapt the resultant layers and take into account the debris as a part of the glacier (See fig. 10).

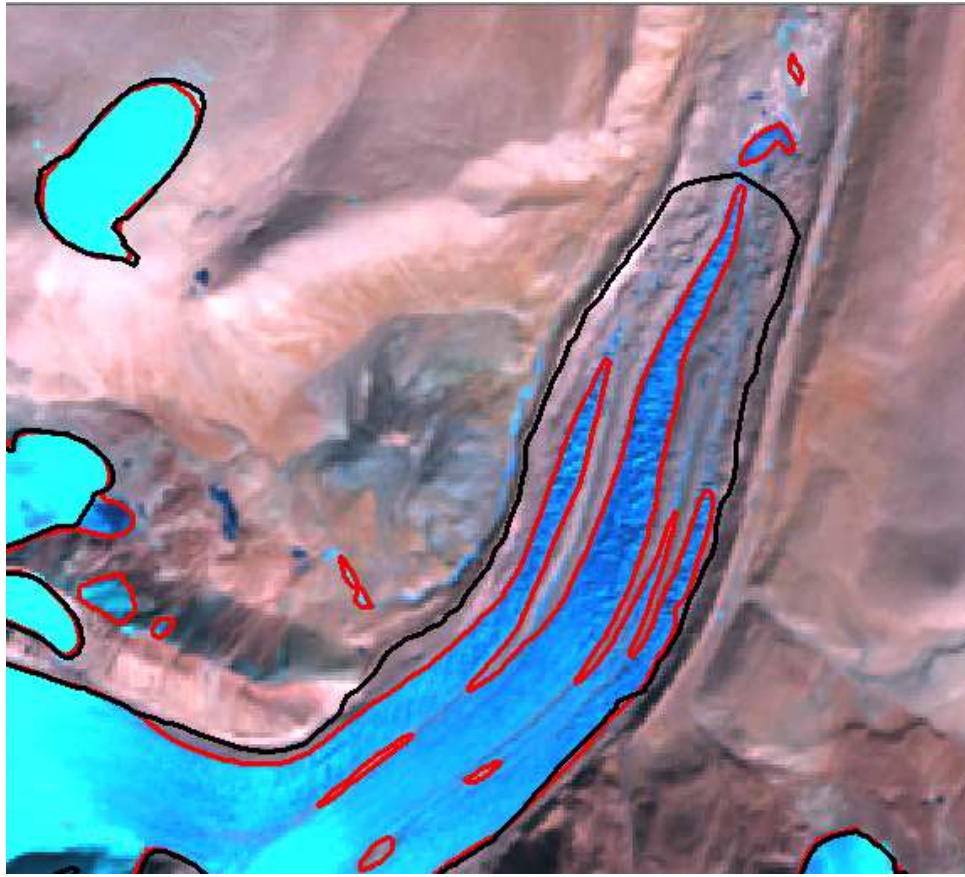


Figure 10. The red line represents the result of the vector layer after the semi-automatized process. The black line is the result of manual edition using the Landsat ETM+ 2000 as base image.

As a first approximation to obtain the ridges of the study area and separate the glaciers individually depending on their flux direction and based upon their constitution, ASTER GDEM V2 was used as the main data source due to its level of accuracy. To find the watersheds, the process performed was a protocol that included: Fill Sinks, Flow Direction, Flow Accumulation, and finally Watershed (Villegas Yepes, 2011). All these tools can be found in the Spatial Analyst Module in the Hydrology Package from ArcGIS©.

Once the ridges were attained, they were added to the outlines vector. Manual editing was necessary to confirm and to adapt not only the outlines but also the watersheds in the most accurate possible way close to reality. In some situations, there was uncertainty of where the border between glaciers might be. A solution was to use Google Earth™ with its 3D option to cross check the terrain and validate the outlines. Also a

hill-shaded relief was created using the SRTM in order to aid the identification of terrain by the effect of illumination. This layer gave a sense of proportion and third dimension over the area of interest in order to facilitate visualization of the surface.

5.2 Adaptation of Glacier Outlines Based on Landsat and ALOS 2010

After obtaining the Year 2000 outlines, the second period that was chosen to process was 2010. It was easier to keep the workflow over images that were terrain corrected and fitted well geometrically.

5.2.1 Landsat Image Selection

The ALOS imagery was purchased by GAF AG¹¹ from JAXA and processed by the Institute of Cartography at Dresden University of Technology. The ALOS imagery and the DEM product of the three scenes were processed by Nikolakakou (2014).

Since the ALOS image does not cover the entire study area, it was necessary to obtain an extra image to complete the necessary spatial coverage in order to adapt the outlines from 2000 to 2010 (see fig.11). The selected image to resolve this deficiency was a Landsat TM. The acquisition date and image specifications can be found in Table 5.

¹¹ Arnulfstr.197 D-80634 Munich – Germany. <http://www.gaf.de/>

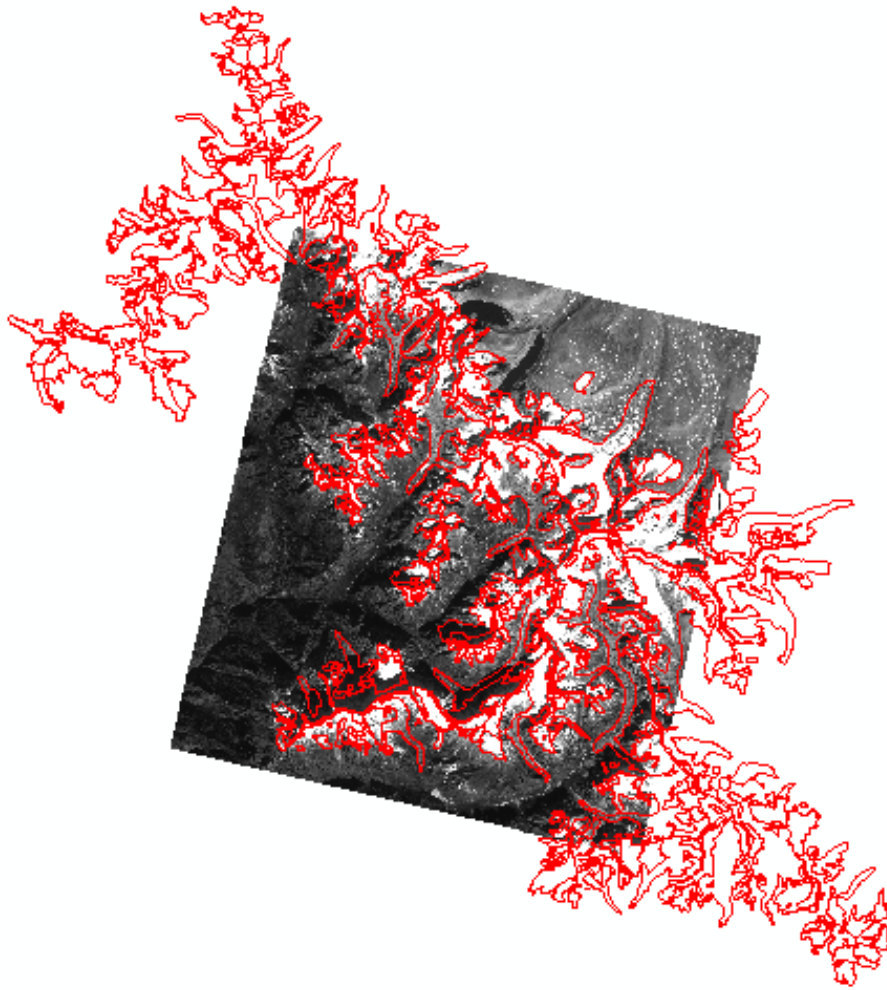


Figure 11. Representation of ALOS image coverage over the AOI. The outlines are shown in red.

Three options were found that could fit the gap in data coverage in the area of interest for 2010 from January, March and April. The Landsat image that was best suited with less than 27% cloud coverage and seasonality feasibility was from April. Some issues with clouds were nevertheless found in the south eastern part of the area but it was manageable.

Table 5. Overall information of imagery used for the project.

Date	Satellite and Sensor	Path/Row or ID	Spatial Resolution	Spectral Bands	Source	Suitability of Scene	Utilization
23-Nov-1974	Hexagon KH-9 (Mission 1209)	DZB1209-500101L007001		Panchromatic	USGS	one schen for the whole area	Outlines adaptation
22-Nov-2000	Landsat ETM (1T)	141/40	15-30 m	panchromatic multispectral thermal	USGS	one schen for the whole area	Base Outlines
03-Dec-2010	Alos PRISM	ALPSMB258793085 ALPSMN258793030 ALPSMF258792975	2.5m (at Nadir)	Panchromatic		the scene covered a part of the area	Outlines adaptation
16-Apr-2010	Landsat TM (1T)	141/40	15-30 m	panchromatic multispectral thermal	USGS	one schen for the whole area	Outlines adaptation
	SRTM		90 m	Elevation		one schen for the whole area	Ortorectification
	DEM ASTER		30 m	Elevation		one schen for the whole area	Flow detection

5.2.2 Manual Editing

The “2000” vector file corresponding to the 2000 outlines and the ridges was duplicated and renamed “2010” before beginning the manual editing. The software used to fulfill this procedure was ArcGIS© with the Editing tool. The part of the AOI that was covered by ALOS was then adapted to it, with a much better accuracy than the one with Landsat. In some cases, it was necessary to consult Google Earth™, in order to distinguish terrain issues like ridges, moraines or steep slopes that could not be detected either by an optical image or by the SRTM when the size of the pixel was inadequate. Any adaptations or modifications of the watersheds done in this layer were applied in the previous 2000 layer to maintain consistency.

5.3 Adaptation of Glacier Outlines Based on HEXAGON 1974

The glacier baselines from the 2000 were modified and adapted to the glacier conditions by superimposing them on the HEXAGON image. The digitalization and adaptation was performed manually (Granshaw and Fountain, 2006).

5.3.1 Image processing

The HEXAGON image was acquired for this work in raw format without any accompanying data to aid correction. It was therefore necessary to run more than one procedure over the image to get a result good enough to obtain a sufficient match with the Landsat images. This extra treatment of the HEXAGON image might be the result of the distortions suffered due to film damage received during years of storage (Surazakov and Aizen, 2010). ERDAS© was used for these procedures.

In order to reduce the size of the image, Surazakov (2010) suggests it should be degraded from the original 0.07 μm to 0.14 μm as. However, the software proved to perform very well with the original size so this step was skipped.

From the complete triplet set of images that were included in the HEXAGON package only one was considered because it covered the whole area (see fig. 12). The name of the image was “DZB1209-500101L007001_7_a”.

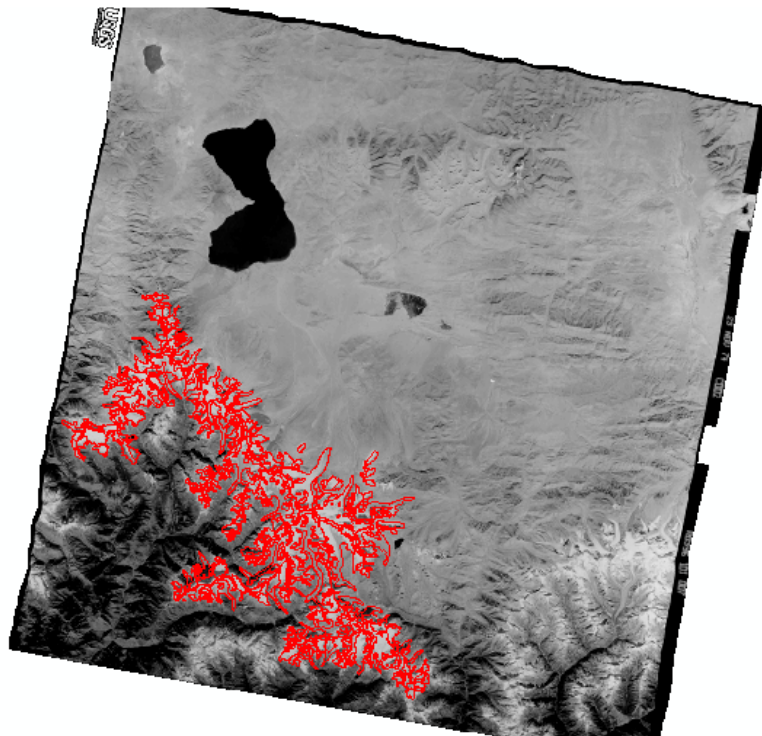


Figure 12. The black & white image corresponds to the chosen HEXAGON image to adapt outlines. In red, the AOI is shown.

The first attempt to orthorectify the image was to georeference it using the tool “Transform & Orthorectify” in the Control Points package from ERDAS® was used. For this procedure, a new project was created, setting Landsat ETM+ band 8 as the reference image, and HEXAGON as the input image. For the “Camera Model Properties” option, only the projection UTM Zone 45 North was defined, taking into account that the Landsat reference image originally came with this information. For the Elevation Datum, World Wide 15 min –Geoid (EGM96) was chosen.

After setting these preferences, the next step was to collect Ground Control Points (GCPs) using the panchromatic band (15 m spatial resolution) from Landsat ETM

2000 as a reference. The chosen GCPs must be distinguishable features of the terrain like lakes, rivers or cliffs (Stallmann et al., 2008). The procedure consisted of placing the points in the input image and then locating the same point in the reference image. After running the procedure, the image was georeferenced but the outlines presented a considerable displacement when they were displayed over the georeferenced image (see fig. 13), meaning the HEXAGON image did not fit geometrically with the Landsat image.

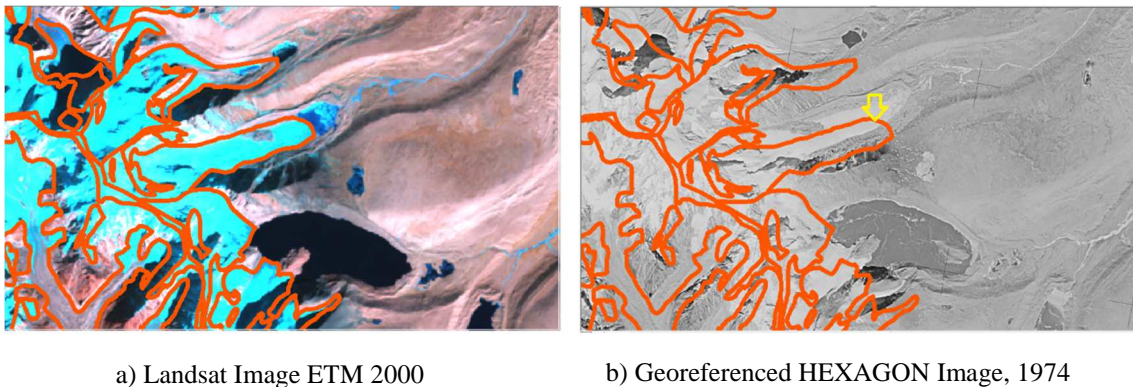


Figure 13. Fig 10a shows the outlines from 2000 fitting perfectly in the ETM image not the same case in the HEXAGON images, where the blue yellow arrow shows the displacement.

The second procedure performed was to orthorectify the georeferenced image using the SRTM as the elevation parameter required in this method.

The selected method was “AutoSync” from ERDAS®. This method was developed by ERDAS® creators and its main function is to georeference raw images by collecting tie points manually or completed automatically when the image is already georeferenced (ERDAS, 2008).

In this case, the attempt of using AutoSync with the raw HEXAGON image was made. However, the result, even after collecting tie points manually, was not as good as the one obtained after getting this image previously georeferenced using the GCP tool formerly mentioned. Therefore, the georeferenced image was used as an input for this tool.

Since the image was previously georeferenced, the steps to follow were simple and required creating a project, selecting an input and a reference image, defining an Automatic Point Measurement (APM) strategy (in this case default settings) and selecting

the geometric model. The geometric model used was a Direct Linear Transformation (DLT) using a DTM as a source, for instance the SRTM resampled to 30 meters. This geometrical model was chosen because DLT “is an excellent approximation for frame cameras, and when it is known that the data comes from a frame camera, this can be used this without knowing the specifics of the frame camera” (ERDAS, 2008).

The software collected automatically a total amount of 3,806 tie points, achieving a RMS of 1.83086. The results were satisfactory (see fig. 14) since there was a sufficient match between images in the terminus and most of the terrain of the features. There was however an issue at the mountain ridges. Those mismatching did not represented a problem since it was not pursued to obtain the DEM from the HEXAGON triplets.

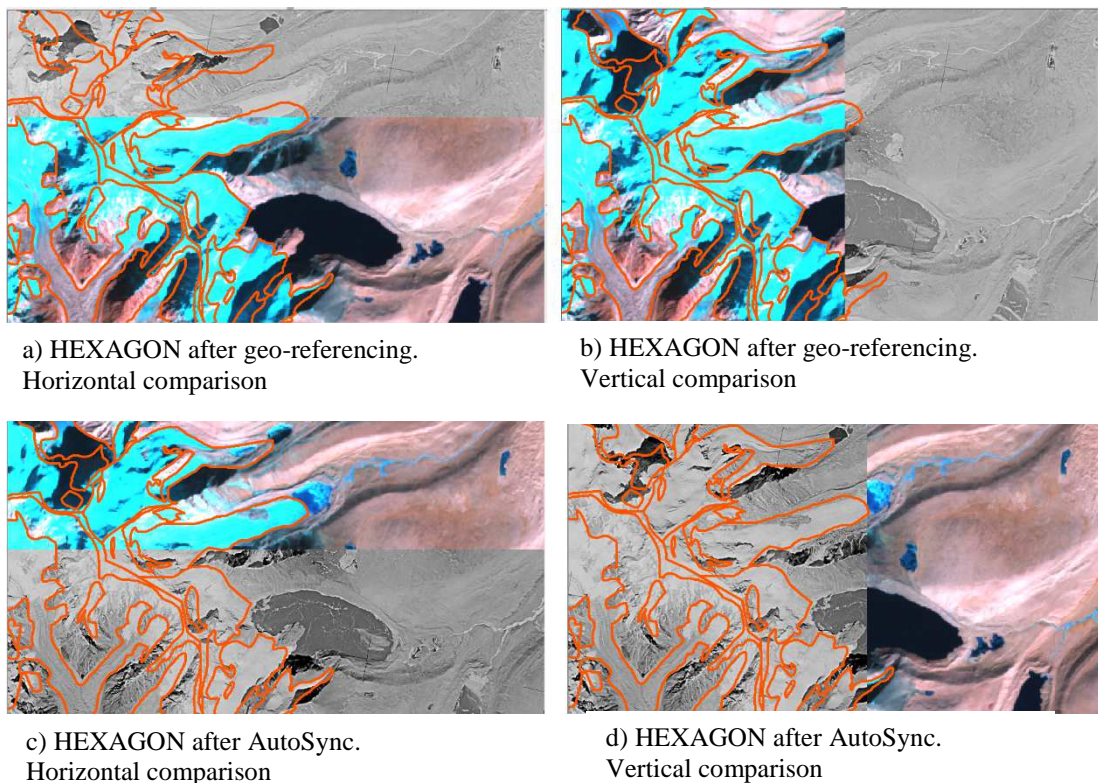


Figure 14. Comparison between the HEXAGON input image (black and white) with different levels of geo-correction and Landsat ETM (color), used as the reference image. The Outlines are shown in orange. Images “c” and “d” display the matching after using AytoSync Tool.

5.3.2 Manual Edition

Once the processing was complete and the image fitted sufficiently with the Landsat ETM+ (reference image) and the rest of the imagery (see fig. 14) the manual editing began. The glacier tongues and some terrain characteristics like lakes and rivers

showed an excellent match with each other, nevertheless the mountain ridges were erroneous. Since the watersheds were created and edited taking into account the Landsat images and SRTM, this HEXAGON's discrepancy presented on mountains was ignored to avoid any further ambiguities that could arise following further editing of the ridges. This error in the HEXAGON image was ignored because previous works note that HEXAGON images had a lower accuracy in mountainous terrain than in flat terrain, even after image processing (Surazakov and Aizen, 2010).

The "2000" outlines and ridges vector file was duplicated and renamed to "1974" and then manual editing began to adapt the outlines to the situation of glaciers present in this year.

5.4 Lengths and Areas of Glaciers

Once the three periods were obtained, these were meticulously checked to see that edges, ridges and the same amount of glaciers coincided in all the periods.

In order to improve the data management of the individual glaciers, each one was named according to their GLIMS¹² identity. The GLIMS ID, taken from the attribute table in the outlines vector layer, was used as a parameter to identify each one of the glaciers by name and to enable the results to be compared with the period to which they belonged. There were some cases where the glacier in the GLIMS catalogue appeared as one single glacier whereas in the digitalization, after identify the components of the glacier¹³, it was clear that there was not only one but two or more glaciers. In such cases, a compromise to split the sections and preserve the original GLIMS ID was attained by adding "a", "b" etc. to the GLIMS name so that the separate glaciers could be easily distinguished.

¹² GLIMS is described in section 4.7

¹³ Some glaciers shrank considerably, therefore one single glacier ended up with more than one snout. One glacier cannot have more than one tongue, thus, the glacier was automatically transformed from one to as many as the amount of terminus appeared (NSIDC, 2014).

5.4.1 Areas

When each one of the glaciers acquired its name from the GLIMS catalog, the calculation of the surface was automatically done by the software ArcGIS®.

The three vector layers containing the calculation of each year's surface area per glacier were joined to enable a comparison of each individual glacier's area and its change over the time periods.

5.4.2 Lengths

Considering that the ice under stress tends to behave like a liquid, there is a relationship between the rate of strain and shear stress. In glaciers, the state of stress is tri-axial with a hydrostatic pressure acting in the deepest part of the ice making this part prone to deformation. At a certain point, the pressure over the element is such that it is close to melting. In this circumstance, this element tends to flow down a uniform plane slope (Nye, 1952).

A glacier's shape is the result of climatic and topographic conditions, thus a glacier can have different kinds of geometry but the tendency will always be to move downhill (Le Bris and Paul, 2013). In glaciology, the measurement of the glacier's length is used to determine glacier dynamics (Purdie et al., 2014). This measurement is represented by a vector line. To determine this line, it is important to generate a flow line (Le Bris and Paul, 2013).

To create the flow lines, requirements must be fulfilled such as the lines must be within the glacier and avoid rock outcrops, since those are not considered as glacier, and finally, the lines must run through the center of the glacier (Le Bris and Paul, 2013).

To obtain the flow lines, it was extremely important that each of the glaciers was delineated as a one single unit (Winsvold, Andreassen and Kienholz, 2014). Based upon each one of the units and using a DEM as a height reference, ASTER GDEM V2 in this case, the centerlines were calculated. This methodology pursued to use the DEM to extract the flow direction by means of different tools with the intention of attaining the flow lines (Winsvold, Andreassen and Kienholz, 2014), (Le Bris and Paul, 2013), (Ender, 2011).

To performance this process, a model builder in ArcGIS© was created with the steps needed to develop the method previously mentioned and utilizing the hydrology tool set from ArcGIS©. The step by step flow chart of the method is outlined in figure 15. Firstly, the Fill tool is applied to remove any holes or areas of no data in the DEM. Then, the Flow Direction tool is added and the third step is to calculate the Flow Accumulation. Next, a raster calculation determines the hydrologic net according to a value defined by the user. A drainage network and the Strahler stream order is then created. The two resultant vector layers are subsequently smoothed to soften their edges after the raster to vector transformation (Pucha Cofrep, 2011). This same procedure was carried out using SRTM as the main source but after comparison, the results obtained from the ASTER GDEM V2 were evidently better, showing a more accurate and denser drainage network. Therefore it was decided to continue using the ASTER GDEM V2 with this procedure.

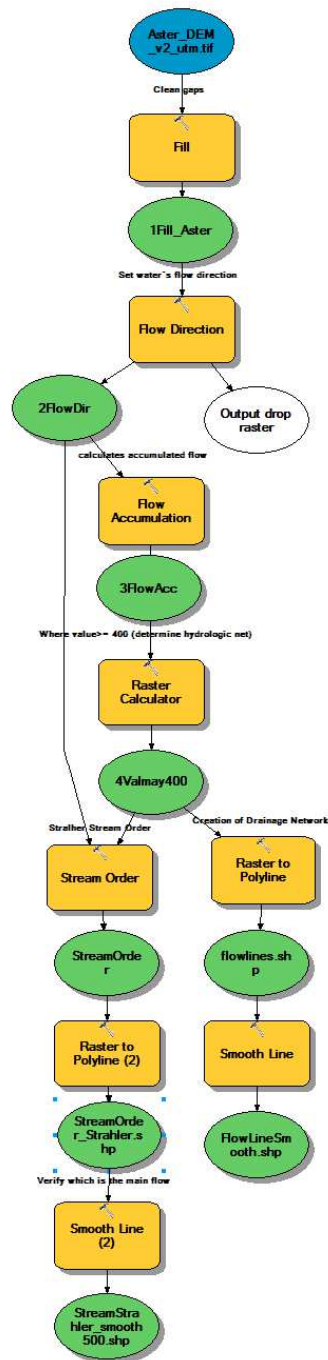


Figure 15. Flow chart of the model builder to get the flow lines.

With this conclusion and the resultant layer, manual editing began. The flow line served to show how the water current runs over the terrain and to be able to determine if retreat occurs between the terminus of different time periods. Using these layers as

a guide, the digitizing of the glacier lengths was completed manually. Any noticeable movement, a retreat or gain, was logged in the attribute table.

When all the observed differences were digitized, the length was calculated automatically using ArcGIS©. This calculation only considered the length in a 2 D. Therefore, the fact that the terrain is not plane was contemplated. Even when the slopes are gradual, the 3rd dimension or height must be compensated to calculate the glacier's true length. To achieve this, the ArcGIS© Add Surface Information¹⁴ tool's main function is to "interpolate surface elevation properties for point, multipoint and polyline features" (ESRI, 2014). This tool interpolates the height data extracted from a DEM, TIN or terrain surface (SRTM was used for this purpose) and then adds this information to the vector layer selected as a target. The process was run and the information was added in an extra field in the attribute table of the vector layer. (Digitized lengths in this case). After the attribute table was completed with the necessary information, the data was exported to for further processing in Excel. This 3D length calculation will be referred as "Surface Length" in subsequent sections.

It is important to remark that the same tool previously mentioned is available in ArcGIS© 10.1 and it offers the option to add surface information to a polygon (ESRI, 2014). The tool was experimented using the outlines in order to get the real 3D surface but unfortunately did not work. Apparently, a bug called "NIM082507"¹⁵ has been reported for this tool and seemed to be fixed in the recently released version of ArcGIS© 10.2. Because of the lack of means access to this version, the 2D surface or projective, was calculated instead for this project.

¹⁴ Add Surface Information. Tool of the 3D analyst used to "Interpolates surface elevation properties for point, multipoint, and polyline features. Slope values for line features are calculated as a percent, or grade, for each line segment. Average slope is obtained by averaging the slope of all line segments after weighing each segment by its 3D length. This results in longer segments having greater influence on the resulting value over shorter segments." (ESRI, 2014)

¹⁵ Errors in ArcGIS were reported in a pdf published in the webpage: http://downloads.esri.com/support/downloads/other_/102-IssuesAddressedList.pdf

6 Uncertainty.

The most common errors present in multi-temporal analysis result from mapping and the differences between spatial and temporal resolutions of source imagery used for the study. Images like Landsat ETM+ present a horizontal shift of less than a half pixel whereas TM images can reach one and HEXAGON up to two pixels or more, depending on the terrain (Bolch et al., 2010).

Some errors are inherent to performing the measurements. Therefore, calculations of this error must be presented (Appalachian State University, 2014). The error propagation was calculated for the change between periods, for lengths as well as for surface.

6.1 Uncertainty Estimations for the Area

The uncertainty for the area was calculated for all of the glaciers individually. To accomplish this, a buffer around the glaciers was defined for each of the periods. The size of the buffer depended on the spatial resolution of the main source image used for the mapping period. The result of this procedure was a new vector layer with an attribute table containing an area field. The original vector layer was subtracted from the new vector layer (corresponding to the buffered area) and the resulting difference was deemed as the uncertainty area (Granshaw and Fountain, 2006). The table 6, shows the buffer sizes according to the image source used for mapping.

Table 6 Details taken into account for the area accuracy (Bolch et al., 2010)

Date	Satellite and Sensor	Path/Row or ID	Spatial Resolution	Horizontal Shift	Size of the buffer
23-Nov-1974	Hexagon KH-9 (Mission 1209)	DZB1209-500101L007001	8 m	between <20 and <40 m	10
22-Nov-2000	Landsat ETM (1T)	141/40	15-30 m	<15 m	7.5
03-Dec-2010	Alos PRISM	ALPSMB258793085 ALPSMN258793030 ALPSMF258792975	2.5m (at Nadir)	2.9 m	2
16-Apr-2010	Landsat TM (1T)	141/40	15-30 m	<30 m	7.5

Table 6 presents the spatial resolution, horizontal shift (Bolch et al., 2010) and the size of the buffer of each image used in this study. This buffer size was taken from the

investigation led by Bolch et al., (2010). In the case of the Landsat image, half of the pixel size was considered, representing a size of 7.5 meters. With HEXAGON, half of the pixel size was not considered the best option because of the geometry issues that this image presented, even after correction (Surazakov and Aizen, 2010), therefore based on previous accuracy works, 10 meters was defined as the buffer size (Bolch et al., 2010). For the 2010 time period, two different kinds of images were available to cover the whole area of interest and digitize the glaciers: ALOS and Landsat TM. The glaciers that were mapped based on ALOS obtained a buffer size of 2 meters and the rest of the mapped area that was digitalized based on Landsat TM acquired a buffer of 7.5 meters.

In the case of ALOS, even when the image resolution can reach 2.5 meters at nadir and half of a pixel would represent 1.25 meters, 2 meters were taken instead. This decision was made taking into account that too many variations of buffer size for a single time period could lead to a considerable variance in the area results.

The error propagation was also calculated from period to period. To accomplish this process, the previous uncertainty result for each year was squared and added up to the next year to compare to, and the square root was applied to the resulting value (see Equation 1). This process was applied for the periods 1974-2000, 2000-2010 and 1974-2010. As mentioned previously, for periods involving the year 2010, the uncertainty was calculated dependent on the image used to digitize the glacier.

$$q = x \pm y \pm z \pm \dots$$

$$\delta q = \sqrt{(\delta x)^2 + (\delta y)^2 + (\delta z)^2 + \dots}$$

Equation 1. In this formula, “q” represents the result of the mathematical operation and “δ” is the uncertainty associated with that measurement (Appalachian State University, 2014).

6.2 Uncertainty Estimations for the Lengths

The lengths were calculated in projective and in a surface mode as explained in the section 5.4.2.

For each change, two measurements were considered and therefore two uncertainties needed to be determined. The formula was the same for both cases (see Equation 1), with the exception that in the case of surface length, the 10 m the relative vertical accuracy of the SRTM was taken into account in the formula (Rignot and Echelmeyer, 2001).

In section 6.1, details referring to calculation of uncertainties for years compared with 2010 were mentioned. Tables 7 and 8 outline the uncertainty calculated according to the source image used for this procedure.

Table 7. Uncertainty calculation for 2 dimensions lengths.

Period	Source	Value for the calculation according to image used (buffer size)	Uncertainty for projective lengths
1974 to 2000	HEXAGON + Landsat	10 m + 7.5 m	± 12.5 m
2000 to 2010	Landsat + Landsat	7.5 m + 7.5 m	± 10.60 m
2000 to 2010	Landsat + ALOS	2 m + 7.5 m	± 7.76 m
1974 to 2010	HEXAGON + Landsat	10 m + 7.5 m	± 12.5 m
1974 to 2010	HEXAGON + ALOS	10 m + 2 m	± 10.2 m

Table 8. Uncertainty calculation for 3 dimensions lengths.

Period	Source	Value for the calculation according to image used (buffer size)	Uncertainty for surface lengths
1974 to 2000	HEXAGON + Landsat + SRTM	10 m + 7.5 m + 10 m	± 16.01 m
2000 to 2010	Landsat + Landsat + SRTM	7.5 m + 7.5 m + 10 m	± 14.58 m
2000 to 2010	Landsat + ALOS + SRTM	2 m + 7.5 m + 10 m	± 12.66 m
1974 to 2010	HEXAGON + Landsat + SRTM	10 m + 7.5 m + 10 m	± 16.01 m
1974 to 2010	HEXAGON + ALOS + SRTM	10 m + 2 m + 10 m	± 14.28 m

7 Results

The interest area encompass in total 213 glaciers with an initial surface area in 1974 of $817.76 \pm 35.06 \text{ km}^2$ (see table 9). In this section, the area and lengths results of a representative sample of glaciers are shown. The full results can be found in the appendix.

7.1 Area

The total area of glaciers was approximately $817.76 \pm 35.06 \text{ km}^2$ in 1974. In 2000 the surface represented an amount of $793.73 \pm 26.56 \text{ km}^2$ and finally in 2010 the area was $784.96 \pm 17.42 \text{ km}^2$ (see table 9).

Table 9. Totals in area in the AOI.

Year	Total area in km^2	Mean km^2
1974	817.76 ± 35.06	3.84 ± 0.16
2000	793.73 ± 26.56	3.73 ± 0.12
2010	784.96 ± 17.42	3.69 ± 0.08

A shrinkage of $24.03 \pm 46.13 \text{ km}^2$ was detected in the period 1974 to 2000. Between the 2000 and 2010, a reduction of $8.77 \pm 32.83 \text{ km}^2$ was identified. For the entire study period, a total area decrease of $-32.8 \pm 34.64 \text{ km}^2$ was calculated (see table 10). The average annual loss was consistent through the years representing a continual loss of less than 1 km^2 per year (see table 10).

Table 10. Absolute difference and averaged totals in area in the AOI

Number of Glaciers	Difference in km^2 between periods			Averaged difference in km^2 per year		
	1974- 2000	2000-2010	1974- 2010	1974-2000	2000-2010	1974-2010
213	$-24.03 \pm$ 46.13	$-8.77 \pm$ 32.83	$-32.8 \pm$ 34.64	$-0.92 \pm$ 1.77	$-0.88 \pm$ 3.28	-0.91 ± 0.96

The relative numbers revealed a reduction of $-2.94 \pm 0.22 \%$ from 1974 to 2000. Due to a shorter period of 10 years, 2000-2010, the reduction obtained was $-1.11 \pm 0.41 \%$. The total amount of shrinkage with regard to the initial 1974 surface was about -4.01 ± 0.12 (see table 11).

Table 11. Relative and averaged relative totals in area in the AOI

Relative difference in percentage between periods			Relative average difference in Area (%) per year		
1974-2000	2000-2010	1974-2010	1974-2000	2000-2010	1974-2010
-2.94 ± 0.22	-1.11 ± 0.41	-4.01 ± 0.12	-0.11 ± 0.01	-0.11 ± 0.04	-0.11 ± 0

Regarding the initial 1974 glacial surface area according to the mapping from the HEXAGON imagery, the biggest glacier (G085720E28299N) had a surface area of 60.56 ± 2.14 km² compared with a mere 0.01 ± 0.01 km² of the smallest glacier (G085815E28296N). This range was quite considerable if we contemplate that the whole area of interest was 817 ± 26.56 km² (see table 9) and that there are a total of 213 glaciers. Whilst digitizing was performed over the various years, it was common to adapt the smaller glaciers more than the bigger ones. In order to find out if there is a relationship between the size and amount of shrinkage of glaciers, it was necessary to define groups of glacier according to their dimensions. To achieve this, a classification over the surface of 1974 was performed with the object of identifying, using the natural breaks¹⁶ method, group sizes that best fitted the behavior of the data (see table 12).

To avoid any bias resulting from manual classification, the natural breaks method helped to find out where the biggest differences in the data were occurring. Once the sizes were defined (see table 12), it turned out that only 9 of the 213 glaciers corresponded to sizes between 22 and 60.45 km², meaning only 4% of the total of glaciers were within this group (see fig. 16a). Nevertheless, comparing with the total area in 1974, this group of glaciers represented 35% of the 817.76 ± 35.06 km² (see fig. 16 b).

¹⁶ “Natural Breaks classes are based on natural groupings inherent in the data. Class breaks are identified that best group similar values and that maximize the differences between classes. The features are divided into classes whose boundaries are set where there are relatively big differences in the data values” (ESRI, 2014).

Table 12. Group Sizes of Glaciers

Group size	Amount glaciers	Proportion according to the total amount of glaciers (%)	Surface in km ²	Proportion according to the entire area of interest (%)
Very Big (22 to 60.45 km ²)	9	4	284.97 ± 9.64	35
Big (8 to 21.9 km ²)	14	6	184.91 ± 7.35	23
Medium (3.88 to 7.99 km ²)	29	14	160.06 ± 5.17	19
Small (0.01 to 3.87 km ²)	161	76	187.82 ± 10.09	23
Total	213	100	817.76 ± 35.06	100

The class named as “Small” corresponded to glaciers in a range size from 0.01 to 3.84 km², this was the only classification that was modified manually to include all the glaciers that were below the mean glacier size 3.84 ± 0.16 km², calculated for 1974 (See table 9). Therefore if the glaciers were less than the mean size calculated for that year they were considered as “Small”

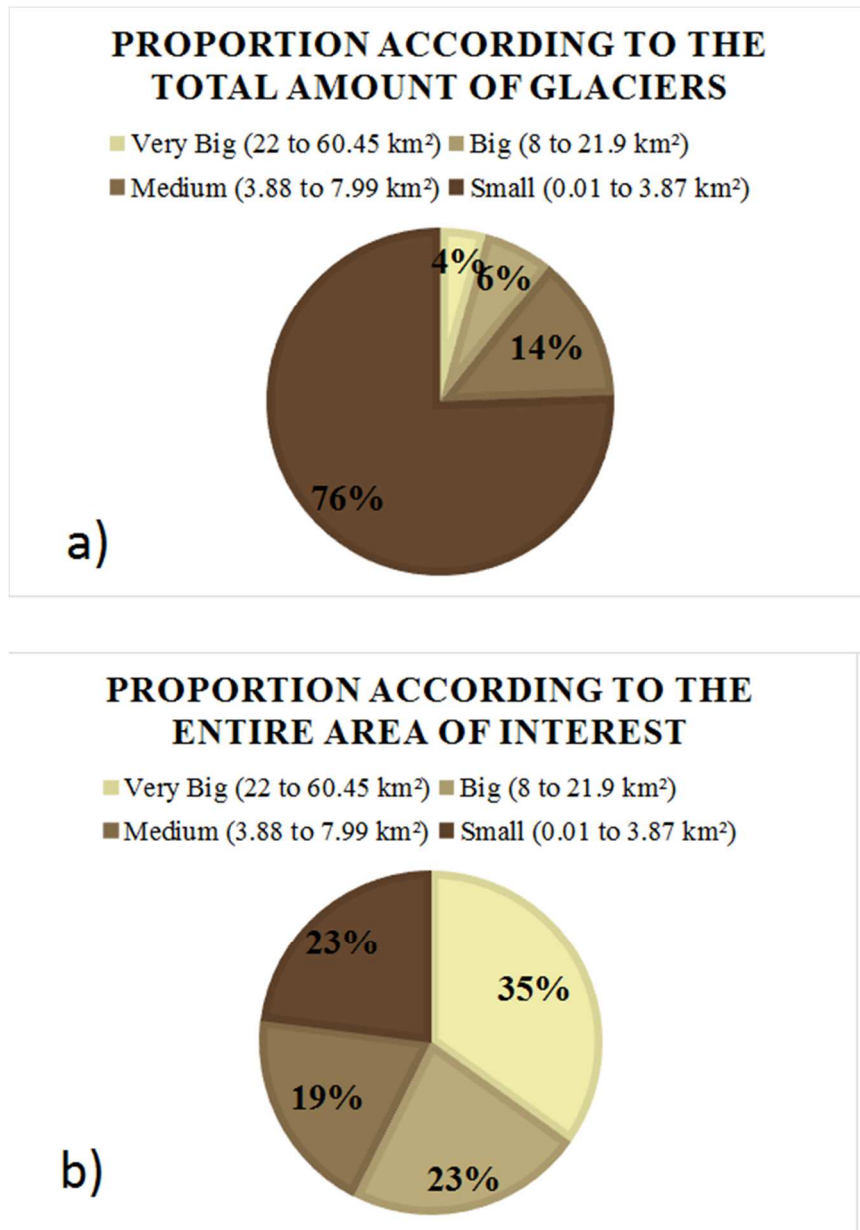


Figure 16. Group size proportion according to the total amount of glaciers (a) and the full surface (b).

A ratio between the total amount of glaciers and the defined sizes was performed to find out the predominant glacier size in the AOI (see fig. 16a). Considering that from 213 glaciers only 9 presented a size from 22 to 60.45 km² and 161 glaciers were included in the range of 0.01 to 3.87 km² this provided a result of 4% forming the “Very Big” glaciers versus 76% of the “Small” ones. On the other hand, comparing the addition of each one of the classes with the entire area (see fig. 16b), the resulting proportion is more related to what we can visualize in figure 17, where there seems to be a

pattern in glaciers' size distribution, nevertheless there is not a remarkable predominance of any particular size.

Figure 16b shows that 36% of the AOI's glaciers correspond to "Very Big" glaciers versus 23% of glaciers that were below the mean and thereby classified as "Small". As a complementary information, glaciers with the size equal or less than 1 km² represented only 5% of the entire area.

This classification was solely done to identify if there is a relationship between glacier sizes and loss and if so, to find out which size of glacier is more prone to changes.

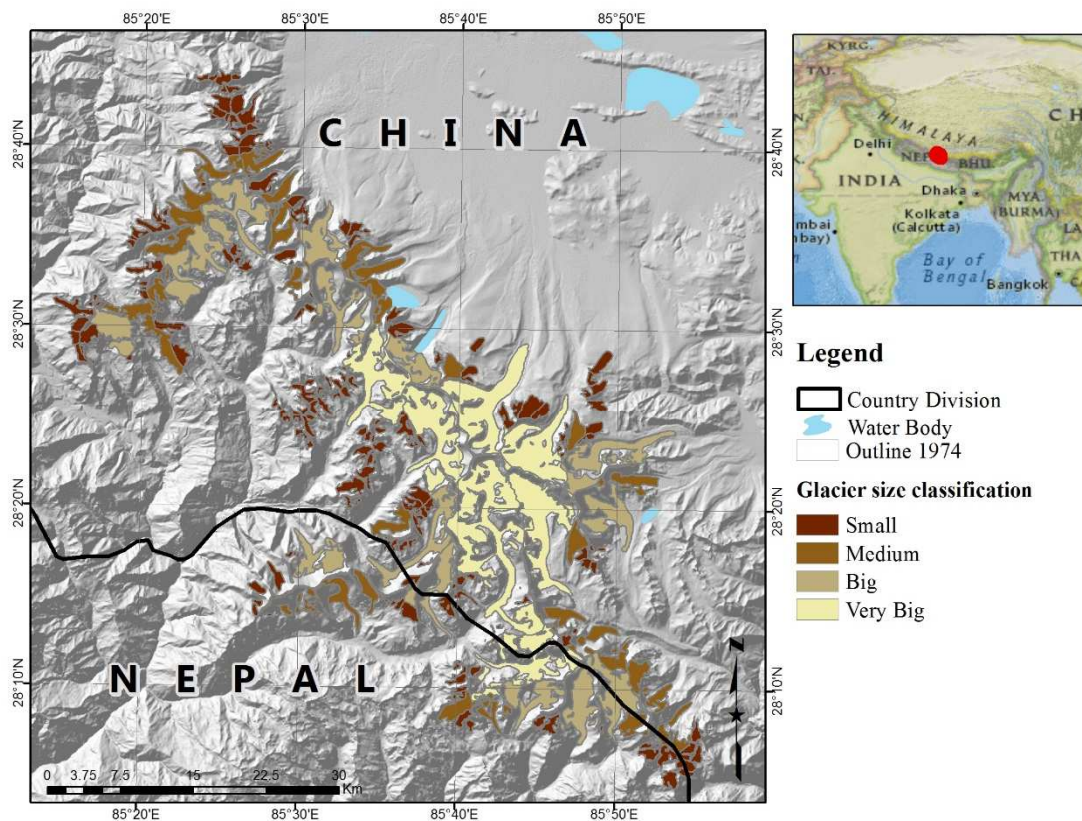


Figure 17. Map showing the group size classification. (Personal compilation based on the raster layers: National Geographic World Map (Esri, 2014) and Shaded Relief from SRTM. The vector files were taken from DIVA-GIS (Hijmans, n.d.) and self-made outlines digitalization)

Based on the previous classification used to define glacier size, the map (see fig. 17) shows a clear pattern within the glaciers' distribution, showing that the largest are located in the middle of the study area and the sizes gradually decrease such that the smallest glaciers by surface area are found at the edges of the study area.

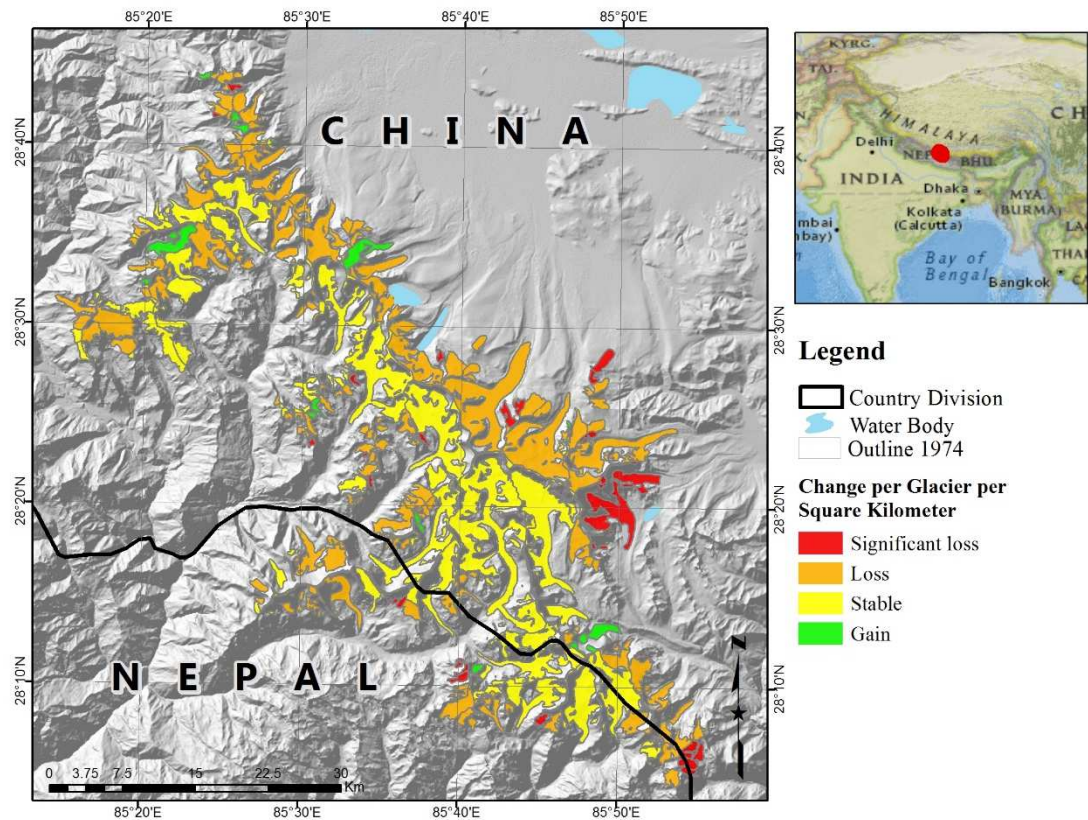


Figure 18. Changes per glacier occurred from 1974 to 2010 normalized by 1974's surface. (Personal compilation based on the raster layers: National Geographic World Map (Esri, 2014) and Shaded Relief from SRTM. The vector files were taken from DIVA-GIS (Hijmans, n.d.) and self-made outlines digitalization)

This map (fig. 18) presents the normalized differences per glacier during the study period from 1974 to 2010. The difference in area per glacier detected for the entire period was normalized with the area that each measured glacier presented in 1974 (difference of area between 2010 and 1974/ total amount of area in 1974). The purpose of this normalization was to detect glaciers that obtained the biggest shrinkage in relation to their original area.

The maximum shrinkage found during this period in a glacier was a loss of -0.66 per km^2 and the highest gain was $+2.3$ per km^2 per their corresponding area in 1974. The ranges created to present the information were defined as follows: The ratio values for loss went from -0.1 to -0.7 per km^2 presented in 96 glaciers, the average was -0.2 , therefore all the glacier presenting a loss below the mean were considered in the range of "Significant loss" (from -0.2 to -0.7 per km^2), the glaciers that presented values in the mean were considered as "Loss". Between -0.01 and 0.01 per km^2 were considered

as "Stable" and finally positive values over 0.01 per km² were considered as "Gain" (see fig. 18).

With the data normalized, it can be seen that only a small number of glaciers shrank considerably, in relation with their initial area. The glacier with bigger sizes seemed to remain stable (see fig. 18).

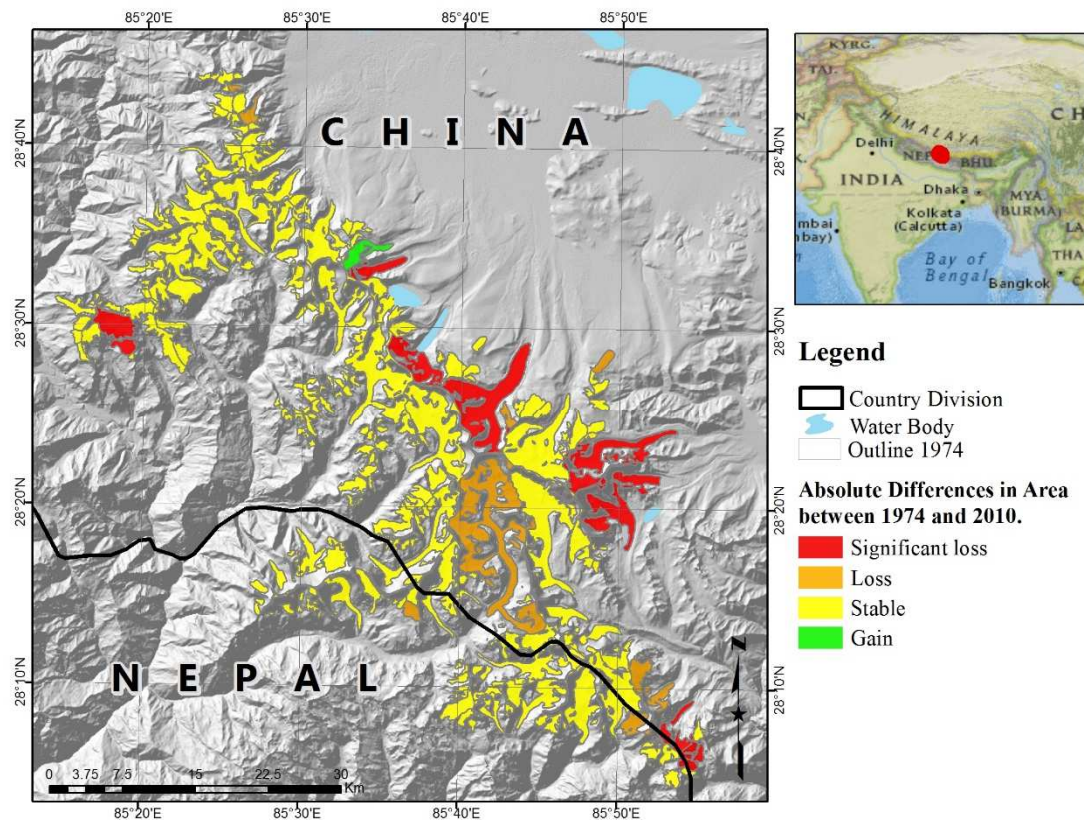


Figure 19 Differences in area between 1974 and 2010. (Personal compilation based on the raster layers: National Geographic World Map (Esri, 2014) and Shaded Relief from SRTM. The vector files were taken from DIVA-GIS (Hijmans, n.d.) and self-made outlines digitalization)

Figure 19 represents the absolute values corresponding to the difference between the total amounts of areas resulting from the period 1974 to 2010. Once again, the mean for the difference between periods was calculated giving a result of -0.58 ± 0.41 km². All the values below the mean were considered as a "Significant loss" (from -3.63 to -0.58 km²). The label "Loss" corresponded to values between -0.57 to -0.42 km². Since the mean uncertainty calculated for this period was ± 0.41 km², values between -0.41 to $+0.41$ were considered as "Stable". Finally, all the values with more than $+0.42$ km² were considered as "Gain".

Ranges for both maps were defined using their mean as a threshold to define classes. This process made it easier to identify significant loss in glaciers that presented values below their mean. Although both maps were showing the same legend, the first map is representing a dependent variable with the original area from 1974 (see fig. 18) and the second an independent variable (fig. 19).

When the results were normalized, it is seen that the greatest changes occurred in small sized glaciers, this means they had lost a higher proportion of surface area relative to their initial surface (see fig. 18). This could support a theory that small glaciers are more prone to extraordinary modifications during time.

Regarding the absolute difference in area found during the whole period (fig. 19), the outlook is different, some small glaciers still appeared to change but it was also shown (in red) that the biggest difference (-3.6 to -0.58 km²) oscillated in glaciers with very big and big sizes (sizes taken from fig. 17). The figure 19 seemed to depict that the majority of the glaciers remained stable for the whole period, nevertheless, the visible conclusion in both maps is the existing decrease of glacier in the area during the study period.

Due to the number of glaciers (213) presented in the entire study area and the multiple possibilities to display the results per glacier, only a sample is given in this section. To see the complete information, check table 21 in the appendix. It is also important to mention that the relative accuracy in glaciers smaller than 1 km² is very high due to the high uncertainty related to small areas. Small areas are prone to obtain high uncertainties because the uncertainty is related to the spatial resolution of the image.

As stated previously, the 213 glaciers were named after their GLIMS ID with some glaciers acquiring an extra letter to discern them within groups of glaciers classified as one entity in the GLIMS catalogue.

Table 13 lists eleven glaciers that exhibited the highest surface reduction during the study period. The surface reduction during the 36-year observation period was calculated by subtracting the 1974 area from the 2010 area. In the table, the field used to sort the results is underlined.

Table 13. Glacier changes sorted by the highest difference (descending order) in area during the period 1974-2010 (underlined field).

GLIMS ID	Area in 1974 (km ²)	Area in 2000 (km ²)	Area in 2010 (km ²)	Difference in Area (km ²) between periods		
				1974-2000	2000-2010	<u>1974-2010</u>
G085813E28330N	14.81 ± 0.61	12.92 ± 0.47	11.18 ± 0.48	-1.89 ± 0.77	-1.74 ± 0.67	-3.63 ± 2.57
G085898E28330N	6.59 ± 0.33	5.02 ± 0.22	3.57 ± 0.22	-1.57 ± 0.4	-1.44 ± 0.31	-3.01 ± 2.13
G085909E28097N	3.08 ± -1.2	1.63 ± 0.05	1.63 ± 0.05	-1.45 ± 1.2	0 ± 0.06	-1.45 ± 1.45
G085690E28418N	33.1 ± 0.75	32.39 ± 0.55	32.2 ± 0.15	-0.71 ± 0.93	-0.19 ± 0.57	-0.9 ± 0.74
G085822E28382N	22.25 ± 0.84	21.7 ± 0.64	21.43 ± 0.63	-0.55 ± 1.05	-0.27 ± 0.9	-0.82 ± 0.61
G085889E28130N	6.54 ± 0.35	5.83 ± 0.24	5.83 ± 0.24	-0.71 ± 0.42	0 ± 0.34	-0.71 ± 0.71
G085579E28556N	5.92 ± 0.25	5.42 ± 0.18	5.23 ± 0.05	-0.5 ± 0.31	-0.18 ± 0.19	-0.69 ± 0.54
G085615E28471N	11.75 ± 0.4	11.01 ± 0.28	11.09 ± 0.08	-0.74 ± 0.49	0.08 ± 0.29	-0.66 ± 0.75
G085304E28490N	11.79 ± 0.26	12.32 ± 0.19	11.19 ± 0.18	0.54 ± 0.32	-1.13 ± 0.26	-0.59 ± 1.25
G085423E28721N	0.85 ± 0.06	0.59 ± 0.03	0.27 ± 0.03	-0.26 ± 0.06	-0.32 ± 0.04	-0.58 ± 0.41
G085817E28470N	2.5 ± 0.08	1.98 ± 0.05	1.93 ± 0.05	-0.53 ± 0.09	-0.05 ± 0.07	-0.57 ± 0.53
Total	119.18 ± 2.72	110.8 ± 2.91	105.56 ± 2.15	-8.38 ± 6.05	-5.24 ± 3.72	-13.61 ± 11.68

To complement the results in table 13, a map was created to highlight where the glaciers with the highest differences were located (see fig. 20). The map coloring was chosen to emphasize the differences in the shrinkage presented in table 13.

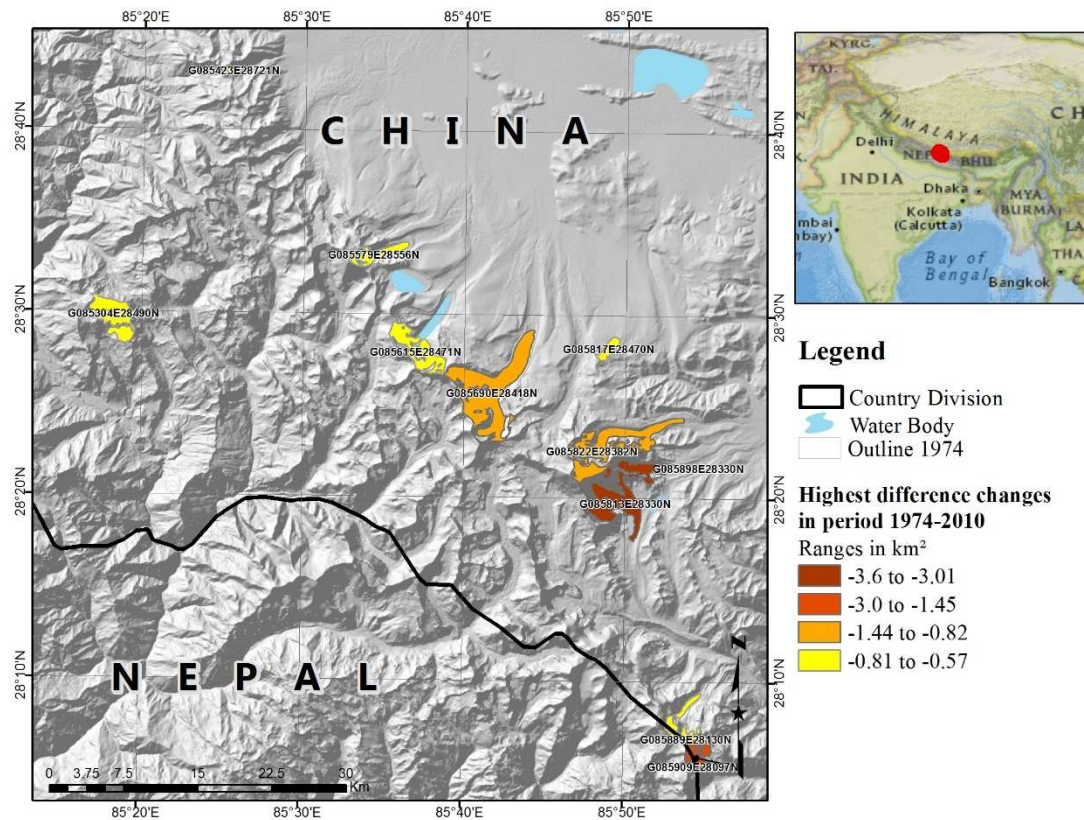


Figure 20. Map showing glacier changes sorted by the highest difference (descending order) in area during the period 1974-2010. (Personal compilation based on the raster layers: National Geographic World Map (Esri, 2014) and Shaded Relief from SRTM. The vector files were taken from DIVA-GIS (Hijmans, n.d.) and self-made outlines digitalization)

In the quest to find a pattern between glacier's size and loss, a second table was included in this section. In this case, table 14 also presents 11 glaciers sorted by the original surface area in 1974. The comparison between these two tables leads us to the conclusion that not necessarily the biggest glaciers had the biggest loss during the study period. Table 14 is joined by fig. 21 that illustrates where glaciers considered in this table are located. Once again, the color shading was chosen to emphasize the sizes between them.

Table 14. Glaciers sorted in descending order by area in 1974 (underlined field).

GLIMS ID	<u>Area in 1974 (Km²)</u>	Area in 2000 (Km ²)	Area in 2010 (Km ²)	Difference in Area (Km ²) between periods		
				1974-2000	2000-2010	1974-2010
G085720E28299N	60.45 ± 2.14	60.08 ± 1.6	60.02 ± 0.43	-0.38 ± 2.67	-0.06 ± 1.65	-0.43 ± 0.38
G085639E28412N	33.22 ± 1.13	33.22 ± 0.85	33.19 ± 0.23	0 ± 1.42	-0.03 ± 0.88	-0.03 ± 0.03
G085690E28418N	33.1 ± 0.75	32.39 ± 0.55	32.2 ± 0.15	-0.71 ± 0.93	-0.19 ± 0.57	-0.9 ± 0.74
G085758E28296N	31.93 ± 1.1	31.78 ± 0.82	31.64 ± 0.81	-0.15 ± 1.37	-0.14 ± 1.15	-0.3 ± 0.21
G085575E28459N	27.65 ± 0.89	27.65 ± 0.67	27.65 ± 0.18	0 ± 1.12	0 ± 0.69	0 ± 0
G085722E28191N	27.03 ± 1.31	26.81 ± 0.97	26.77 ± 0.98	-0.22 ± 1.63	-0.04 ± 1.38	-0.26 ± 0.22
G085752E28395N	26.89 ± 0.53	26.55 ± 0.39	26.55 ± 0.11	-0.34 ± 0.66	0 ± 0.41	-0.34 ± 0.34
G085434E28603N	22.44 ± 0.94	22.08 ± 0.69	22.52 ± 0.68	-0.36 ± 1.16	0.44 ± 0.97	0.08 ± 0.56
G085822E28382N	22.25 ± 0.84	21.7 ± 0.64	21.43 ± 0.63	-0.55 ± 1.05	-0.27 ± 0.9	-0.82 ± 0.61
G085545E28527N	17.28 ± 0.99	17.28 ± 0.74	17.28 ± 0.2	0 ± 1.24	0 ± 0.77	0 ± 0
G085840E28159N	17.17 ± 0.56	17.17 ± 0.42	17.17 ± 0.42	0 ± 0.7	0 ± 0.59	0 ± 0
Total	319.42 ± 11.19	316.72 ± 8.34	316.42 ± 4.81	-2.71 ± 13.96	-0.3 ± 9.97	-3 ± 3.1

In both tables (13 and 14), a couple of rows are marked in red. These rows highlight coincidences presented in both tables regarding the glaciers. The glaciers that appeared in both tables were G085690E28418N and G085822E28382N.

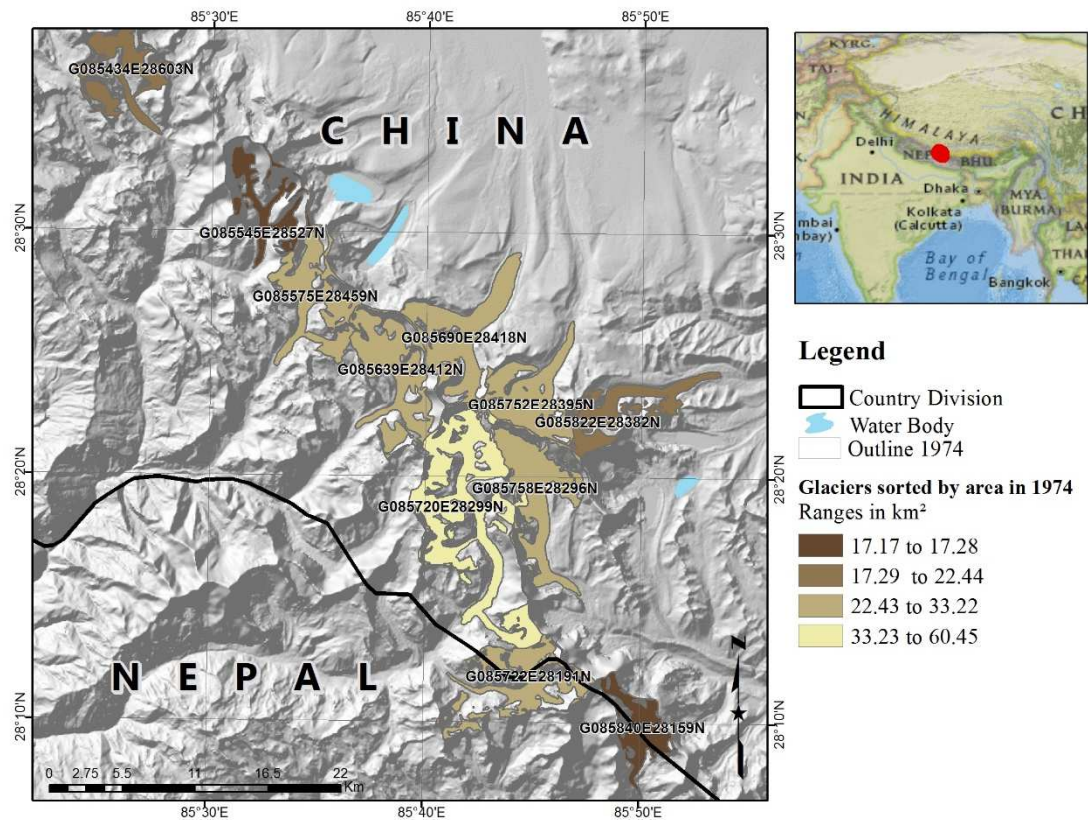


Figure 20. Map showing glaciers sorted in descending order by area in 1974. (Personal compilation based on the raster layers: National Geographic World Map (Esri, 2014) and Shaded Relief from SRTM. The vector files were taken from DIVA-GIS (Hijmans, n.d.) and self-made outlines digitalization)

7.2 Lengths

Whilst working with the lengths' results, it was found that there were some glaciers that presented a growth instead of a retreat, this surprising result did not represent a considerable number, nevertheless, it is important to mention all the dynamics found in the interest area. From the whole group of glaciers measured through these 36 years, the relative majority presented a change in lengths though the whole period. Table 15 presents the various dynamics that occurred during the different periods. To produce this table, the activity of all glaciers was summarized as retreat, gain or no change (stable) and their number was then calculated as a percentage of the total number of glaciers. The complete information for all the glaciers is showed in the appendix (table 21)

Table 15. Percentage of dynamics of the glaciers over the AOI per period.

Status	Period	Period	Period
	1974-2000	2000-2010	1974-2010
Retreat	60 %	36 %	66 %
Advance	1 %	7 %	2 %
Stable	39 %	57 %	32 %
Total	100 %	100 %	100 %

The period that showed the least change was 2000-2010 but nevertheless this time also revealed the highest percentage of glacier advance compared with the other periods. The multi-temporal analysis does not have equal durations between observation periods (see table 15) and therefore, this capricious result could be related to the short time period taken into account, only 10 years, in comparison with 26 years from the previous period, or the whole period itself (36 years).

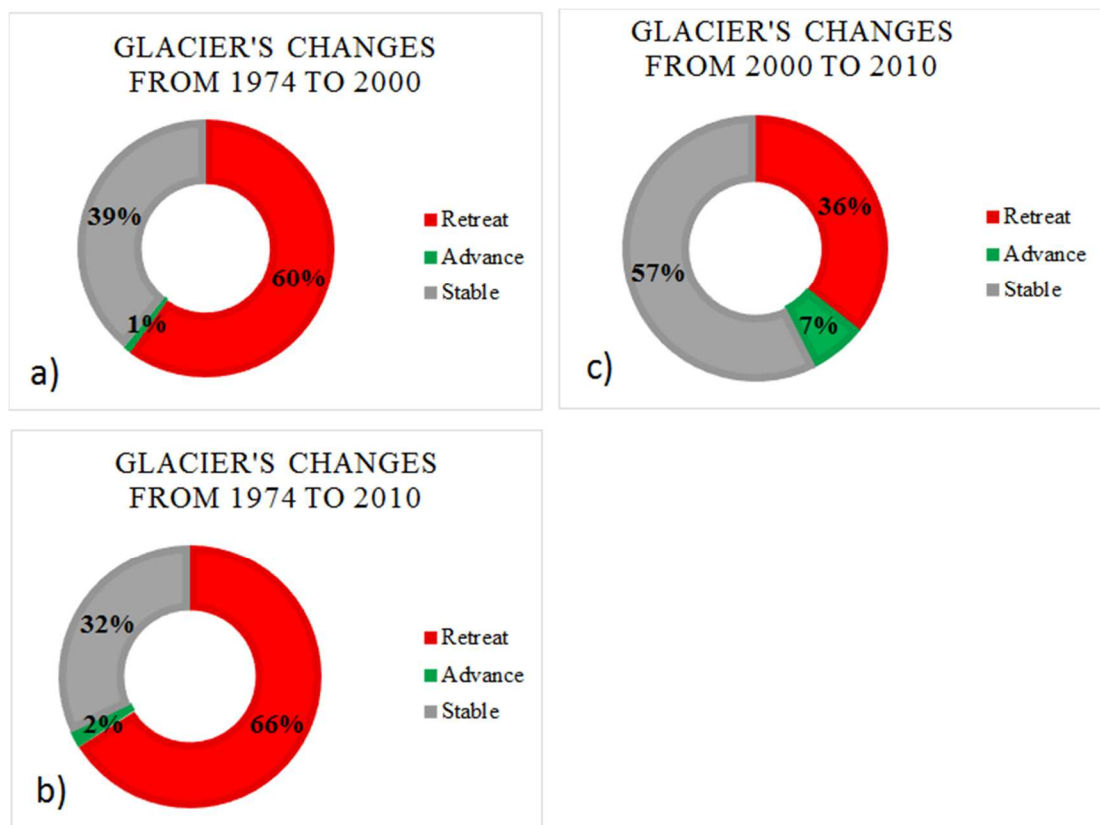


Figure 21. Charts that explain the changes of the glaciers in the AOI during different periods.

Table 15 is accompanied by a group of charts (see fig. 22) that portray the changes that occurred in the study area during the different periods measured.

Taking into consideration that 36 years corresponding to the period 1974-2010, it is shown that there was a retreat in 66% of the glaciers, while 32% remained stable and only 2 percent of the glaciers advanced (fig. 22b). The behavior of glaciers between 2000 and 2010 was somewhat different showing a higher percentage in length advance in respect to the other two graphs (Fig. 22c).

Table 16 shows the total amount of retreat counted by observation period. Considering the lengths resulted from the interpolated distance with the SRTM (surface length), during the 1974-2010 period, -56.25 ± 2.12 km were lost. The difference between this quantity and the one provided by the projective lengths of -41.67 ± 1.61 km, also for the entire period is about 2.39 km.

Table 16. Total length changes per period.

Period	Total Surface Length (km)	Average Surface Length per year (km)	Total Projective Length (km)	Average Projective Length per year (km)
1974 to 2000	-43.48 ± 2.07	-1.67 ± 0.08	-41.67 ± 1.61	-1.6 ± 0.06
2000 to 2010	-12.77 ± 1.22	-1.28 ± 0.12	-12.18 ± 0.82	-1.22 ± 0.08
1974 to 2010	-56.25 ± 2.12	-1.56 ± 0.04	-53.85 ± 1.56	-1.5 ± 0.04

On average per year in the entire period, the retreat presented was about -1.56 ± 0.04 km (surface length) or -1.5 ± 0.04 km (projective length) in the complete study area.

To illustrate the situation with lengths in the AOI for the entire period, the map “Surface Length Changes during the period 1974-2010” was added.

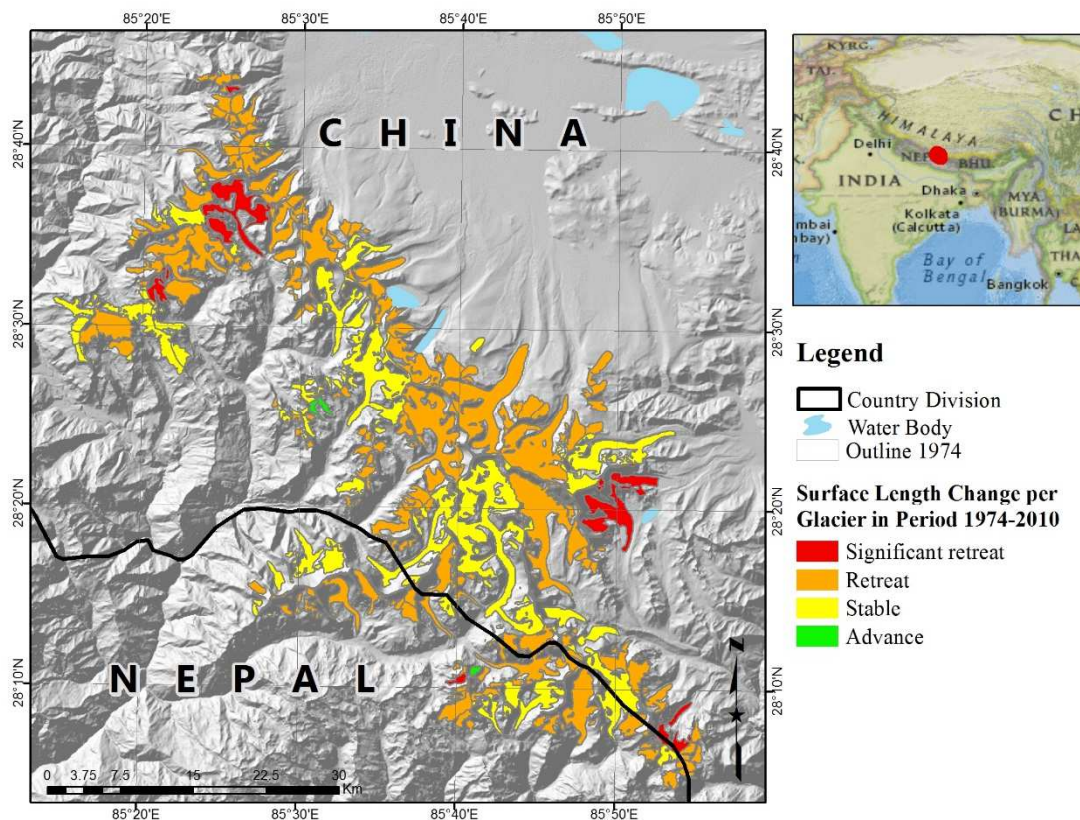


Figure 22. Length changes sorted by 3D Lengths during the period 1974-2010. . (Personal compilation based on the raster layers: National Geographic World Map (Esri, 2014) and Shaded Relief from SRTM. The vector files were taken from DIVA-GIS (Hijmans, n.d.) and self-made outlines digitalization)

The highest uncertainty calculated for the period 1974-2010 regarding the surface lengths was ± 16.01 meters (see table 8). Based on this uncertainty, all the lengths that presented values between -16.01 and $+16.01$ meters were considered as “Stable”. Lengths with values from -999.9 to -16.02 meters were considered as “Retreat”. From -3017.18 to -1000 meters it was considered as “Significant retreat” and values above 16 meters were taken as “Advance”.

Figure 23 highlights the distance in ranges of glaciers that either retreated or advanced in the AOI. The ranges were calculated based upon the field that provided the changes in lengths that occurred between 1974 and 2010. The map was produced taking into

account the interpolated distances that result from using the elevation properties of the SRTM to calculate the surface length aided by the ArcGIS© Tool “Add Surface Information”.

This map emphasizes the greatest changes that occurred in glaciers in the whole area in the 1974-2010 period. The decision to present the changes in lengths from this perspective was made based on the fact that at this scale it is easier to notice changes in polygons than in lines.

Taken the whole 36 years observation period into consideration, it is evident that the majority of glaciers in the entire study area have experienced retreat rather than advance (see fig. 23).

The table 17 presents the more significant retreat occurred in the period 1974-2010. Some of the glaciers presented in this table are depicted in the figure 24.

Table 17. Lengths of the 11 more significant retreats

GLIMS_ID	Surface length 1974-2010 (meters)	Projective Length 1974-2010 (meters)	Average surface length per year 1974-2010 (meters)	Average projective length per year 1974-2010 (meters)
G085898E28330N	-3017.99 ± 16.01	-3013.05 ± 12.5	-83.83 ± 0.35	-83.7 ± 0.35
G085813E28330N	-2147.96 ± 16.01	-2127.93 ± 12.5	-59.67 ± 0.35	-59.11 ± 0.35
G085889E28130N	-1460.93 ± 14.14	-1458.76 ± 10	-40.58 ± 0.28	-40.52 ± 0.28
G085423E28721N	-1175.8 ± 16.01	-1137.3 ± 12.5	-32.66 ± 0.35	-31.59 ± 0.35
G085671E28175N	-1070.35 ± 14.14	-1026.4 ± 10	-29.73 ± 0.28	-28.51 ± 0.28
G085353E28530N	-1051.27 ± 16.01	-950.59 ± 12.5	-29.2 ± 0.35	-26.41 ± 0.35
G085434E28603N	-1017.43 ± 16.01	-1010.25 ± 12.5	-28.26 ± 0.35	-28.06 ± 0.35
G085304E28490N	-935.91 ± 16.01	-924.36 ± 12.5	-26 ± 0.35	-25.68 ± 0.35
G085277E28492N	-924.15 ± 16.01	-789.93 ± 12.5	-25.67 ± 0.35	-21.94 ± 0.35
G085579E28556N	-908.21 ± 14.28	-908.04 ± 10.2	-25.23 ± 0.28	-25.22 ± 0.28
G085524E28586N	-892.89 ± 16.01	-883.89 ± 12.5	-24.8 ± 0.35	-24.55 ± 0.35

Figure 24 shows the outlines' evolution during the different periods where the biggest changes occurred. The HEXAGON image is presented as a background image because

that was the starting point of the multi-temporal study. This subset area was chosen to depict the glaciers that suffered the highest retreat. The small image shows where the biggest changes in the entire area occurred. The lengths accompany the outlines to show the track and direction followed during the glacier's retreat.

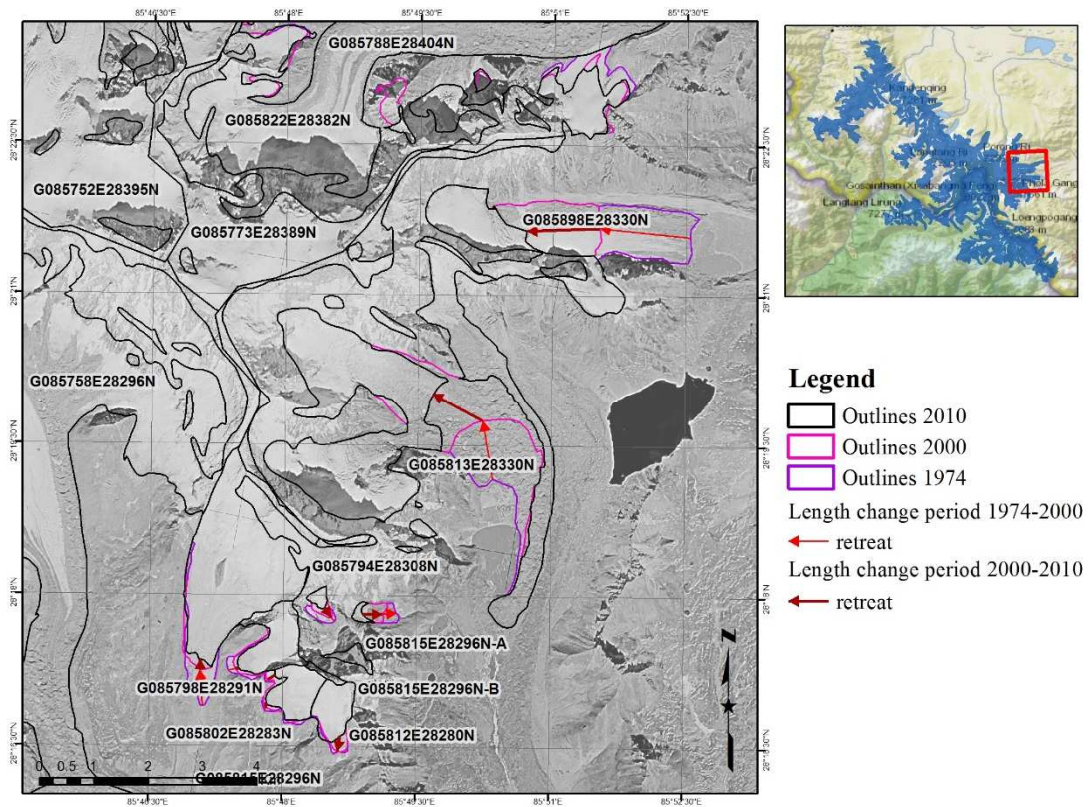


Figure 24. Outlines and Lengths. (Personal compilation based on the raster layers: National Geographic World Map (Esri, 2014) HEXAGON image in the background. The vector files were the result of self-made outlines digitalization.)

8 Discussion

Previous works using multi-temporal analysis to detect changes of ice and debris coverage such as Bolch, Pieczonka, & Benn (2011), Pan, et al., (2012), Bolch, et al., (2010) among others, have been developed in the Tibetan Plateau.

Monitoring in the Gongga Mountains in the south-eastern Tibetan Plateau was performed using Landsat and ASTER as the main satellite imagery source, implementing the ratio TM4/TM5, defining a threshold to differentiate ice from no ice and adapting the results to the debris coverage to ultimately conclude that of 74 glaciers that covered

the area, a shrinkage of 11.3% or 29.2km² from 1966 to 2009 was detected (Pan et al., 2012).

In other research in the south and west of Mt. Everest, 10 glaciers with a total area of 50 km² were studied with aerial images (Cartosat-1) and stereo pair images (Corona) for the period 1970-2007. The result was mass loss 0.32 ± 0.08 meter of water equivalent per year (mw.e. a⁻¹) of for 1970–2007 is . It is worth noting that the authors stated that due to a high uncertainty of the results, the outcome mentioned was barely contemplated (Bolch, Pieczonka and Benn, 2011).

In the majority of studies reviewed for this current project, a glacier shrinkage/retreat has been documented, showing consistency in the loss of glacier in the Tibetan Plateau.

The outcomes of this work were also compared with the results of mass balance and volume previously developed by Nikolakakou (2014). Table 18 shows the results in volume and mass balance change taken from Nikolakakou (2014). According to these results, every glacier presents a loss both in volume and mass balance.

Table 18 Glaciers' mass and volume changes (Nicolakakou, 2014)

GLIMS ID	Name	Volume change (10-3km ³)	Mass balance (m w.e.a ⁻¹)
G085544E28246N	Lirung	-9.8 ± 8.1	-0.061 ± 0.488
G085545E28527N	Gangpengqing	-229.6 ± 12.1	-0.640 ± 0.488
G085575E28459N	Lalaga	-204.8 ± 13.8	-0.438 ± 0.488
G085639E28412N	Purepu	-136.7 ± 14.7	-0.256 ± 0.488
G085690E28418N	Kangjiaruo	-271.0 ± 14.1	-0.552 ± 0.488
G085720E28299N	Langtang	-301.9 ± 20.0	-0.305 ± 0.488
G085752E28395N	Yebokangjiale	-80.6 ± 12.0	-0.226 ± 0.488

Table 19 presents the conclusions of Nikolakakou's work in area difference for the same glaciers showed in table 18. The majority of the glaciers exhibited in table 18, show a change, nevertheless, in comparison with the results registered in the present study for the entire area, the glaciers from table 19 are among those that experienced the least loss (see table 13).

Table 19. Area and differences in area for the Glaciers considered in Nikolakakou (2014)

GLIMS ID	Name	Area in 1974 (Km ²)	Area in 2000 (Km ²)	Area in 2010 (Km ²)	Difference in Area (Km ²) between periods		
					1974-2000	2000-2010	1974-2010
G085544E28246N	Lirung	7.07 ± 0.45	6.94 ± 0.33	6.95 ± 0.09	-0.13 ± 0.56	0 ± 0.35	-0.12 ± 0.13
G085545E28527N	Gangpengqing	17.28 ± 0.99	17.28 ± 0.74	17.28 ± 0.2	0	0	0
G085575E28459N	Lalaga	27.65 ± 0.89	27.65 ± 0.67	27.65 ± 0.18	0	0	0
G085639E28412N	Purepu	33.22 ± 1.13	33.22 ± 0.85	33.19 ± 0.23	0	-0.03 ± 0.88	-0.03 ± 0.03
G085690E28418N	Kangjiaruo	33.1 ± 0.75	32.39 ± 0.55	32.2 ± 0.15	-0.71 ± 0.93	-0.19 ± 0.57	-0.9 ± 0.74
G085720E28299N	Langtang	60.45 ± 2.14	60.08 ± 1.6	60.02 ± 0.43	-0.38 ± 2.67	-0.06 ± 1.65	-0.43 ± 0.38
G085752E28395N	Yebokangjiale	26.89 ± 0.53	26.55 ± 0.39	26.55 ± 0.11	-0.34 ± 0.66	0	-0.34 ± 0.34

Table 20 shows lengths' results for the entire study period for the glaciers considered in table 18.

The glacier that presented the greatest retreat according to table 20 was the Kangjiaruo glacier with an average retreat per year of -6.64 ± 14.14 meters the same one presented a volume loss of -271.0 ± 14.1 km³ and a mass balance of -0.552 ± 0.488 mw.e.a⁻¹ (see table 17), (Nikolakakou, 2014).

Table 20 Length and length average for the Glaciers considered in Nikolakakou (2014)

GLIMS ID	Name	1974-2010			
		Lenght3D (meters)	Lenght2D (meters)	Average Length3D 36 years	Average Length2D 36 years
G085544E28246N	Lirung	-537.18 ± 14.14	-537.14 ± 10	-14.92 ± 14.14	-14.92 ± 10
G085545E28527N	Gangpengqing	0.0	0	0.0	0
G085575E28459N	Lalaga	0.0	0	0.0	0
G085639E28412N	Purepu	-122.45 ± 14.28	-122.26 ± 10.2	-3.4 ± 14.28	-3.4 ± 10.2
G085690E28418N	Kangjiaruo	-639.21 ± 14.28	-638.75 ± 10.2	-17.76 ± 14.28	-17.74 ± 10.2
G085720E28299N	Langtang	0.0	0	0.0	0
G085752E28395N	Yebokangjiale	-239.03 ± 14.14	-239 ± 10	-6.64 ± 14.14	-6.64 ± 10

The behavior of the glaciers' variables represented in tables 17, 18 and 19, suggests that the loss in those studied glaciers could have been in height rather than in surface

area. Similar behavior has been identified in the area of Muztag Ata (Eater Pamir) in a work that is still in preparation (Holzer et al., 2014)

The aim of this comparison is none other than to demonstrate that several studies have been made in the area and that the results also suggest that there is a decrease in the glaciers. This investigation supports the fact that there is a hazard jeopardizing the water reservoir in the Tibetan Plateau linked directly to glacier existence (Richardson and Reynolds, 2000).

Despite drawbacks, remote sensing methods prove to be a very useful tool for tracking changes in glaciers, especially because these mountainous regions are extremely difficult to difficult access and survey (Richardson and Reynolds, 2000).

9 Conclusions

The method followed for a quick first detection of ice coverage proved to be efficient and saved a considerable amount of time, nonetheless it was still necessary to improve results with manual digitalization in order to include debris coverage.

The total study area consisted of 213 glaciers with a total area in 1974 of 817.76 ± 35.06 km². The last observed year, 2010, reported a total surface of 784.96 ± 17.42 km² (see table 9).

The final report of surface loss in the entire study area during the complete 36-year period is 32.8 ± 34.64 km² with an average retreat per year of approximately 0.91 km² (see table 10). The loss rate per year during the observation period was consistent having less than 1 km² loss per period. For the averaged result, the uncertainty turned out to be higher than the result itself, despite this, the changes occurred in the area imply a diminishing in glacier coverage than can crucially help to understand the condition of glaciers (Pellikka and Rees, 2009).

The changes presented in the AOI between the 36 years considered show that there was actually a retreat in 66% of the glacier's lengths (see fig 22b). The period from 2000 to 2010 showed a slightly different behavior with the obtained results revealing 7% of the 213 glaciers advanced instead of retreated (see fig 22c). This could be related

to the lower number of years considered in that second period, only 10 years in comparison to 26 years in the first period. This second period was less than half of the first one. This difference in duration between observation periods could explain the different behavior exposed by the glaciers.

Considering the present results, it could be suggested that those glaciers with a larger initial surface area are more stable than glaciers with a smaller initial surface area.

Results that can be achieved thanks to remote sensing have not only helped scientists to arrive at the conclusion that glaciers are diminishing but also have aided further research into the several hazards associated with a reduction in glacier coverage including threats to mankind living in vulnerable locations as well as effects on the infrastructure such as hydropower plants located in these mountainous regions (Richardson and Reynolds, 2000).

10 Outlook

In a discussion with my colleague José de Jesús Díaz Torres¹⁷, he manifested to me that he is working in the field of solar radiation and how this is influencing the response of vegetation. He suggested to me that it would be interesting to reveal if the interaction between the atmosphere and solar radiation had changed considerably enough to compromise the water reservoir in ice form during the time period comprised in this study over the area of interest.

Interactions between the incoming energy from the sun and the earth's atmosphere as scattering and reflection can be jeopardized by aerosols and other gases absorbed in the atmosphere (Dubayah and Rich, 1995). Any change in this relationship can signify a misbalance that can represent a threat to the climate (Trenberth, Fasullo and Kiehl, 2009).

¹⁷ Centro de Investigación y Asistencia en Tecnología y Diseño del Estado de Jalisco (CIATEJ), Av. Normalistas No. 800, Col. Colinas de la Normal, CP 44270, Guadalajara, Jal., México. Email: jdiaz@ciatej.net.mx

Several statements have been made about the fact that the shrinkage of glaciers is clear evidence of the climate changing and how this is affecting water storage in the world (Lei et al., 2014), (Paul and Andreassen, 2009), (Immerzeel, van Beek and Bierkens, 2010). Since one of the main goals of this thesis was to verify how much global warming is jeopardizing the glacier storage, accompanying it with an extra section that explain and prove the fact that there is a modification in the interaction with the atmosphere and the amount of reflection and absorption in the earth surface (Pellicciotti et al., 2011) would be a recommendation to complement this premise.

To fulfill this proposal, the necessary altitude and climate data which could be free to download in the web. Climate data available from the past 50 years is also available to calculate it. The proposed methodology to follow was created by Dubayah (1994). This model was applied over the Rio Grande area and proved that is possible to get radiation results using pyranometer data, satellite images, and digital elevation model (Dubayah and Rich, 1995).

A glacier's behavior is related to many variables including elevation, slope, debris coverage, topography, climate, precipitation and mass balance (Maurer, 2013), so these variables should be considered in order to have a complete report of the situation in the study area. The conclusion that there is glacier shrinkage due to climate change needs to be analyzed further since so many variables are involved in glacier processes and they should all be taken into account in further studies in order to obtain a more complete analysis.

11 Appendix

Table 21. Results per glacier

GLIMS_ID	Area per glacier (km ²).			Differ- ence in area 1974-2010 (km ²).	Surface length 1974- 2010 (me- ters)	Projective Length 1974-2010 (meters)
	1974	2000	2010			
G085898E28330N	6.59 ± 0.33	5.02 ± 0.22	3.57 ± 0.22	-3.01 ± 2.13	-3017.99 ± 16.01	-3013.05 ± 12.5
G085813E28330N	14.81 ± 0.61	12.92 ± 0.47	11.18 ± 0.48	-3.63 ± 2.57	-2147.96 ± 16.01	-2127.93 ± 12.5
G085889E28130N	6.54 ± 0.35	5.83 ± 0.24	5.83 ± 0.24	-0.71 ± 0.71	-1460.93 ± 14.14	-1458.76 ± 10
G085423E28721N	0.85 ± 0.06	0.59 ± 0.03	0.27 ± 0.03	-0.58 ± 0.41	-1175.8 ± 16.01	-1137.3 ± 12.5
G085671E28175N	1.37 ± 0.11	1.06 ± 0.07	1.06 ± 0.07	-0.31 ± 0.31	-1070.35 ± 14.14	-1026.4 ± 10
G085353E28530N	4.31 ± 0.27	4.31 ± 0.2	4.1 ± 0.19	-0.21 ± 0.21	-1051.27 ± 16.01	-950.59 ± 12.5
G085434E28603N	22.44 ± 0.94	22.08 ± 0.69	22.52 ± 0.68	0.08 ± 0.56	-1017.43 ± 16.01	-1010.25 ± 12.5
G085304E28490N	11.79 ± 0.26	12.32 ± 0.19	11.19 ± 0.18	-0.59 ± 1.25	-935.91 ± 16.01	-924.36 ± 12.5
G085277E28492N	2.7 ± 0.09	2.48 ± 0.07	2.33 ± 0.07	-0.37 ± 0.27	-924.15 ± 16.01	-789.93 ± 12.5
G085579E28556N	5.92 ± 0.25	5.42 ± 0.18	5.23 ± 0.05	-0.69 ± 0.54	-908.21 ± 14.28	-908.04 ± 10.2
G085524E28586N	13.25 ± 0.38	12.89 ± 0.27	12.86 ± 0.27	-0.4 ± 0.37	-892.89 ± 16.01	-883.89 ± 12.5
G085615E28471N	11.75 ± 0.4	11.01 ± 0.28	11.09 ± 0.08	-0.66 ± 0.75	-888.63 ± 14.28	-880.98 ± 10.2
G085442E28699N	2.8 ± 0.13	2.61 ± 0.08	2.35 ± 0.08	-0.45 ± 0.32	-880.73 ± 14.14	-851.32 ± 10
G085478E28628N	4.2 ± 0.17	4.21 ± 0.12	3.95 ± 0.11	-0.25 ± 0.26	-880.49 ± 16.01	-879.82 ± 12.5
G085628E28395N	0.73 ± 0.08	0.47 ± 0.05	0.46 ± 0.01	-0.27 ± 0.26	-872.38 ± 14.28	-843.13 ± 10.2
G085794E28308N	5.04 ± 0.16	4.83 ± 0.11	4.73 ± 0.11	-0.31 ± 0.23	-857.71 ± 16.01	-849.33 ± 12.5
G085758E28296N	31.93 ± 1.1	31.78 ± 0.82	31.64 ± 0.81	-0.3 ± 0.21	-846.8 ± 16.01	-845.27 ± 12.5
G085502E28614N- B	1.41 ± 0.06	1.28 ± 0.04	1.3 ± 0.04	-0.11 ± 0.13	-801.47 ± 16.01	-757.98 ± 12.5
G085870E28159N	8.89 ± 0.38	8.42 ± 0.26	8.42 ± 0.26	-0.47 ± 0.47	-792.28 ± 14.14	-775.92 ± 10
G085519E28243N	4.22 ± 0.37	3.91 ± 0.27	3.85 ± 0.07	-0.36 ± 0.31	-756.22 ± 14.28	-670.25 ± 10.2
G085514E28415N	0.43 ± 0.03	0.43 ± 0.02	0.53 ± 0.01	0.1 ± 0.1	-745.32 ± 14.28	-728.16 ± 10.2
G085841E28198N	5.09 ± 0.24	4.9 ± 0.17	4.9 ± 0.17	-0.19 ± 0.19	-724.17 ± 14.14	-723.57 ± 10
G085430E28708N	2.42 ± 0.08	2.33 ± 0.07	2.22 ± 0.06	-0.2 ± 0.14	-723.1 ± 14.14	-713.94 ± 10

G085415E28709N	2.28 ± 0.08	2.08 ± 0.05	1.9 ± 0.05	-0.38 ± 0.27	-720.96 ± 14.14	-666.55 ± 10
G085462E28636N	3.45 ± 0.19	3.33 ± 0.14	3.28 ± 0.14	-0.17 ± 0.13	-657.16 ± 16.01	-641.64 ± 12.5
G085620E28148N	0.85 ± 0.09	0.78 ± 0.06	0.71 ± 0.06	-0.14 ± 0.1	-650.28 ± 14.14	-628.24 ± 10
G085501E28521N	2.07 ± 0.17	1.91 ± 0.12	1.77 ± 0.03	-0.3 ± 0.21	-649.1 ± 14.28	-643.54 ± 10.2
G085423E28563N	1.04 ± 0.06	0.97 ± 0.03	0.97 ± 0.03	-0.07 ± 0.07	-639.28 ± 14.14	-457.63 ± 10
G085690E28418N	33.1 ± 0.75	32.39 ± 0.55	32.2 ± 0.15	-0.9 ± 0.74	-639.21 ± 14.28	-638.75 ± 10.2
G085815E28296N-A	0.53 ± 0.07	0.45 ± 0.05	0.32 ± 0.04	-0.2 ± 0.15	-625.22 ± 16.01	-621.6 ± 12.5
G085481E28592N	7.19 ± 0.33	7.04 ± 0.24	6.99 ± 0.24	-0.19 ± 0.15	-604.76 ± 16.01	-510.65 ± 12.5
G085408E28648N	7.24 ± 0.39	7.19 ± 0.29	7.13 ± 0.29	-0.11 ± 0.08	-601.39 ± 16.01	-600.78 ± 12.5
G085665E28186N	1 ± 0.1	0.74 ± 0.06	0.71 ± 0.06	-0.29 ± 0.26	-582.52 ± 14.14	-513.48 ± 10
G085502E28614N-A	2.58 ± 0.18	2.48 ± 0.13	2.53 ± 0.13	-0.06 ± 0.12	-581.89 ± 14.14	-581.32 ± 10
G085451E28651N	6.05 ± 0.27	5.88 ± 0.2	5.85 ± 0.19	-0.2 ± 0.17	-578.19 ± 16.01	-575.71 ± 12.5
G085544E28246N	7.07 ± 0.45	6.94 ± 0.33	6.95 ± 0.09	-0.12 ± 0.13	-537.18 ± 14.14	-537.14 ± 10
G085374E28549N	11.37 ± ± 0.34	11.25 ± 0.25	11.41 ± 0.25	0.04 ± 0.2	-497.86 ± 14.14	-495.77 ± 10
G085918E28129N	1.48 ± 0.07	1.25 ± 0.04	1.36 ± 0.05	-0.12 ± 0.26	-480.96 ± 16.01	-475.94 ± 12.5
G085909E28097N	1.82 ± 0.06	1.63 ± 0.05	1.63 ± 0.05	-0.19 ± 0.19	-468.35 ± 14.14	-466.02 ± 10
G085909E28097N	3.08 ± -1.2	1.63 ± 0.05	1.63 ± 0.05	-1.45 ± 1.45	-468.35 ± 14.14	-466.02 ± 10
G085911E28090N	0.84 ± 0.04	0.57 ± 0.03	0.57 ± 0.03	-0.27 ± 0.27	-458.2 ± 14.14	-388.96 ± 10
G085659E28466N	4.07 ± 0.11	3.96 ± 0.08	3.89 ± 0.02	-0.18 ± 0.13	-456.7 ± 14.28	-449.06 ± 10.2
G085387E28623N	4.63 ± 0.13	4.54 ± 0.1	4.53 ± 0.09	-0.1 ± 0.08	-454.42 ± 16.01	-448.22 ± 12.5
G085672E28166N	0.7 ± 0.06	0.64 ± 0.04	0.64 ± 0.04	-0.06 ± 0.06	-426.99 ± 14.14	-362.55 ± 10
G085858E28197N	0.17 ± 0.03	0.09 ± 0.01	0.09 ± 0.01	-0.08 ± 0.08	-421.6 ± 14.14	-389.7 ± 10
G085615E28339N	2.1 ± 0.11	2.01 ± 0.07	1.98 ± 0.02	-0.12 ± 0.1	-419.54 ± 14.28	-370.14 ± 10.2
G085423E28655N	0.05 ± 0.01	0.04 ± 0.01	0.16 ± 0.02	0.11 ± 0.12	-415.94 ± 16.01	-364.74 ± 12.5
G085397E28569N	10.77 ± ± 0.38	10.5 ± 0.28	10.5 ± 0.28	-0.27 ± 0.27	-415.34 ± 14.14	-414.71 ± 10
G085728E28427N	1.23 ± 0.07	1.05 ± 0.04	0.99 ± 0.01	-0.25 ± 0.19	-408.87 ± 14.14	-383.27 ± 10
G085618E28255N	12.21 ± ± 0.56	12.12 ± 0.41	12.21 ± 0.11	0 ± 0.13	-407.73 ± 14.14	-401.22 ± 10
G085354E28573N	7 ± 0.32	6.92 ± 0.24	7.34 ± 0.23	0.34 ± 0.42	-406.75 ± 16.01	-394.84 ± 12.5

G085768E28135N	2 ± 0.11	1.75 ± 0.08	1.75 ± 0.08	-0.25 ± 0.25	-390.97 ± 14.14	-380.28 ± 10
G085612E28242N-B	0.66 ± 0.04	0.5 ± 0.03	0.51 ± 0.01	-0.15 ± 0.16	-377.23 ± 14.28	-360.87 ± 10.2
G085891E28084N	2.19 ± 0.09	2.01 ± 0.06	1.94 ± 0.06	-0.26 ± 0.2	-372.39 ± 16.01	-313.2 ± 12.5
G085612E28242N-C	0.28 ± 0.03	0.15 ± 0.02	0.1 ± 0	-0.18 ± 0.14	-369.61 ± 14.28	-350.91 ± 10.2
G085570E28372N	2.6 ± 0.16	2.5 ± 0.12	2.45 ± 0.03	-0.15 ± 0.11	-365.71 ± 14.14	-363.94 ± 10
G085574E28352N	0.46 ± 0.04	0.25 ± 0.02	0.22 ± 0.01	-0.24 ± 0.21	-364.18 ± 14.28	-359.78 ± 10.2
G085409E28700N	1.43 ± 0.07	1.33 ± 0.05	1.29 ± 0.05	-0.13 ± 0.1	-353.18 ± 14.14	-344.35 ± 10
G085414E28730N	1.62 ± 0.07	1.5 ± 0.05	1.39 ± 0.05	-0.22 ± 0.16	-346.75 ± 14.14	-336.76 ± 10
G085812E28280N	0.72 ± 0.04	0.7 ± 0.03	0.65 ± 0.02	-0.07 ± 0.05	-340.17 ± 16.01	-307.04 ± 12.5
G085815E28296N-B	0.3 ± 0.05	0.23 ± 0.03	0.18 ± 0.03	-0.12 ± 0.09	-336.64 ± 16.01	-300.52 ± 12.5
G085612E28242N-A	2.53 ± 0.08	2.33 ± 0.05	2.07 ± 0.02	-0.46 ± 0.33	-327.89 ± 14.28	-309.7 ± 10.2
G085742E28430N	3.74 ± 0.09	3.48 ± 0.06	3.32 ± 0.02	-0.41 ± 0.3	-323.57 ± 14.28	-319.46 ± 10.2
G085447E28686N	0.88 ± 0.06	0.88 ± 0.04	0.72 ± 0.03	-0.16 ± 0.16	-321.93 ± 14.14	-293.86 ± 10
G085454E28262N	1.62 ± 0.11	1.46 ± 0.08	1.37 ± 0.02	-0.25 ± 0.18	-302.65 ± 14.28	-280.78 ± 10.2
G085346E28556N	2.69 ± 0.15	2.65 ± 0.11	2.62 ± 0.11	-0.07 ± 0.05	-296.66 ± 16.01	-295.91 ± 12.5
G085789E28219N	1.31 ± 0.09	1.19 ± 0.06	1.19 ± 0.06	-0.12 ± 0.12	-289.32 ± 14.14	-288.35 ± 10
G085495E28547N	4.24 ± 0.3	4.24 ± 0.23	4.24 ± 0.06	0 ± 0.01	-279.21 ± 14.28	-274.96 ± 10.2
G085546E28594N	1.25 ± 0.05	1.18 ± 0.04	1.05 ± 0.04	-0.21 ± 0.15	-277.5 ± 16.01	-267.91 ± 12.5
G085569E28377N	0.08 ± 0.02	0.06 ± 0.01	0.05 ± 0	-0.03 ± 0.02	-272.77 ± 14.28	-267.95 ± 10.2
G085585E28391N	1.33 ± 0.09	1.11 ± 0.06	1.12 ± 0.02	-0.21 ± 0.21	-271.15 ± 14.28	-269.9 ± 10.2
G085444E28671N	3.01 ± 0.12	2.96 ± 0.08	2.96 ± 0.08	-0.04 ± 0.04	-270.62 ± 14.14	-243.06 ± 10
G085677E28457N	1.91 ± 0.09	1.54 ± 0.06	1.57 ± 0.02	-0.34 ± 0.38	-269.4 ± 14.28	-269.4 ± 10.2
G085562E28337N	0.41 ± 0.06	0.35 ± 0.04	0.33 ± 0.01	-0.08 ± 0.07	-267.95 ± 14.28	-229.86 ± 10.2
G085609E28297N	0.77 ± 0.07	0.72 ± 0.05	0.66 ± 0.01	-0.1 ± 0.07	-267.01 ± 14.28	-244.41 ± 10.2
G085809E28455N	0.89 ± 0.05	0.73 ± 0.04	0.68 ± 0.04	-0.21 ± 0.16	-264.58 ± 16.01	-244.14 ± 12.5
G085612E28242N-D	0.24 ± 0.05	0.18 ± 0.03	0.1 ± 0.01	-0.14 ± 0.1	-258.03 ± 14.28	-223.47 ± 10.2
G085722E28191N	27.03 ± ± 1.31	26.81 ± 0.97	26.77 ± 0.98	-0.26 ± 0.22	-255.55 ± 14.14	-196.45 ± 10
G085808E28409N	1.76 ± 0.06	1.65 ± 0.04	1.46 ± 0.04	-0.31 ± 0.22	-245.52 ± 16.01	-245.45 ± 12.5

G085752E28395N	26.89 ± 0.53	26.55 ± 0.39	26.55 ± 0.11	-0.34 ± 0.34	-239.03 ± 14.14	-239 ± 10
G085333E28543N	0.25 ± 0.04	0.25 ± 0.03	0.3 ± 0.03	0.05 ± 0.05	-233.94 ± 16.01	-199.37 ± 12.5
G085553E28334N	0.62 ± 0.06	0.56 ± 0.04	0.53 ± 0.01	-0.1 ± 0.07	-233 ± 14.28	-193.28 ± 10.2
G085602E28318N	6.19 ± 0.29	6.15 ± 0.21	6.04 ± 0.06	-0.15 ± 0.12	-229.48 ± 14.28	-215.77 ± 10.2
G085343E28593N	2.33 ± 0.13	2.35 ± 0.1	2.35 ± 0.1	0.02 ± 0.02	-228.64 ± 14.14	-209.35 ± 10
G085645E28473N	0.62 ± 0.04	0.43 ± 0.02	0.36 ± 0.01	-0.26 ± 0.2	-228.21 ± 14.28	-224.44 ± 10.2
G085814E28430N	1.54 ± 0.06	1.38 ± 0.05	1.44 ± 0.05	-0.1 ± 0.18	-222.88 ± 14.14	-219.22 ± 10
G085431E28683N	0.98 ± 0.06	0.93 ± 0.05	1.04 ± 0.04	0.07 ± 0.13	-220.06 ± 16.01	-215.66 ± 12.5
G085671E28138N	2.16 ± 0.11	2.03 ± 0.08	1.98 ± 0.08	-0.17 ± 0.13	-214.25 ± 14.14	-187.62 ± 10
G085670E28257N	2.92 ± 0.27	2.82 ± 0.2	2.86 ± 0.05	-0.06 ± 0.11	-213.82 ± 14.14	-213.12 ± 10
G085585E28525N	6.56 ± 0.3	6.33 ± 0.22	6.15 ± 0.06	-0.41 ± 0.29	-211.32 ± 14.28	-205.36 ± 10.2
G085817E28470N	2.5 ± 0.08	1.98 ± 0.05	1.93 ± 0.05	-0.57 ± 0.53	-209.83 ± 14.14	-209.28 ± 10
G085508E28390N	0.49 ± 0.05	0.36 ± 0.03	0.32 ± 0.01	-0.18 ± 0.14	-203.8 ± 14.28	-184.53 ± 10.2
G085393E28731N	0.64 ± 0.04	0.62 ± 0.03	0.65 ± 0.04	0.01 ± 0.03	-202.94 ± 16.01	-200.5 ± 12.5
G085570E28389N	1.95 ± 0.12	1.73 ± 0.08	1.67 ± 0.02	-0.28 ± 0.23	-199.73 ± 14.28	-199.31 ± 10.2
G085798E28291N	1.13 ± 0.06	1.08 ± 0.04	1 ± 0.04	-0.13 ± 0.09	-197.83 ± 16.01	-192.33 ± 12.5
G085576E28254N	4.29 ± 0.26	4.16 ± 0.19	4.26 ± 0.05	-0.04 ± 0.17	-197.01 ± 14.28	-181.58 ± 10.2
G085788E28404N	4.1 ± 0.14	4.05 ± 0.1	4.03 ± 0.1	-0.08 ± 0.06	-196.53 ± 14.14	-191.17 ± 10
G085429E28674N	0.5 ± 0.05	0.49 ± 0.03	0.48 ± 0.03	-0.01 ± 0.01	-182.13 ± 16.01	-170.34 ± 12.5
G085601E28297N	0.57 ± 0.05	0.51 ± 0.03	0.5 ± 0.01	-0.07 ± 0.06	-182.11 ± 14.28	-173.73 ± 10.2
G085605E28500N	3.25 ± 0.15	3.19 ± 0.11	3.19 ± 0.03	-0.06 ± 0.06	-180.95 ± 14.14	-179.64 ± 10
G085593E28299N	0.52 ± 0.06	0.49 ± 0.04	0.46 ± 0.01	-0.06 ± 0.04	-179.76 ± 14.28	-168.91 ± 10.2
G085498E28408N	1.22 ± 0.12	1.18 ± 0.09	1.11 ± 0.02	-0.11 ± 0.09	-179.73 ± 14.28	-171.74 ± 10.2
G085565E28379N	0.17 ± 0.02	0.12 ± 0.01	0.1 ± 0	-0.07 ± 0.05	-179.57 ± 14.28	-170.02 ± 10.2
G085416E28719N	0.4 ± 0.04	0.42 ± 0.03	0.39 ± 0.03	0 ± 0.04	-178.91 ± 14.14	-174.54 ± 10
G085666E28148N	5.07 ± 0.14	4.92 ± 0.1	4.92 ± 0.1	-0.16 ± 0.16	-175.02 ± 14.14	-140.2 ± 10
G085802E28443N	0.56 ± 0.04	0.48 ± 0.03	0.48 ± 0.03	-0.08 ± 0.08	-167.82 ± 14.14	-166.25 ± 10
G085716E28420N	1.92 ± 0.08	1.45 ± 0.05	1.45 ± 0.01	-0.47 ± 0.47	-167.08 ± 14.14	-164.53 ± 10

G085564E28401N	0.66 ± 0.04	0.58 ± 0.03	0.58 ± 0.01	-0.07 ± 0.07	-165.39 ± 14.14	-160.1 ± 10
G085537E28440N	0.49 ± 0.05	0.41 ± 0.04	0.42 ± 0.01	-0.07 ± 0.09	-160.89 ± 14.28	-133.86 ± 10.2
G085474E28429N	0.35 ± 0.03	0.35 ± 0.02	0.32 ± 0.01	-0.04 ± 0.04	-155.65 ± 14.28	-129.92 ± 10.2
G085756E28139N	1.11 ± 0.07	0.86 ± 0.04	0.86 ± 0.04	-0.25 ± 0.25	-155.27 ± 14.14	-149.51 ± 10
G085800E28158N	15.09 ± ± 0.62	15.06 ± 0.46	15.06 ± 0.46	-0.03 ± 0.03	-144.15 ± 14.14	-114.17 ± 10
G085802E28283N	0.87 ± 0.04	0.83 ± 0.03	0.73 ± 0.03	-0.14 ± 0.11	-143.52 ± 16.01	-138.9 ± 12.5
G085854E28138N	4.89 ± 0.22	4.47 ± 0.17	4.47 ± 0.17	-0.43 ± 0.43	-138.33 ± 14.14	-133.59 ± 10
G085426E28691N	0.7 ± 0.04	0.77 ± 0.04	0.76 ± 0.04	0.06 ± 0.07	-132.14 ± 16.01	-129.88 ± 12.5
G085814E28447N	1.5 ± 0.06	1.4 ± 0.04	1.45 ± 0.04	-0.05 ± 0.11	-128.23 ± 14.14	-127.61 ± 10
G085625E28348N	2.45 ± 0.08	2.45 ± 0.06	2.37 ± 0.02	-0.08 ± 0.08	-123.37 ± 14.28	-122.31 ± 10.2
G085639E28412N	33.22 ± ± 1.13	33.22 ± 0.85	33.19 ± 0.23	-0.03 ± 0.03	-122.45 ± 14.28	-122.26 ± 10.2
G085643E28314N-A	0.88 ± 0.05	0.85 ± 0.03	0.84 ± 0.01	-0.04 ± 0.03	-117.36 ± 14.14	-107.11 ± 10
G085421E28665N	1.86 ± 0.09	1.83 ± 0.07	1.83 ± 0.07	-0.03 ± 0.03	-113.88 ± 14.14	-108.49 ± 10
G085754E28423N	1.76 ± 0.07	1.69 ± 0.05	1.54 ± 0.01	-0.22 ± 0.16	-108.05 ± 14.28	-106.96 ± 10.2
G085608E28411N	3.07 ± 0.19	2.7 ± 0.14	2.65 ± 0.03	-0.42 ± 0.37	-105.75 ± 14.28	-105.39 ± 10.2
G085619E28301N	0.63 ± 0.06	0.63 ± 0.05	0.62 ± 0.01	0 ± 0	-105.45 ± 14.28	-103.44 ± 10.2
G085426E28733N	0.44 ± 0.03	0.44 ± 0.02	0.4 ± 0.02	-0.04 ± 0.04	-105.33 ± 16.01	-102.68 ± 12.5
G085440E28557N	1.38 ± 0.09	1.3 ± 0.06	1.3 ± 0.06	-0.08 ± 0.08	-104 ± 14.14	-98.47 ± 10
G085862E28115N	2.55 ± 0.15	2.53 ± 0.12	2.53 ± 0.12	-0.02 ± 0.02	-103.88 ± 14.14	-77.84 ± 10
G085419E28692N	0.38 ± 0.04	0.38 ± 0.02	0.31 ± 0.02	-0.08 ± 0.07	-100.82 ± 14.14	-94.65 ± 10
G085780E28410N	0.18 ± 0.02	0.17 ± 0.01	0.2 ± 0.02	0.03 ± 0.03	-99.8 ± 16.01	-98.15 ± 12.5
G085776E28402N	0.49 ± 0.04	0.48 ± 0.03	0.46 ± 0.03	-0.03 ± 0.02	-93.48 ± 14.14	-82.02 ± 10
G085406E28694N	0.3 ± 0.03	0.3 ± 0.02	0.24 ± 0.02	-0.07 ± 0.07	-87.51 ± 16.01	-81.94 ± 12.5
G085316E28575N	0.6 ± 0.05	0.54 ± 0.04	0.54 ± 0.04	-0.05 ± 0.05	-84.71 ± 14.14	-73.75 ± 10
G085603E28515N	1.32 ± 0.08	1.32 ± 0.06	1.28 ± 0.02	-0.03 ± 0.03	-84.6 ± 14.28	-78.35 ± 10.2
G085551E28440N	0.79 ± 0.05	0.79 ± 0.04	0.65 ± 0.01	-0.13 ± 0.13	-79.25 ± 14.28	-75.49 ± 10.2
G085334E28540N	0.4 ± 0.03	0.4 ± 0.02	0.53 ± 0.03	0.13 ± 0.13	-79.2 ± 16.01	-77.77 ± 12.5
G085405E28731N	0.45 ± 0.04	0.51 ± 0.03	0.41 ± 0.03	-0.03 ± 0.11	-66.67 ± 14.14	-61.51 ± 10

G085327E28587N	1.16 ± 0.06	1.12 ± 0.05	1.13 ± 0.05	-0.03 ± 0.03	-65.48 ± 16.01	-57.24 ± 12.5
G085554E28593N	1.56 ± 0.08	1.54 ± 0.06	1.54 ± 0.06	-0.03 ± 0.03	-55.81 ± 14.14	-55.12 ± 10
G085629E28324N	0.49 ± 0.05	0.48 ± 0.04	0.46 ± 0.01	-0.03 ± 0.02	-53.85 ± 14.14	-47.26 ± 10
G085489E28568N	2.54 ± 0.18	2.54 ± 0.13	2.51 ± 0.03	-0.04 ± 0.04	-47.35 ± 14.28	-46.95 ± 10.2
G085564E28572N-B	0.85 ± 0.05	0.79 ± 0.04	0.83 ± 0.04	-0.02 ± 0.08	-2.5 ± 16.01	-2.49 ± 12.5
G085263E28491N	1.14 ± 0.05	1.14 ± 0.04	1.14 ± 0.04	0 ± 0	0 ± 0	0 ± 0
G085264E28519N	3.48 ± 0.19	3.34 ± 0.14	3.11 ± 0.13	-0.37 ± 0.27	0 ± 0	0 ± 0
G085267E28501N	1.76 ± 0.06	1.76 ± 0.04	1.64 ± 0.05	-0.12 ± 0.12	0 ± 0	0 ± 0
G085270E28469N	1.13 ± 0.06	1.13 ± 0.05	1.13 ± 0.05	0 ± 0	0 ± 0	0 ± 0
G085275E28471N-A	0.18 ± 0.03	0.18 ± 0.02	0.18 ± 0.02	0 ± 0	0 ± 0	0 ± 0
G085275E28471N-B	0.14 ± 0.02	0.14 ± 0.02	0.14 ± 0.02	0 ± 0	0 ± 0	0 ± 0
G085275E28471N-C	0.26 ± 0.03	0.26 ± 0.02	0.26 ± 0.02	0 ± 0	0 ± 0	0 ± 0
G085286E28529N	0.35 ± 0.04	0.35 ± 0.03	0.35 ± 0.03	0 ± 0	0 ± 0	0 ± 0
G085290E28524N	0.3 ± 0.04	0.3 ± 0.03	0.3 ± 0.03	0 ± 0	0 ± 0	0 ± 0
G085309E28517N	5.6 ± 0.27	5.6 ± 0.2	5.6 ± 0.2	0 ± 0	0 ± 0	0 ± 0
G085320E28470N	0.32 ± 0.03	0.32 ± 0.02	0.32 ± 0.02	0 ± 0	0 ± 0	0 ± 0
G085320E28580N	0.29 ± 0.03	0.29 ± 0.02	0.29 ± 0.02	0 ± 0	0 ± 0	0 ± 0
G085335E28529N	0.68 ± 0.04	0.68 ± 0.03	0.64 ± 0.03	-0.04 ± 0.04	0 ± 0	0 ± 0
G085335E28535N	0.18 ± 0.02	0.18 ± 0.02	0.18 ± 0.02	0 ± 0	0 ± 0	0 ± 0
G085336E28498N	7.33 ± 0.29	7.33 ± 0.22	7.33 ± 0.22	0 ± 0	0 ± 0	0 ± 0
G085346E28605N	1.03 ± 0.08	1.03 ± 0.06	1.03 ± 0.06	0 ± 0	0 ± 0	0 ± 0
G085356E28601N	0.54 ± 0.05	0.54 ± 0.04	0.54 ± 0.04	0 ± 0	0 ± 0	0 ± 0
G085359E28497N	2.49 ± 0.14	2.49 ± 0.1	2.49 ± 0.1	0 ± 0	0 ± 0	0 ± 0
G085371E28473N	2.48 ± 0.09	2.48 ± 0.07	2.48 ± 0.07	0 ± 0	0 ± 0	0 ± 0
G085374E28603N	5.53 ± 0.18	5.53 ± 0.14	5.53 ± 0.14	0 ± 0	0 ± 0	0 ± 0
G085395E28631N	0.25 ± 0.02	0.25 ± 0.02	0.24 ± 0.02	0 ± 0	0 ± 0	0 ± 0
G085428E28571N	1.01 ± 0.08	1.16 ± 0.07	1.01 ± 0.06	0 ± 0.21	0 ± 0	0 ± 0
G085453E28237N	0.62 ± 0.05	0.62 ± 0.04	0.62 ± 0.01	0 ± 0	0 ± 0	0 ± 0

G085457E28245N	0.6 ± 0.07	0.58 ± 0.05	0.56 ± 0.01	-0.04 ± 0.03	0 ± 0	0 ± 0
G085460E28671N	0.55 ± 0.05	0.55 ± 0.04	0.55 ± 0.04	0 ± 0	0 ± 0	0 ± 0
G085466E28236N	0.18 ± 0.04	0.18 ± 0.03	0.18 ± 0.01	0 ± 0	0 ± 0	0 ± 0
G085476E28425N	0.2 ± 0.02	0.2 ± 0.02	0.2 ± 0	0 ± 0	0 ± 0	0 ± 0
G085481E28267N	2.42 ± 0.2	2.42 ± 0.15	2.42 ± 0.04	0 ± 0	0 ± 0	0 ± 0
G085481E28414N	0.48 ± 0.05	0.48 ± 0.03	0.48 ± 0.01	0 ± 0	0 ± 0	0 ± 0
G085488E28414N	0.51 ± 0.04	0.5 ± 0.03	0.5 ± 0.01	-0.01 ± 0.01	0 ± 0	0 ± 0
G085490E28286N	0.66 ± 0.08	0.66 ± 0.06	0.66 ± 0.02	0 ± 0	0 ± 0	0 ± 0
G085502E28397N	0.33 ± 0.04	0.33 ± 0.03	0.31 ± 0.01	-0.02 ± 0.02	0 ± 0	0 ± 0
G085502E28437N	3.83 ± 0.28	3.83 ± 0.21	3.84 ± 0.06	0.01 ± 0.01	0 ± 0	0 ± 0
G085510E28407N	1.17 ± 0.08	1.17 ± 0.06	1.14 ± 0.02	-0.03 ± 0.03	0 ± 0	0 ± 0
G085525E28439N	0.5 ± 0.06	0.45 ± 0.04	0.49 ± 0.01	-0.01 ± 0.06	0 ± 0	0 ± 0
G085536E28454N	1.89 ± 0.17	1.89 ± 0.13	1.89 ± 0.03	0 ± 0	0 ± 0	0 ± 0
G085538E28285N	12.47 ± 0.62	12.36 ± 0.46	12.2 ± 0.12	-0.26 ± 0.19	0 ± 0	0 ± 0
G085545E28527N	17.28 ± 0.99	17.28 ± 0.74	17.28 ± 0.2	0 ± 0	0 ± 0	0 ± 0
G085548E28472N	0.17 ± 0.02	0.17 ± 0.01	0.17 ± 0	0 ± 0	0 ± 0	0 ± 0
G085554E28353N	3.31 ± 0.17	3.31 ± 0.13	3.31 ± 0.03	0 ± 0	0 ± 0	0 ± 0
G085554E28453N	0.75 ± 0.07	0.75 ± 0.05	0.6 ± 0.01	-0.16 ± 0.16	0 ± 0	0 ± 0
G085564E28572N-A	5.86 ± 0.22	5.86 ± 0.16	6.4 ± 0.16	0.53 ± 0.53	0 ± 0	0 ± 0
G085570E28342N	0.11 ± 0.03	0.11 ± 0.02	0.11 ± 0.01	0 ± 0	0 ± 0	0 ± 0
G085575E28459N	27.65 ± 0.89	27.65 ± 0.67	27.65 ± 0.18	0 ± 0	0 ± 0	0 ± 0
G085583E28407N	0.95 ± 0.08	0.85 ± 0.06	0.92 ± 0.02	-0.03 ± 0.12	0 ± 0	0 ± 0
G085584E28303N	0.3 ± 0.04	0.3 ± 0.03	0.3 ± 0.01	0 ± 0	0 ± 0	0 ± 0
G085617E28265N	1.37 ± 0.09	1.37 ± 0.07	1.37 ± 0.02	0 ± 0	0 ± 0	0 ± 0
G085627E28314N	0.95 ± 0.07	1.05 ± 0.07	1.04 ± 0.02	0.09 ± 0.09	0 ± 0	0 ± 0
G085633E28274N	0.47 ± 0.08	0.47 ± 0.06	0.47 ± 0.02	0 ± 0	0 ± 0	0 ± 0
G085633E28327N	0.65 ± 0.04	0.65 ± 0.03	0.63 ± 0.01	-0.01 ± 0.01	0 ± 0	0 ± 0
G085643E28314N	15.78 ± 0.74	15.78 ± 0.56	15.79 ± 0.15	0.01 ± 0.01	0 ± 0	0 ± 0

G085657E28240N	2.14 ± 0.1	2.14 ± 0.07	1.96 ± 0.02	-0.18 ± 0.18	0 ± 0	0 ± 0
G085669E28239N	0.3 ± 0.03	0.3 ± 0.02	0.32 ± 0.01	0.01 ± 0.01	0 ± 0	0 ± 0
G085686E28486N	1.25 ± 0.05	1.02 ± 0.03	1.22 ± 0.01	-0.02 ± 0.31	0 ± 0	0 ± 0
G085699E28143N	4.56 ± 0.32	4.51 ± 0.24	4.5 ± 0.23	-0.06 ± 0.05	0 ± 0	0 ± 0
G085707E28225N	0.53 ± 0.09	0.53 ± 0.07	0.53 ± 0.02	0 ± 0	0 ± 0	0 ± 0
G085720E28299N	60.45 ± 2.14	60.08 ± 1.6	60.02 ± 0.43	-0.43 ± 0.38	0 ± 0	0 ± 0
G085736E28271N	1 ± 0.19	1 ± 0.14	1 ± 0.04	0 ± 0	0 ± 0	0 ± 0
G085749E28150N	12.27 ± 0.51	12.27 ± 0.38	12.27 ± 0.38	0 ± 0	0 ± 0	0 ± 0
G085773E28389N	0.69 ± 0.08	0.69 ± 0.06	0.69 ± 0.06	0 ± 0	0 ± 0	0 ± 0
G085774E28232N	5.46 ± 0.29	5.46 ± 0.22	5.46 ± 0.22	0 ± 0	0 ± 0	0 ± 0
G085801E28399N	0.83 ± 0.06	0.76 ± 0.04	0.62 ± 0.05	-0.21 ± 0.15	0 ± 0	0 ± 0
G085807E28212N	5.2 ± 0.25	5.2 ± 0.19	5.59 ± 0.19	0.39 ± 0.39	0 ± 0	0 ± 0
G085815E28296N	0.01 ± 0.01	0.01 ± 0.01	0.01 ± 0.01	0 ± 0	0 ± 0	0 ± 0
G085819E28132N	0.23 ± 0.03	0.23 ± 0.02	0.23 ± 0.02	0 ± 0	0 ± 0	0 ± 0
G085822E28382N	22.25 ± 0.84	21.7 ± 0.64	21.43 ± 0.63	-0.82 ± 0.61	0 ± 0	0 ± 0
G085840E28159N	17.17 ± 0.56	17.17 ± 0.42	17.17 ± 0.42	0 ± 0	0 ± 0	0 ± 0
G085870E28096N	0.16 ± 0.03	0.16 ± 0.02	0.16 ± 0.02	0 ± 0	0 ± 0	0 ± 0
G085886E28098N	2.39 ± 0.1	2.28 ± 0.08	2.28 ± 0.08	-0.1 ± 0.1	0 ± 0	0 ± 0
G085528E28427N	1.13 ± 0.07	1.13 ± 0.05	1.06 ± 0.01	-0.07 ± 0.07	59.18 ± 14.28	58.2 ± 10.2
G085686E28182N	0.82 ± 0.06	0.83 ± 0.04	0.85 ± 0.04	0.04 ± 0.03	103.99 ± 16.01	100.22 ± 12.5
G085521E28419N	1.13 ± 0.07	1.13 ± 0.05	1.22 ± 0.01	0.09 ± 0.09	191.22 ± 14.28	189.66 ± 10.2
G085465E28672N	0.15 ± 0.02	0.15 ± 0.01	0.18 ± 0.02	0.03 ± 0.03	211.98 ± 16.01	188.57 ± 12.5
Totals	817.72 ± 35.05	793.69 ± 26.55	784.81 ± 17.4	-32.91 ± 34.53	-56248.19 ± 2123.02	-53850.39 ± 1556.41
Mean	3.84 ± 0.16	3.73 ± 0.12	3.69 ± 0.08	-0.15 ± 0.16	-264.08 ± 9.97	-252.82 ± 7.31

Acknowledgments

I want to thank Nicolai Holzer for his guide and patience teaching me the wonderful world of glaciers and its marvels. I am really grateful with Professor Manfred F. Buchroithner for his un-stoppable will and the support that he provided to me during the developing of this Master.

I am really thankful with CONACYT (Consejo Nacional de Ciencia y Tecnología) for all the support given and all the effort that this organization is still doing to promote the science in youth in my country.

I would like to mentioned the suport provided by the BMBF F&E (Bundesministerium für Bildung und Forschung, Forschung & Entwicklung), the research project WET (Vari-ability and Trends in Water Balance Components of Benchmark Drainage Basins on the Tibetan Plateau).

Since the gratitude comes from the heart, and my heart express itself better in spanish I will thank in the best way I could, from the bottom of my heart... my mexican-speaking heart. I hope I am not breaking any law.

Gracias a CONACYT que sin su apoyo, esta maestría y todo lo que obtuve seguiría en un sueño.

Gracias a mi mamita la guerrera incansable por enseñarme a ser libre. También al Pelón por entrarle duro al quite y no rajarse. Obvio a mis hermanitos y al Yopitol nomás porque les quiero agradecer. A Lupita por ser tan chida y estar siempre presente. A toda mi familia paterna que siempre ha estado siempre en las buenas y malas.

Tengo que reconocer el apoyo incondicional que obtuve del Toñito, que lidió como un guerrero con mis dramas, crisis y atorones. Ni qué olvidarme del Jesús Díaz por los consejillos tan cereros. A la Tony por compartir y estar. A todos mis amigos en México que no me han olvidado. También incluida en la gratitud mí maestra Bertha Márquez por su recomendación para hacer esta maestría. Gracias a mis amiguitos Tania, Katja, Cath y Christian, que hicieron de esta travesía una aventura maravillosa. Y de aquí, a lo que sigue.... Continuará/To be continued/つづく.

References

Appalachian State University (2014) *Error Propagation*, [Online], Available:

<http://physics.appstate.edu/undergraduate-programs/laboratory/resources/error-propagation>

[03 January 2015].

Archives, N. (2002) *Press Release*, 2002 Oct, [Online], Available:

<http://www.archives.gov/press/press-releases/2003/nr03-02.html> [27 November 2014].

Barnett, T.P., Adam, J.C. and Lettenmaier, D.P. (2005) 'Potential impacts of a warming climate on water availability in snow-dominated regions', *Nature*, vol. 438, pp. 303-309.

Bolch, T., Pieczonka, T. and Benn, D.I. (2011) 'Multi-decadal mass loss of glaciers in the Everest area (Nepal Himalaya) derived from stereo imagery', *The Cryosphere*, vol. 5, no. 2, pp. 349-358.

Bolch, T., Yao, T., Kang, S., Buchroithner, M.F., Scherer, D., Maussion, F., Huintjes, E. and Schneider, C. (2010) 'A glacier inventory for the western Nyainqentanglha Range and the Nam Co Basin, Tibet, and glacier changes 1976–2009', *The Cryosphere*, vol. 4, no. 3, pp. 419-433.

Braithwaite, R.J. and Raper, S.C.B. (2009) 'Estimating equilibrium-line altitude (ELA) from glacier inventory data', *Annals of Glaciology*, vol. 50, no. 53, pp. 127-132.

Burnett, M.G. (2012) *HEXAGON (KH-9) Mapping Camera Program and Evolution*, Virginia.

Center, C.I.I. *China's Tibet Facts and Figures 2002*, [Online], Available:

<http://www.china.org.cn/english/tibet-english/dili.htm> [22 November 2014].

Ch'ang, C.-f., Zheng, X.-l. and Pan, Y.-s. (1977) *The geological history, tectonic zonation and origin of uplifting of the Himalayas*, Pekin.

Cogley, J.G., R. Hock, L.A., Rasmussen, A.A.A., A. Bauder, R.J.B., P. Jansson, G.K., M. Möller, L.N. and Zemp, M. (2011) *Glossary of Glacier Mass Balance and Related Terms*, Paris, France.

Cryosphere Glossary (2014), [Online], Available: <https://nsidc.org/cryosphere/glossary/> [25 November 2014].

- Cubasch, U. and Cess, R.D. (1990) 'Processes and Modelling', in Houghton, J.T., Jenkins, G.J. and Ephraums, J.J. *Climate Change The IPCC Scientific Assessment*, First Edition edition, Cambridge: Intergovernmental Panel on Climate Change.
- de Blasio, F.V. (2011) 'Friction, Cohesion, and Slope Stability', in de Blasio, F.V. *Introduction to the Physics of Landslides*, Springer.
- Dubayah, R. and Rich, P.M. (1995) 'Research Article Topographic solar radiation models for GIS', *Geographical information Systems*, vol. 9, no. 4, pp. 405-419.
- Ender, A. (2011) *Glacier volume and mass balance in the Ala Ala Archa National Park (Kyrgyz Ala-Too/Kyrgyzstan)*, Technische Universität Dresden.
- ERDAS (2008) 'IMAGINE AutoSync User ' s Guide'.
- ESRI (2014) *ArcGIS Resource Center*, December, [Online], Available: <http://help.arcgis.com/en/arcgisdesktop/10.0/help/index.html#/> [16 December 2014].
- Esri (2014) *Maps and Map Layers*, 21 August, [Online], Available: <http://www.esri.com/software/arcgis/arcgisonline/maps/maps-and-map-layers> [24 November 2014].
- GLIMS (2014) *GLIMS*, 04 August, [Online], Available: <http://www.glims.org/> [10 November 2014].
- Goward, S.N., Masek, J.G., Williams, D.L., Irons, J.R. and Thompson, R.J. (2001) 'The Landsat 7 mission: Terrestrial research and applications for the 21st century', *Remote Sensing of Environment*, vol. 78, no. 1-2, pp. 3-12.
- Granshaw, F.D. and Fountain, A.G. (2006) 'Glacier change (1958 – 1998) in the North Cascades National Park Complex', *Journal of Glaciology*, vol. 52, no. 177, pp. 251-256.
- Hijmans, R.J. *DIVA-GIS Data*, [Online], Available: <http://www.diva-gis.org/gdata> [28 November 2014].
- Hijmans, R.J., Cameron, S. and Parra, J. *WorldClim*, [Online], Available: <http://www.worldclim.org> [09 December 2014].
- Hijmans, R.J., Cameron, S. and Parra, J. *WorldClim- Global Climate Data Download*, [Online], Available: <http://www.worldclim.org/current> [25 November 2014].

- Hijmans, R.J., Cameron, S.E., Parra, J.L., Jones, P.G. and Jarvis, A. (2005) 'Very high resolution interpolated climate surfaces for global land areas', *International Journal of Climatology*, vol. 25, no. 15, pp. 1965-1978.
- Holzer, N., Vijay, S., Yao, T., Xu, B., Buchroithner, M. and Bolch, T. (2014) 'Four decades of glacier variations at Muztag Ata (Eastern Pamir): a multi-sensor study including Hexagon KH-9 and Pléiades data'.
- Immerzeel, W.W., van Beek, L.P.H. and Bierkens, M.F.P. (2010) 'Climate Change Will Affect the Asian Water Towers', *Science*, vol. 328, no. 5984, pp. 1382-1385.
- JAXA (2001) *Advanced Land Observing Satellite "DAICHI" (ALOS)*, 20 October, [Online], Available: <http://global.jaxa.jp/projects/sat/alos/> [11 December 2014].
- Kropáček, J., Maussion, F., Chen, F., Hoerz, S. and Hochschild, V. (2013) 'Analysis of ice phenology of lakes on the Tibetan Plateau from MODIS data', *The Cryosphere*, pp. 287-301.
- Laboratory, J.P. (2014) *Jet Propulsion Laboratory*, October, [Online], Available: <http://www2.jpl.nasa.gov/srtm/> [18 November 2014].
- Lauer, D.T., Morain, S.A. and Salomonson, V.V. (1997) 'The Landsat Program : Its Origins , Evolution , and Impacts', *Photogrammetric Engineering & Remote Sensing*, vol. 63, no. 7, pp. 831-838.
- Le Bris, R. and Paul, F. (2013) 'An automatic method to create flow lines for determination of glacier length: A pilot study with Alaskan glaciers', *Computers & Geosciences*, vol. 52, pp. 234-245.
- Lei, Y., Yang, K., Wang, B., Sheng, Y., Bird, B.W. and Zhang, G. (2014) 'Response of inland lake dynamics over the Tibetan Plateau to climate change', *Climatic Change*, vol. 125, no. 2, pp. 281-290.
- Liu, X. and Chen, B. (2000) 'Climatic warming int the Tibetan Plateau during recent decades', *International Journal of Climatology*, vol. 20, no. 14, pp. 1729-1742.
- Maurer, J. (2013) *Evaluation of Hexagon Imagery for Regional Mass Balance Study in the Bhutan Himalayas*, Utah: Utah Space Grant Consortium.
- NASA (2011) *ASTER*, [Online], Available: <http://asterweb.jpl.nasa.gov/gdem.asp> [8 December 2014].

- NASA (2014) *Landsat 7*, 2 December, [Online], Available: <http://landsat.gsfc.nasa.gov/?p=3184> [3 December 2014].
- NASA (2014) *Landsat Science*, 02 December, [Online], Available: <http://landsat.gsfc.nasa.gov/?p=3180> [3 December 2014].
- NGA (2014) *NGA in History*, [Online], Available: <https://www.nga.mil/About/History/NGAinHistory/Pages/HEXAGON.aspx> [27 November 2014].
- Nikolakakou, P. (2014) *Investigation and visualization of glacier mass balances at Mt. Shishapangma (Tibet, China) based on multi-temporal remote sensing data*, Technische Universität Dresden.
- NSIDC (2014) *All about glaciers*, [Online], Available: <http://nsidc.org/cryosphere/glaciers/questions/components.html> [12 December 2014].
- Nye, J.F. (1952) 'The mechanics of glacier flow', *Journal of Glaciology*, no. 11, pp. 82-93.
- Pan, B.T., Zhang, G.L., Wang, J., Cao, B., Geng, H.P. and Zhang, C. (2012) 'Glacier changes from 1966–2009 in the Gongga Mountains, on the south-eastern margin of the Qinghai-Tibetan Plateau and their climatic forcing', *The Cryosphere*, vol. 6, no. 5, pp. 1087-1101.
- Paul, F. and Andreassen, L.M. (2009) 'A new glacier inventory for the Svartisen region, Norway, from Landsat ETM+ data: challenges and change assessment', *Journal of Glaciology*, vol. 55, no. 192, pp. 607-618.
- Paul, F., Barry, R.G., Cogley, J.G., Frey, H., Haeberli, W., Ohmura, A., Ommanney, C.S.L., Raup, B., Rivera, A. and Zemp, M. (2009) 'Recommendations for the compilation of glacier inventory data from digital sources', *Annals of Glaciology*, vol. 50, no. 53, pp. 119-126.
- Paul, F., Huggel, C. and Kääb, A. (2004) 'Combining satellite multispectral image data and a digital elevation model for mapping debris-covered glaciers', *Remote Sensing of Environment*, pp. 510-518.
- Paul, F., Huggel, C., Kääb, A., Kellenberger, T. and Maisch, M. (2002) 'Comparison of TM-Derived Glacier Areas with Higher Resolution Data Sets', EARSel Workshop on remote sensing of land ice and snow, Bern.

- Pellicciotti, F., Raschle, T., Huerlimann, T., Carezzo, M. and Burlando, P. (2011) 'Transmission of solar radiation through clouds on melting glaciers: a comparison of parameterizations and their impact on melt modelling', *Journal of Glaciology*, vol. 57, no. 202, pp. 367-381.
- Pellikka, P. and Rees, W.G. (2009) *Remote Sensing of Glaciers*, London, U.K.: Taylor & Francis Group.
- Phillips, E. (2013) *Glossary of Glacier Terminology - Text Version*, 12 January, [Online], Available: <http://pubs.usgs.gov/of/2004/1216/text.html> [25 November 2014].
- Pucha Cofrep, F. (2011) *Delimitar automáticamente una cuenca hidrográfica en ArcGIS*, 31 August, [Online], Available: <http://acolita.com/como-delimitar-automaticamente-una-cuenca-hidrografica-en-arctis-hidrologia/> [11 September 2014].
- Purdie, H., Anderson, B., Chinn, T., Owens, I., Mackintosh, A. and Lawson, W. (2014) 'Franz Josef and Fox Glaciers, New Zealand: Historic length records', *Global and Planetary Change*, vol. 121, pp. 41-52.
- Richardson, S.D. and Reynolds, J.M. (2000) 'An overview of glacial hazards in the Himalayas', *Quaternary International*, vol. 66, pp. 31-47.
- Rignot, E. and Echelmeyer, K. (2001) 'Penetration depth of interferometric synthetic-aperture radar signals in snow and ice', *Geophysical Research Letters*, vol. 28, no. 18, pp. 3501-3504.
- Space (2014) *Just Declassified: Spy Satellite KH-9 Hexagon*, [Online], Available: <http://www.space.com/13004-declassified-spy-satellite-kh-9-hexagon.html> [26 November 2014].
- Stallmann, C., Meyer, J., Pretorius, L. and Maass, F. (2008) *An Open Source Implementation of Automated Orthorectification using a Rational Polynomial Coefficients Model*, Pretoria: University of Pretoria.
- Surazakov, A. and Aizen, V. (2010) 'Positional accuracy evaluation of declassified Hexagon KH-9 mapping camera imagery', *Photogrammetric Engineering & Remote Sensing*, vol. 76, pp. 603-608.
- Trenberth, K.E., Fasullo, J.T. and Kiehl, J. (2009) 'Earth's Global Energy Budget', *Bulletin of the American Meteorological Society*, vol. 90, no. 3, pp. 311-323.

- U.S. Department of the Interior (2013), 16 January, [Online], Available: <http://landsat.usgs.gov> [14 November 2014].
- USGS (2013) *Frequently Asked Questions about the Landsat Missions*, 19 September, [Online], Available: http://landsat.usgs.gov/what_is_landsat.php [2 February 2014].
- Villegas Yepes, P.P. (2011) *Delimitación de cuencas con ArcGIS*, [Online], Available: <http://www.aguaysig.com/2011/03/delimitacion-de-cuencas-con-arcgis.html> [7 December 2014].
- Winsvold, S.H., Andreassen, L.M. and Kienholz, C. (2014) 'Glacier area and length changes in Norway from repeat inventories', *The Cryosphere*, vol. 8, no. 5, pp. 1885-1903.
- Yao, T., Pu, J., Lu, A., Wang, Y. and Yu, W. (2007) 'Recent Glacial Retreat and Its Impact on Hydrological Processes on the Tibetan Plateau , China , and Surrounding Regions Recent Glacial Retreat and Its Impact on Hydrological Processes on the Tibetan Plateau , China , and Surrounding Regions', *Arctic, Antarctic, and Alpine Research*, vol. 39, no. 4, pp. 642-650.
- Yao, T., Thompson, L.G., Mosbrugger, V., Zhang, F., Ma, Y., Luo, T., Xu, B., Yang, X., Joswiak, D.R., Wang, W., Joswiak, M.E., Devkota, L.P., Tayal, S., Jilani, R. and Fayziev, R. (2012) 'Third Pole Environment (TPE)', *Environmental Development*, vol. 3, pp. 52-64.
- Yu, H. (2010) *Monitoring Glacier Elevation Changes Over the Tibetan Plateau Using ALOS PRISM and ICESat*.
- Zheng, B. (1988) 'Quaternary glaciation of Mt. Qomolangma-Xixabangma region', *GeoJournal*, vol. 17, no. 4, pp. 525-543.